Geological Survey of Finland

Bulletin 308

The granulite complex of Finnish Lapland: petrology and metamorphic conditions in the Ivalojoki - Inarijärvi area

by Paul Karl Hörmann, Michael Raith, Peter Raase, Dietrich Ackermand and Friedrich Seifert

Geologinen tutkimuslaitos
Espoo 1980

Geological Survey of Finland, Bulletin 308

THE GRANULITE COMPLEX OF FINNISH LAPLAND: PETROLOGY AND METAMORPHIC CONDITIONS IN THE IVALOJOKI–INARIJÄRVI AREA

BY

PAUL KARL HÖRMANN, MICHAEL RAITH, PETER RAASE, DIETRICH ACKERMAND AND FRIEDRICH SEIFERT

with 45 figures, 28 tables in the text and one appendix

GEOLOGINEN TUTKIMUSLAITOS
ESPOO 1980

Hörmann, Paul Karl; Raith, Michael; Raase, Peter; Ackermand, Dietrich and Seifert, Friedrich, 1980. The granulite complex of Finnish Lapland: petrology and metamorphic conditions in the Ivalojoki—Inarijärvi area. *Geological Survey of Finland, Bulletin 308.* 95 pages, 45 figures, 28 tables and one appendix.

The Precambrian metamorphic rocks of the granulite complex and the adjacent West Inari schist zone and granite gneiss complex had both magmatic and sedimentary source rocks. In the Ivalojoki—Inarijärvi area the West Inari schist zone is characterized by predominant tholeiitic and dacitic source rocks and only subordinate sediments (greywackes). In the granulite complex the magmatogenic rocks originated from calc-alkaline basalts to rhyolites with abundant andesites. Metasediments in this unit (greywackes, arkoses, quartzites, pelites) are particularly important in the central and northeastern parts. Tholeiitic and dacitic source rocks constitute the major part of the granite gneiss complex in the study area.

The geochemical characteristics of the magmatogenic rocks of the individual units suggest the existence of an old (Pre-Karelian) island arc system, with the West Inari schist zone constituting the tholeiitic outer arc and the granulite complex the calc-alkaline inner arc system, and a stable continental block in the northeast.

The metamorphic evolution of the series was polyphase: The assemblages and textures only reflect the metamorphism of Karelian age. An early, synkinematic event of this cycle (2150 Ma) is still preserved in the southwestern part of the granulite complex. The strongly foliated and sheared rocks (with platy quartz textures) crystallized in hypersthene granulite facies at low X_{H_2O} (below 0.3). The subsequent postkinematic event (1 900 Ma) overprinted the entire area. In the granulite complex X_{H_2O} increased but was still only in the order of 0.3, leading to hornblende granulite facies rocks and extensive anatexis in the central and northeastern parts. Temperatures ranged from 700—750°C, at pressures around 5 kbars. The West Inari schist zone and the granite gneiss complex were subjected to high-grade amphibolite facies metamorphism at temperatures ranging from 650—700°C and high X_{H_2O}. Temperatures and pressures varied continuously over the profile, whereas X_{H_2O} shows a sharp decrease at the border between the West Inari schist zone and the granulite complex.

Key words: petrology, petrography, geochemistry, mineralogy, metamorphic rocks, granulite, metamorphism, metamorphic zones, polymetamorphism, P-T conditions, Precambrian, Finland, Lapland

Authors' address:
Mineralogisch — Petrographisches Institut und Museum der Universität Kiel, Olshausenstrasse 40—60, 2300 Kiel, BRD

ISBN 951-690-122-0
ISSN 0367-522x

Helsinki 1980. Valtion painatuskeskus.

CONTENTS

INTRODUCTION

The granulite belt of northern Finland represents one of the classical areas of high-grade Precambrian metamorphic rocks. Its petrology became particularly known through the studies by Eskola (e.g. 1952) and served for a definition of the granulite facies in terms of mineral assemblages and conditions of formation (Eskola 1939). Some data on the geochemistry of the rocks and the structures have been given by Sahama (1933, 1936, 1945). Mikkola (1941) mapped the region joining the granulite belt in the south and southwest and gave an account on the petrography and structures of the rocks. The granulite belt proper and its adjacent rock units have been mapped in admirable detail by Meriläinen (1965). His excellent paper on the petrography, stratigraphy and tectonics of the Precambrian of northern Finland (Meriläinen 1976) presents a thorough and lucid description of the rocks and, on the basis of radiometric data, establishes the age of the rocks and the sequence of the metamorphic and magmatic events. This work was of fundamental importance for the present investigation.

In view of the recent developments in Precambrian geology and petrology (cf. Windley 1976) it was deemed necessary to obtain more information on the genesis of the very old source rocks and their physicochemical conditions of metamorphism, thus amplifying our knowledge of the Finnish granulites in particular and of Precambrian rock-forming processes in general. To achieve this goal, an extensive data set on the compositions of rocks and minerals, assemblages and textural relationships has to be established and evaluated applying modern concepts and recent results of geochemistry and phase petrology.

GEOLOGICAL SETTING

On the basis of lithology, structures and radiometric data Meriläinen (1976) distinguished four different rock units in the crystalline basement of northern Finland. His subdivision will be adopted in the present paper. In the following, only the most important characteristics are given, for more detail the reader is referred to the paper by Meriläinen (1976) and the ensuing discussion.

From the northeast towards the southwest the following complexes are encountered (Fig. 1):

1. The granite gneiss complex consisting mainly of intermediate to acid gneisses and amphibolites intruded by synkinematic granites to quartz diorites. Within this sequence the oldest rocks of the Finnish Precambrian have been dated (2 865—2 739 Ma), but there are also indications of two younger thermal events (2 500 and 1 900 Ma).
2. As complex synclinoria within the granite gneiss complex the younger schist zones of Apukasjärvi, Vätsäri and Kuorboaivi are encountered. They bear a great variety of rocks of sedimentary, volcanic and plutonic origin. The latter give ages in the range

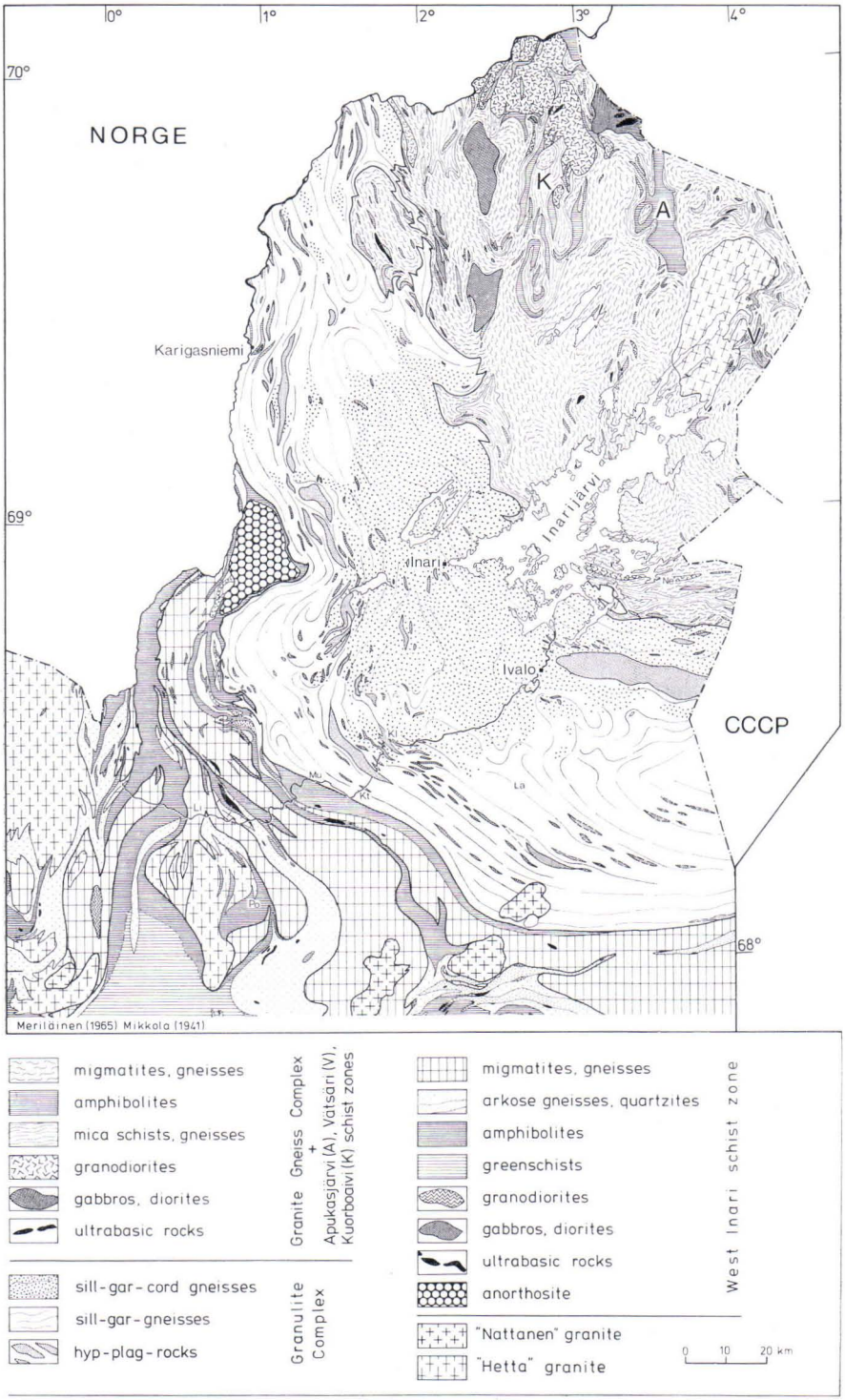

Fig. 1. Geological map of the Precambrian of northern Finland according to Mikkola (1941) and Meriläinen (1965). Abbreviations for localities are explained in Fig. 2.

1 735—2 093 Ma, but an age older than 2 500 Ma is assumed for the metasediments and metavolcanics.

3. The granulite complex consists mainly of garnet gneisses, garnet–cordierite gneisses, and hypersthene–plagioclase rocks. In its marginal zones, however, quartz-feldspar gneisses, hornblende gneisses and amphibolites predominate. The oldest radiometric data (2 500 Ma, based on whole-rock common lead) are interpreted by Meriläinen (1976) as the age of an early amphibolite facies metamorphism. Ages around 2 150 Ma, which were determined on granulitic garnet gneisses in the southwestern part of the granulite complex from U/Pb in zircons are assigned to a granulite facies metamorphic stage. On the other hand, the anatectic garnet–cordierite gneisses in the northeastern part of the granulite complex gave U/Pb monazite ages of 1 900 Ma, which is the age of a younger high-grade metamorphic event under static conditions, leading to the anatectic overprint. This process is termed a diaphthoresis by Meriläinen (1976) whereas the present study suggests that the temperatures were similar to those during granulitisation.
4. The West Inari schist zone is composed mainly of greenschists, amphibolites, quartz-feldspar gneisses and quartzites besides syn-kinematic granite intrusions (Hetta-type 1 832 Ma). The age relationships are still, obscure but ages above 2 500 Ma are assumed by Meriläinen (1976).

The radiometric data indicate that the entire region has suffered its last high-grade metamorphism at 1 900 Ma during the Karelian orogeny leading to amphibolite facies metamorphism in the eastern part of the West Inari schist zone, the granite gneiss complex and the associated schist zones but to hornblende granulite facies rocks in the granulite complex. Most of the mineral assemblages encountered today in all the different rock units originated during this episode. Only in the basal parts of the granulite complex an older event is recognized in addition by Meriläinen (1976) and related to hypersthene granulite metamorphism at an age of 2 150 Ma (see above).

At the end of the Karelian orogenetic cycle postorogenic intrusions of granites (Nattanen-type) took place at 1 730 Ma.

For a characterization of the origin of the source rocks and the physicochemical conditions of metamorphism in all rock units the present study concentrates on samples from a profile along the Ivalojoki river and the shores of Inarijärvi (Fig. 2). The profile starts near Lisma in the middle part of the West Inari schist zone, cuts the eastern parts of the West Inari schist zone, the granulite complex and its two marginal zones, and ends in the granite gneiss complex northeast of Nellimö (cf. Fig. 1).

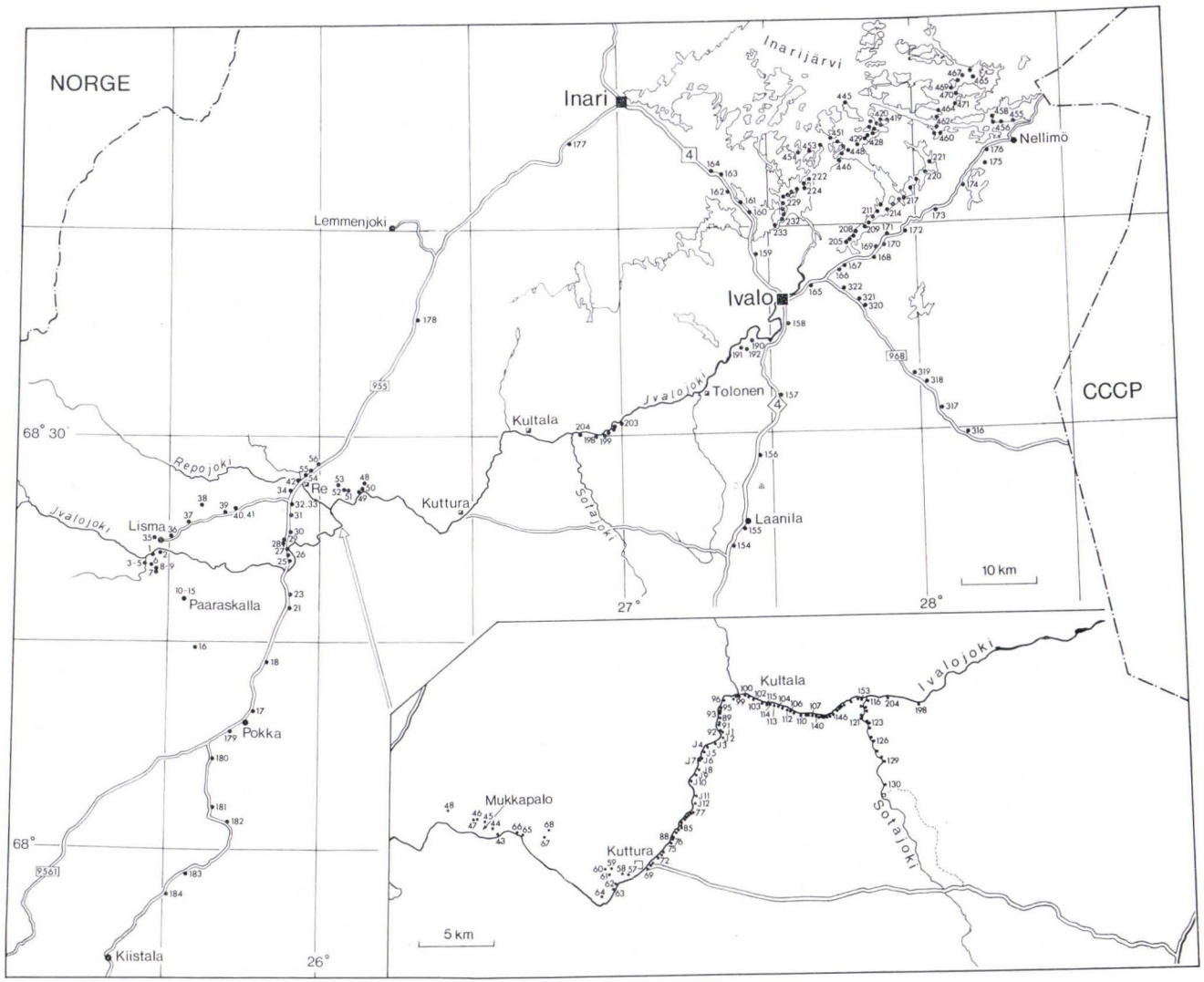

Fig. 2. Sample localities and sample numbers in the profile studied. For the geological setting of the samples cf. Fig. 1.

PETROGRAPHY

The metamorphic rock sequence, its petrography, mineral contents and petrofabrics as it is exposed along the Ivalojoki—Inarijärvi section (cf. Figs. 8 and 9) will only briefly be described here. For details the reader is referred to the paper by Meriläinen (1976).

West Inari schist zone

The rocks of this zone form a heterogeneous sequence comprising three distinct subunits: In the western part, the so-called Peltotunturi zone, which has not been studied here, quartzites, mica schists, gneisses and greenschists predominate. The central part is mainly built up of amphibolites and hornblende gneisses, whereas in the eastern part fine-grained light quartz–feldspar gneisses grading into hornblende gneisses and amphibolites are exposed. The series contains ultramafics as small lenses in the gneisses (Mikkola and Sahama 1936) and highly aluminous amphibolites with corundum, sapphirine and kornerupine (Haapala *et al.* 1971).

The amphibolites of the central and eastern part vary from fine-grained, banded and foliated types to coarse-grained, massive rocks with schlieren texture. In the field, dark green amphibolites, plagioclase amphibolites and garnet amphibolites can be distinguished. All types can contain clinopyroxene and quartz and, as accessories, apatite, sphene, and rare opaques.

Because of the geochemical data to be presented below it is believed that these rocks were derived from tholeiitic magmatic rocks, the banded varieties might represent former tuffs with mainly volcanic matter (cf. also Meriläinen 1976).

The hornblende gneisses are rocks transitional from amphibolites to light banded gneisses (quartz–feldspar gneisses according to Meriläinen 1976). They are partly finely banded, partly coarse-grained rocks with schlieren texture made up of plagioclase, quartz, garnet, hornblende as well as microcline and biotite in varying proportions. A particularly microcline-rich, fine-grained variety occurs near Ivalon Matti at the road Pokka—Inari. Its accessories are sphene, apatite, and magnetite. The parent rocks were probably tuffaceous sediments.

The quartz–feldspar gneisses of the eastern part are fine-grained greyish rocks often with massive migmatic texture. The main mineral components are microcline, quartz and plagioclase with minor biotite and occasional garnet and hornblende. Accessories are zircon, apatite and small amounts of magnetite and ilmenite. The geochemical data presented below hint to a magmatic origin (dacite to rhyolite).

The concordant bodies of ultramafics are mostly coarse-grained metaperidotites often with relic olivine. They consist of bronzite, tremolite, chlorite and little spinel. Besides carbonate, serpentine minerals and talc are present. In their marginal parts these rocks are transformed into strongly sheared tremolite–chlorite schists with some serpentine, talc and carbonate. As premetamorphic rocks harzburgites to dunites can be assumed.

The southwestern marginal zone of the granulite complex

This heterogeneous zone follows to the northeast of the West Inari schist zone and forms the transition to the granulite complex. Because of the similarity of rock types and lack of outcrops the boundary towards the West Inari schist zone is poorly defined (Meriläinen 1976).

However, the appearance of light garnet–quartz–feldspar gneisses with the typical platy quartz texture and the change in mineral assemblages indicate the boundary towards the granulite complex proper in the northeast. These changes occur over a rather narrow zone less than 500 meters wide. It will be shown below by the detailed mineralogical data that the southwestern marginal zone forms the transition zone between the West Inari schist zone and the granulite complex in terms of metamorphic conditions.

In the area investigated the marginal zone consists of a sequence of amphibolites to hornblende gneisses and quartz–feldspar gneisses alternating on a small scale (Lechner 1978, Wiens 1978). These rocks show in some places strong anatexis.

Contrary to the West Inari schist zone the quartz–feldspar gneisses are characterized by the widespread occurrence of garnet, hornblende and clinopyroxene. Adjacent to the granulite complex (at Mukkapalo) these rocks develop platy quartz textures; in addition the metabasic rocks contain orthopyroxene for the first time, besides hornblende, clinopyroxene and garnet. In this zone nearly pure garnet–quartz rocks with only minor plagioclase and orthopyroxene occur as bands several meters thick.

The coarse-grained hornblende–plagioclase flaser gneisses and massive rock types exposed near Repojoki can be derived from gabbros or diorites. The series contains typically small concordant lenses of metaperidotites (cf. Mikkola and Sahama 1936), pyroxenites and hornblendites. As a particularity small discordant bodies of metatroctolite exhibiting characteristic corona textures have been encountered at Mukkapalo.

The granulite complex

This unit can be subdivided into two parts according to the structure and mineral assemblages of the garnet gneisses (Meriläinen 1976):

In the southwestern part (up to 1 km south of Kultala) fine-grained light garnet–quartz–feldspar gneisses with platy quartz texture predominate. These rocks might be considered as the most typical granulite rocks in the area. They contain schlieren, streaks and bands of coarser-grained garnet–biotite gneisses with mostly flaser texture. These can be further subdivided into garnet–biotite–K-feldspar gneisses and garnet–biotite–plagioclase gneisses. All gneisses, in particular the garnet–biotite–K-feldspar gneisses, may contain coarse prismatic sillimanite. Zircon, monazite, sparse apatite, and opaques (rutile, ilmenite, pyrite) are the accessories. Some gneisses contain graphite which, by analogy to the results of Rankama (1948) on the origin of graphite in other metamorphic rocks, has been taken as evidence for a sedimentary origin by Eskola (1952).

The central and northeastern part of the granulite complex is built up mainly of medium- to coarce-grained sillimanite–garnet–biotite gneisses and anatexites often characterized by the occurrence of cordierite. Contrary to the granulitic gneisses of the southwestern part these rocks are rather massive, the anatectic mobilization generally increases towards the northeast. Simultaneously, by this process, the rocks become coarser-grained and the platy quartz textures vanish. The garnet–cordierite gneisses contain as accessories zircon, monazite, rutile, hercynite and graphite besides a complex assemblage of opaques (pyrrhotite, pyrite, ilmenite, pentlandite and chalcopyrite).

Hypersthene-bearing rocks are widespread over the entire granulite complex in the form of lenses or bands (partly boudinized) ranging in thickness from tenths of a meter to several

meters. Where the granulitic garnet gneisses grade into the anatectic, cordierite-bearing garnet gneisses a zone with abundant massive to gneissose hypersthene-plagioclase rocks occurs. These form concordant bodies with thicknesses up to several hundred meters. Besides hypersthene and plagioclase they always contain biotite and varying amounts of hornblende, clinopyroxene, quartz and occasionally also garnet and K-feldspar. The colour of these rocks depends mainly on the varying hypersthene—plagioclase ratio. Accessories are apatite, zircon and opaques (magnetite, ilmenite/hematite, pyrite, pyrrhotite, bornite and chalcopyrite).

In the northeastern part the hypersthene–plagioclase rocks bear cummingtonite and/or anthophyllite. These rocks grade into the cummingtonite-bearing, hypersthene-free amphibolites of the northeastern marginal zone of the granulite complex (see below).

According to Meriläinen (1976) the garnet gneisses of the granulite complex are mostly metamorphosed pelitic sediments, greywackes and intermediate tuffites, whereas the hypersthene-plagioclase rocks are derived from basic to andesitic volcanics. The geochemical data reported below indicate that magmatic rocks also played an important role as parent rocks of the garnet gneisses.

The northeastern marginal zone of the granulite complex

Towards the northeast the granulite complex is bordered by a zone some 5—10 km wide consisting of a heterogeneous sequence of quartz–feldspar gneisses, garnet-bearing mica gneisses, hornblende gneisses and amphibolites as well as quartzites. These rocks differ from the coarse-grained and rather massive anatexites of the adjacent part of the granulite complex by their fine to medium grain size, a well-defined foliation and their amphibolite facies assemblages. The boundary of this unit towards the granite gneiss complex in the northeast is poorly defined and, according to Meriläinen (1976), may be drawn at the base of a southwest-dipping quartzite series occurring on the islands Kaamassaari and Lusmasaari. The border is thus defined by the lithology and does not necessarily represent a sudden change in metamorphic conditions. Meriläinen (1976) suggests a sedimentary and volcanogenic origin of these rocks.

Main minerals of the quartz–feldspar gneisses and mica gneisses are plagioclase, quartz, biotite, and garnet. In addition, minor microcline and hornblende may occur. Accessories are zircon, rutile, ilmenite, magnetite and pyrite. Sillimanite and cordierite have been found in some migmatic garnet gneisses similar to those of the northeastern part of the granulite complex. The schlieren texture and specific mineral assemblage of the rocks as well as the strong folding of the lithologic boundary between the granulite complex and the northeastern marginal zone suggests that these rocks belong chemically in fact to the granulite complex.

Hornblende gneisses and amphibolites contain as major minerals plagioclase and hornblende besides minor biotite, garnet, cummingtonite, clinopyroxene, scapolite and quartz. Accessories are apatite, zircon, and opaques (ilmenite, magnetite, pyrrhotite, and pyrite).

The rocks of the northeastern marginal zone are particularly affected by retrograde alteration. It led to the formation of andalusite, kyanite, chlorite, muscovite, and sphene in the gneisses, and of epidote, chlorite, sphene, actinolite and carbonate in the metabasites.

The granite gneiss complex

In the profile studied the granite gneiss complex consists of a monotonous suite of fine- to medium-grained migmatic gneisses interlayered with hornblende gneisses and amphibolites. The rock sequence is veined and gneissose, sometimes strongly folded and often cut by pegmatites.

The migmatic gneisses of quartzdiorite to granodiorite composition usually contain plagioclase, quartz, and biotite besides minor microcline and hornblende. Garnet is typically absent. Accessories are apatite, zircon and opaques. These rocks grade continuously into hornblende gneisses. Amphibolites form distinct layers and lenses. Besides plagioclase and hornblende as major constituents some clinopyroxene, biotite, and accessories (apatite and opaques) may occur. Local intense retrogression led to the formation of epidote, chlorite, white mica, prehnite, and sphene.

GEOCHEMISTRY

Some data on the major element compositions of rocks of the West Inari schist zone and the granulite complex have already been presented by Eskola (1952), Mikkola (1941), Mikkola and Sahama (1936) and Meriläinen (1976). Trace element data of rocks from the southern part of the area were published by Sahama (1945).

The authors agree that the rock sequence is built up of rocks of magmatic as well as of sedimentary origin. Eskola (1952) concluded that the ultramafic and mafic rocks of the granulite complex had magmatic source rocks (peridotites, pyroxenites, basalts, andesites), but most of the more acid rock types, except the granites, were assigned to sedimentary source rocks. According to Meriläinen (1976) the acid gneisses originated largely from sedimentary rocks (greywackes, subgreywackes, arkoses, quartzites) interbedded locally with volcanics (lavas, tuffs, sills).

Since the studies of Sahama (1945) and Eskola (1952) more information on the major and trace element composition of specific magmatic and sedimentary rock types is available (e.g. Wedepohl 1969, 1975) and thus the question of source rocks has to be reinvestigated. In addition, the recent knowledge of the relationships between volcanic rock composition and geological setting might allow a characterization of the tectonic environment during the formation of the source rocks. For a discrimination of magmatic and sedimentary materials various methods have been developed (e.g. Shaw 1972) which are also applicable to high-grade metamorphic rocks. To achieve these goals, an extensive data set on major and trace element compositions of the rocks has been collected.

The representation of the CIPW norm data for the analyses available in the Q–A–P Streckeisen diagram (Fig. 3) and the Alk–F–M diagrams (Fig. 4) reveals a distribution pattern typical of tholeiitic and calc-alkaline rocks of the

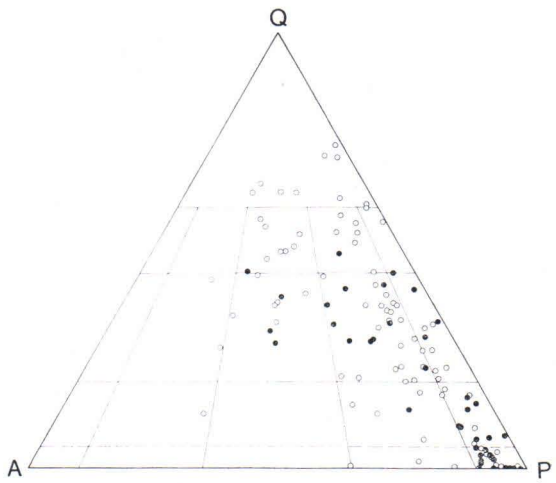

Fig. 3. Q–A–P Streckeisen diagram of the rocks of the West Inari schist zone and the granulite complex based on CIPW norm data. Dots: rocks of the West Inari schist zone; circles: rocks of the granulite complex.

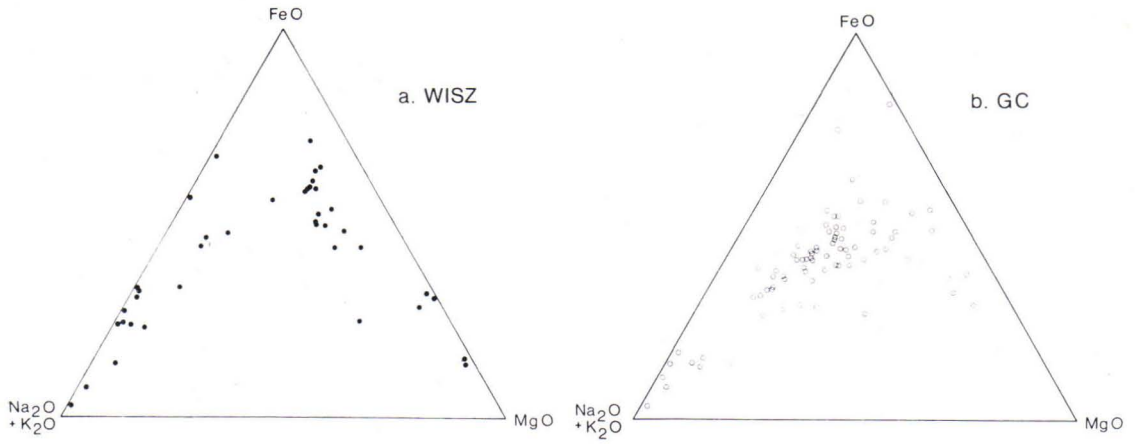

Fig. 4. Alk–F–M diagrams of the rocks of the West Inari schist zone (a) and the granulite complex (b).

continental margins (Jakeš and White 1972, Miyashiro 1974, Dostal *et al.* 1977, Hörmann and Pichler 1980). There exists also a striking geochemical similarity to Archean volcanic rocks of the old greenstone belts of Canada (Baragar 1966, Baragar and Goodwin 1969), the United States (Condie 1972, Bayley *et al.* 1973) and South Africa (Viljoen and Viljoen 1969).

For a discrimination of source rocks (magmatogenic versus sedimentary origin) the methods proposed by Shaw (1972), Köhler and Raaz (1951) and Bilâl (1978) have been used. All these methods critically hinge on the assumption that the high-grade metamorphic processes did not considerably change the bulk rock chemistry. Even then, primitive sediments (e.g. greywackes) may be indistinguishable from magmatic rocks. From factor analysis Shaw (1972) derived a discriminant function

$DF = 10.44 - 0.21\ SiO_2 - 0.32\ Fe_2O_3$ (total Fe) $- 0.98\ MgO + 0.55\ CaO + 1.46\ Na_2O + 0.54\ K_2O$

which is applicable only to quartz–feldspar rocks with $MgO < 6$ % and $SiO_2 < 80$ %. Igneous parentage is indicated by positive values of DF, whereas negative values point to a sedimentary origin. Bilâl (1978) discriminated basalts and the similarly composed greywackes by the method of Köhler and Raaz (1951) and by alk/si Niggli diagrams. By both methods, magmatic compositions are represented on smooth trendlines in the diagrams, whereas sedimentary compositions display quite irregular scattering. Bilâl (1978) checked these methods for low-grade metasedimentary and metavolcanic rocks of the Tampere schist belt of southwestern Finland (Simonen 1953) and from other areas. All these methods of discrimination depend on loss of feldspar component from magmatic debris during the sedimentary process.

In this section the main geochemical features are described. The inferred source rocks are given in parentheses.

West Inari schist zone

Major element composition

Ultramafic rocks (komatiite or picrite): These rocks occur as lenses and schlieren-like bodies within the amphibolites and hornblende gneisses. Two different rock types can be distinguished on the basis of their chemical composition. The ultramafic rock 22 I(No. 1 in Table 1) has a composition close to garnet peridotite (Carswell

Table 1
Chemical composition of ultramafic rocks, recalculated onto a water-free basis.

	1.	2.	3.	4.	5.	6.
SiO_2	48.75	46.98 ±2.06	45.55±0.83	47.1	47.37	44.2
Al_2O_3	0.99	7.36 ±0.37	8.29±1.86	6.6	6.79	6.4
TiO_2	0.05	0.37 ±0.19	0.75±0.35	0.3	0.46	1.44
Fe_2O_3	4.10	3.96 ±1.46	3.59±1.36	1.0	1.18	2.96
FeO	3.57	6.37 ±3.26	8.52±1.99	7.7	8.08	7.4
MnO	0.104	0.192±0.021	0.20±0.06	0.2	0.19	0.19
MgO	39.00	26.81 ±2.76	24.76±4.13	30.2	20.39	22.4
CaO	2.66	7.00 ±1.26	7.60±1.39	6.8	8.31	8.3
Na_2O	0.72	0.84 ±0.75	0.51±0.42	0.2	0.39	0.64
K_2O	0.06	0.085±0.043	0.26±0.10	0.02	0.06	0.40
P_2O_5	0.003	0.021±0.021	—	—	0.05	0.17

1. Ultramafic rock 22 I, West Inari schist zone.
2. Average of ultramafic rocks 5 I, 38 I, 38 II, 39 I, West Inari schist zone.
3. Average of 4 chlorite-amphibole rocks, Kittilä Greenstone Province (Mikkola 1941).
4. Peridotite with quench texture (Nesbitt 1972).
5. Peridotitic komatiite, Geluk type, Onverwacht group, South Africa (Viljoen and Viljoen 1969).
6. Picrite, Deccan, India (Krishnamurthy and Cox 1977).

Table 2
Chemical composition of amphibolites.

	1.	2.	3.	4.	5.
SiO_2	51.23 ±1.57	51.88±1.28	51.57	49.60	51.18
Al_2O_3	14.38 ±0.91	14.25±1.49	15.91	16.03	15.20
TiO_2	1.31 ±0.59	1.20±0.80	0.80	1.43	1.62
Fe_2O_3	3.11 ±1.04	n. d.			
FeO	8.42 ±1.29	10.76±2.09	7.04	9.18	11.00
MnO	0.206±0.026	n. d.	0.17	0.17	0.18
MgO	6.99 ±0.94	7.88±1.31	6.73	7.94	6.12
CaO	9.97 ±0.80	10.33±1.74	11.74	11.25	10.11
Na_2O	2.69 ±0.39	2.70±0.70	2.41	2.47	2.37
K_2O	0.60 ±0.15	0.27±0.21	0.44	0.21	0.84
P_2O_5	0.136±0.070	n. d.	0.11	0.14	0.22

1. Average of amphibolites 4 I, 18 II, 19 I, 20 I, 21 I, 24 I, 27 I, 29 I, 30 I, 44 I, West Inari schist zone.
2. Average of 13 samples of Tertiary basalts from the basic igneous complex of Ecuador and Columbia (Goossens *et al.* 1977).
3. Island arc tholeiites (Jakeš and White 1972).
4. Abyssal oceanic tholeiites (Wedepohl 1975).
5. Continental tholeiites (Wedepohl 1975).

and Dawson 1970). The other, more abundant, ultramafic rocks (No. 2 in Table 1) are similar to those encountered in the komatiite series of the Precambrian old greenstone belts (Viljoen and Viljoen 1969, Nesbitt 1972, Gelinas *et al.* 1977, Nisbet *et al.* 1977, Schau 1977, Jahn 1977, Blais 1978). Picrites are similarly composed (Krishnamurthy and Cox 1977). Mikkola (1941) found rocks of comparable composition in the neighbouring Kittilä greenstone province (No. 3 in Table 1).

Amphibolites (tholeiite): The amphibolites form a chemically homogeneous group with the composition of SiO_2-saturated tholeiites (Table 2). Alkali-basaltic rocks are not encountered. The tholeiitic amphibolites of the West Inari schist zone are compositionally identical to the Precambrian amphibolites of Greenland and the

Table 3
Examples for the chemical composition of the hornblende gneisses.

	34 I	54 I	46 III	53 I	Andesite	Dacite
SiO_2	56.97	61.08	67.37	63.95	57.40	65.1
Al_2O_3	18.11	15.10	13.37	14.56	15.60	16.5
TiO_2	1.33	0.51	0.74	0.08	1.25	0.51
Fe_2O_3	2.06	3.71	1.31	2.17	3.48	—
FeO	5.01	4.36	2.85	6.89	5.01	3.68
MnO	0.098	0.135	0.078	0.140	—	—
MgO	1.98	2.69	1.95	1.66	3.38	1.48
CaO	7.36	7.29	6.78	4.57	6.14	4.57
Na_2O	4.48	2.69	4.03	2.72	4.20	4.60
K_2O	1.14	0.68	0.30	1.45	0.43	2.05
P_2O_5	0.023	0.097	0.221	0.290	0.44	0.51
$H_2O + CO_2$	0.98	1.12	0.94	0.85	—	—
	99.54	99.46	99.94	99.33		

34 I, 54 I, 46 III: plagidacitic rocks
53 I: dacitic rock
Andesite: according to Jakeš and White (1972)
Dacite: according to Taylor (1969)

Table 4
Chemical composition of quartz-feldspar gneisses.

	1.	2.	3.	4.
SiO_2	74.47±2.69	74.21±2.10	79.20	75.3
Al_2O_3	13.18±1.45	11.73±1.14	11.10	13.5
TiO_2	0.23±0.16	0.36±0.10	0.23	0.27
Fe_2O_3	1.24±0.92	1.49±0.51	0.52	
FeO	1.28±0.75	1.79±0.59	0.90	1.68
MnO	0.05±0.03	0.08±0.03	n.d.	n.d.
MgO	0.41±0.33	0.14±0.09	0.36	0.25
CaO	2.40±1.49	1.23±0.23	2.04	1.49
Na_2O	4.16±0.99	2.96±0.79	3.40	4.12
K_2O	1.82±1.39	5.30±0.46	1.58	3.39
P_2O_5	0.04±0.03	0.03±0.03	n. d.	0.27

1. Average of the plagidacitic gneisses 8 II, 16 I, 19 II, 26 I, 31 I, 40 I, 43 I, 48 I, 51 I, 52 I, 55 I.
2. Average of the rhyolitic gneisses 24 II, 41 I, 42 I, 42 II.
3. Tholeiitic dacite, according to Jakeš and White (1972).
4. Calc-alkaline rhyolite, according to Taylor (1969).

Canadian shield (Baragar and Goodwin 1969, Rivalenti 1976).

The notably low Al_2O_3 contents and high FeO/MgO ratios seem to be a major characteristic of basalts of Precambrian age (Gunn 1976). The rocks do not correspond to modern continental nor to abyssal tholeiites or tholeiites of the island arcs (Table 2). However, they are similar in composition to basalts of the Tertiary Basic Igneous Complex of Ecuador and Columbia (Goossens *et al.* 1977) (No. 2 in Table 2), and consequently basalts with low Al_2O_3 and high FeO/MgO ratio do occur present-day in continental margins. It is believed that this type of basalt is more abundant, but has been largely overlooked to date.

Hornblende gneisses (andesites—dacites): The hornblende gneisses form a chemically very variable rock group. Factor analysis (Shaw 1972) indicates an igneous parentage. As with the amphibolites, the hornblende gneisses follow a strongly tholeiitic trend in the Alk–F–M–diagram (Fig. 4).

Table 5
Chemical composition of amphibolites and hornblende gneisses (meta-greywackes).

	1.	2.
SiO_2	51.81 ±2.07	51.23 ±1.57
Al_2O_3	13.62 ±0.66	14.38 ±0.91
TiO_2	1.28 ±0.37	1.31 ±0.59
Fe_2O_3	2.66 ±0.99	3.11 ±1.04
FeO	10.16 ±1.86	8.42 ±1.29
MnO	0.244±0.028	0.206±0.026
MgO	5.90 ±1.41	6.99 ±0.94
CaO	10.27 ±0.73	9.97 ±0.80
Na_2O	2.02 ±0.49	2.69 ±0.39
K_2O	0.42 ±0.27	0.60 ±0.15
P_2O_5	0.128±0.07	0.136±0.07

1. Average of amphibolites and hornblende gneisses (meta-greywackes) 1 I, 2 I, 8 I, 9 I, 17 I, 18 I, 36 I.
2. Average of amphibolites (meta-tholeiites) from Table 2.

The rocks have the composition of tholeiitic plagidacites and dacites (Table 3). Metavolcanic rocks of this composition are present in many other Precambrian areas, e.g. the Archean greenstone belts of the Canadian shield (Baragar and Goodwin 1969).

Quartz–feldspar gneisses (plagidacites–rhyolites): The rock compositions of the quartz–feldspar gneisses (Table 4) fall into two groups which differ significantly in their Na_2O/K_2O ratios. The most abundant type has plagidacitic composition (No. 1 in Table 4) with high Na_2O/K_2O ratios and high SiO_2 contents. Less abundant are the rhyolitic types with low Na_2O/K_2O ratio (No. 2 in Table 4). Factor analysis (Shaw 1972) indicates a magmatic origin for both rock types.

Plagidacites of comparable composition are found in the island arc systems (tholeiitic dacites, according to Jakeš and White 1972). Rhyolites are present in the island arc systems (Ewart *et al.* 1973) as well as in the calc-alkaline andesite series (Taylor 1969). They are rare in Precambrian rock sequences (e.g. about 15 per cent in the Archean volcanic belts of the Superior Province, Canada, Goodwin 1977).

Amphibolites and hornblende gneisses (greywackes): The metasediments encountered in the eastern part of the West Inari schist zone are mainly meta-greywackes, now transformed to amphibolites and hornblende gneisses. The rock compositions (Table 5) are very similar to that of basalts, but they are characterized by lower alkali and alumina contents which indicate that the basalts have lost feldspar component during the sedimentary process.

Trace element composition

The trace element compositions of the major rock units of the West Inari schist zone are shown by Table 6 and the Figs. 5 and 6. Four rock groups are distinguishable by their specific trace element contents.

Ultramafic rocks (komatiite or picrite): The high Ni and Cr contents (Table 6) as well as the Ni/Cr ratios are typical of picrites as well as komatiites, but other trace element contents are different. According to Frey (1969), Sun and Nesbitt (1978) and Herrmann *et al.* (1976) peridotitic komatiites have very low REE contents, e.g. Ce in the O.X—X ppm order of magnitude. Both the REE and the other trace elements of the rocks studied here exceed the values expected for peridotitic komatiites, but are closer to those encountered in picrites (Krishnamurthy and Cox 1977, Alexander and Gibson 1977).

Amphibolites (tholeiite): It is shown in Table 6 that the rocks of this group have trace element compositions intermediate between continental and oceanic tholeiites (Wedepohl 1975). The REE are equally concentrated by factors 10—40 compared with chondrites. The La_N/Yb_N ratios are 0.9—2 (Hörmann and Schock 1980).

Tholeiitic rocks from the Archean greenstone belts, e.g. of the Canadian shield (Baragar and Goodwin 1969, Shaw *et al.* 1976) have similar trace element contents. There also exists a close correspondence with the tholeiitic rocks of the Tertiary Basic Igneous Complex of Ecuador and Colombia (Goossens *et al.* 1977).

Hornblende gneisses (andesites—dacites) and *quartz–feldspar gneisses* (plagidacites—rhyolites): The rocks of this group, though variable in

Table 6
Average trace element content (in ppm) of rocks of the West Inari schist zone.

	1.	2.	3.	4.	5.	6.
Li	5.4	8.8	6.0	6.2	7.6	5.6
Rb	2.8	20	41	36	151	15
Ba	91	247	429	460	1 355	263
Sr	85	115	159	193	10	84
Ni	1 771	90	5.2	5.7	2.0	22
Cr	2 654	167	6.1	8.6	3.3	30
V	115	190	68	12	2.5	217
La	14	14	15	15	89	13
Ce	52	44	39	32	187	48
Y	9.6	17	29	27	136	24
Th	2.9	4.9	7.3	5.4	14.1	5.8
U	0.5	0.5	0.5	0.5	0.9	0.6

1. 5 ultramafic rocks (picrite).
2. 10 amphibolites (tholeiite).
3. 5 hornblende gneisses (andesite-dacite).
4. 9 quartz-feldspar gneisses (plagidacite).
5. 5 quartz-feldspar gneisses (rhyolite).
6. 7 amphibolites (greywacke).

The standard deviation of the values ranges from 10—30 per cent.

major element composition, have very similar trace element contents (Tab. 6).

The contents of the large cations Rb, Sr, Ba increase regularly with increasing K_2O content (Tab. 6, Fig. 5). The Rb contents are low, except in the rhyolites. Removal of Rb from the gneisses during progressive metamorphism and an increase of the K/Rb ratio was envisaged by Heier (1960) and Lambert and Heier (1968). On the other hand, Lewis and Spooner (1973) found that rocks of Precambrian granulite terrains often have K/Rb ratios similar to modern volcanic rocks. The K/Rb ratios of the gneisses, the most abundant values of which are 200—300 (ranging from 100—600), are similar to those of more recent crustal rocks, e.g. the Cenozoic volcanic rocks of the Andes of Ecuador (Hörmann and Pichler 1980). Therefore it is presumed that Rb actually was not removed from the rocks and that the low Rb contents reflect the andesitic and dacitic source rocks.

The abundances of the highly charged cations U and Th increase irregularly by a factor of 2 from the andesitic to the rhyolitic gneisses (Fig. 5). The U contents are about half as large as in the Cenozoic volcanic rocks of the Andes whereas the Th contents are approximately the same (Hörmann and Pichler 1980).

Consequently, the Th/U ratios are twice that of the volcanic rocks of the Andes, indicating that either 50 percent of the U was removed during metamorphism or that the source rocks had low U contents. It is suggested that the latter explanation is most likely. According to Heier (1962) and Heier and Adams (1965) mobilization of U and Th during progressive metamorphism occurs mainly in the granulite facies. Archean intrusive tonalitic and granodioritic rocks have higher U and Th contents (e.g. Rye and Roy 1978) than the rocks studied here.

Hornblende gneisses and plagidacitic quartz–feldspar gneisses are similar with respect to most trace element contents (Table 6) but differ considerably in their REE distribution patterns. In the hornblende gneisses as in the amphibolites, the REE are concentrated by factors 10—40 compared to chondrites. The La_N/Yb_N ratios are 1—3 (Hörmann and Schock 1980) and some samples have negative Eu anomalies.

The plagidacitic quartz–feldspar gneisses have highly fractionated REE spectra. The LREE abundances are similar to those of the hornblende gneisses, the HREE much lower. The La_N/Yb_N ratios are consequently 10—25 (Hörmann and Schock 1980). Eu anomalies, if present, are positive.

Thus, the REE distribution in the hornblende gneisses can be compared best with that in island arc andesites (Ewart *et al.* 1973), whereas that in the plagidacitic quartz–feldspar gneisses with that in calc-alkaline volcanic rocks (Taylor 1969, Dostal *et al.* 1977). The strong enrichment of LREE compared with HREE is a characteristic property of the andesitic and dacitic rocks of the old greenstone belts (e.g. Condie and Baragar 1974).

The contents of the ferromagnesian elements Ni, Cr, V (Table 6) are comparable to those in andesites and decrease with decreasing MgO contents (Fig. 6). The correlation of Ni and Cr

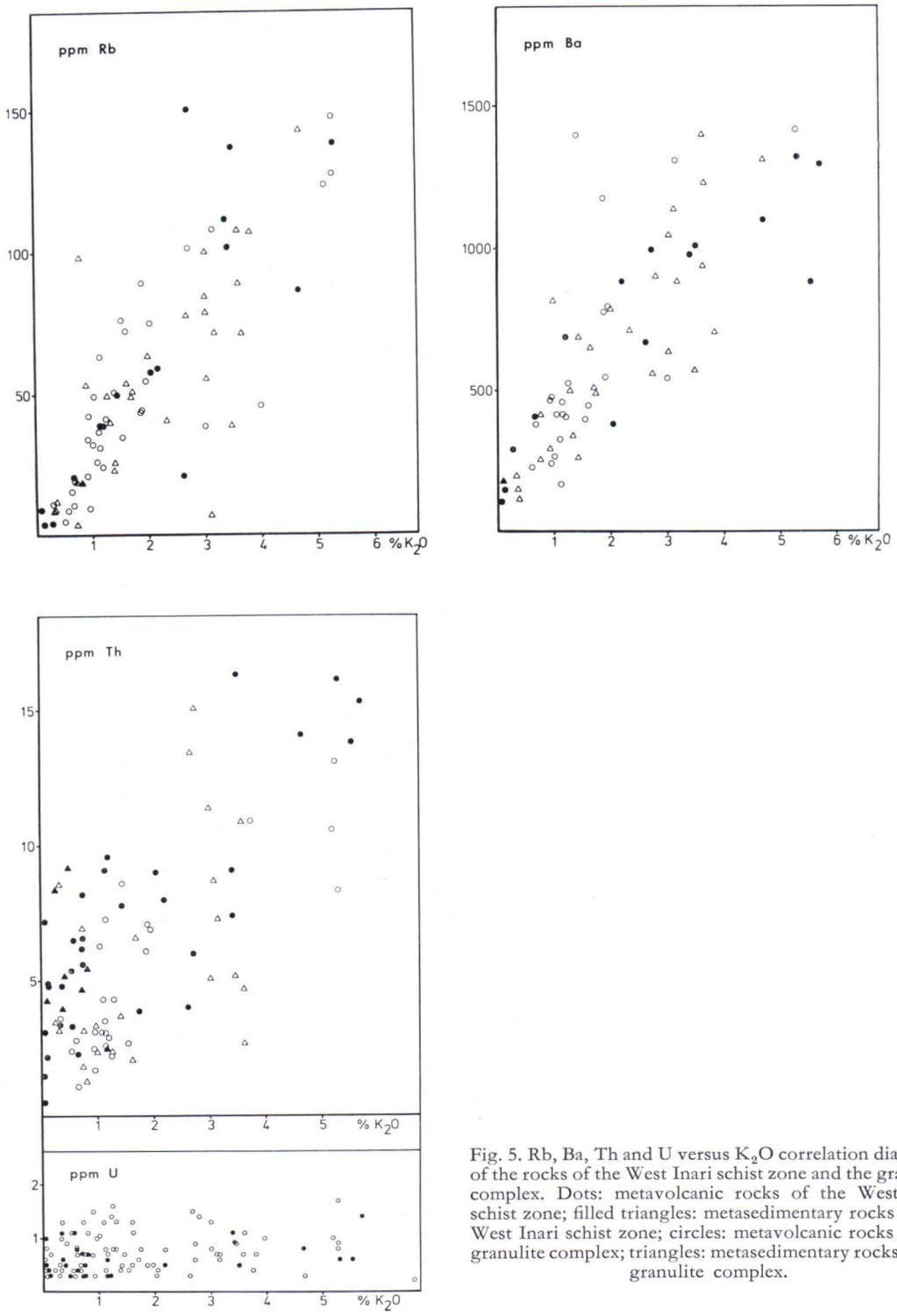

Fig. 5. Rb, Ba, Th and U versus K_2O correlation diagrams of the rocks of the West Inari schist zone and the granulite complex. Dots: metavolcanic rocks of the West Inari schist zone; filled triangles: metasedimentary rocks of the West Inari schist zone; circles: metavolcanic rocks of the granulite complex; triangles: metasedimentary rocks of the granulite complex.

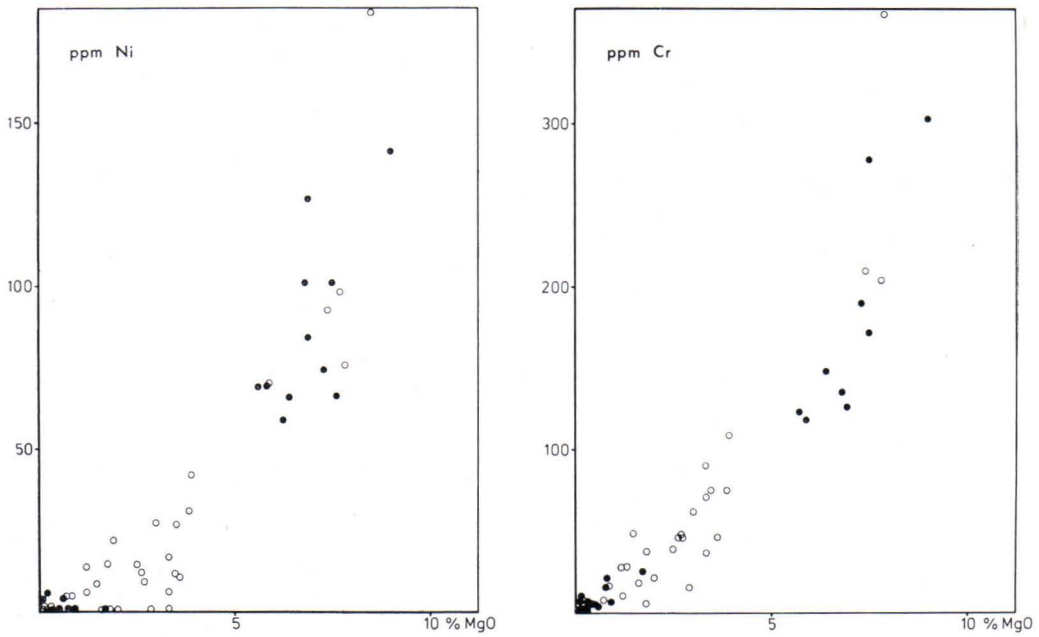

Fig. 6. Ni and Cr versus MgO correlation diagrams of the rocks of the West Inari schist zone and the granulite complex. Dots: metavolcanic rocks of the West Inari schist zone; circles: metavolcanic rocks of the granulite complex.

with MgO provides a strong support for the magmatic origin of the rocks.

Amphibolites and hornblende gneisses (greywackes): The rocks of this group have trace element contents very similar to those of the basaltic amphibolites. However, the Ni and Cr contents are distinctly lower, and the Ni/MgO and Cr/MgO correlations which are so typical for the amphibolites of basaltic origin are absent.

Granulite complex

Major element composition

Basic hypersthene gneisses (high-alumina basalt): The gneisses of this group are abundant mainly in the southwestern part of the complex and they have the composition of quartz-normative high-alumina tholeiites. Such basalts occur as the most primitive members in the Andean-type, calc-alkaline volcanic rock suites of the continental margins (Taylor 1969), and also in the Archean greenstone belts (Baragar and Goodwin 1969). The main chemical characteristics are high Al_2O_3, K_2O and SiO_2 contents, FeO/ MgO ratios of about 1, and low TiO_2 contents (Table 7).

Table 7

Chemical composition of basic hypersthene gneisses.

	1.	2.	3.
SiO_2	52.56 ±0.71	50.91	53.52
Al_2O_3	19.46 ±0.76	19.54	18.18
TiO_2	0.60 ±0.15	1.08	1.19
Fe_2O_3	1.56 ±0.77		
FeO	6.80 ±0.69	9.02	9.06
MnO	0.218±0.118	—	—
MgO	5.81 ±0.69	4.32	4.82
CaO	8.10 ±0.96	8.87	7.87
Na_2O	2.96 ±0.48	3.80	4.18
K_2O	0.61 ±0.07	1.04	1.12
P_2O_5	0.08 ±0.02	—	—

1. Average of the samples 97 I, 97 II, 116 III, 141 I.
2. and 3. Calc-alkaline high-alumina basalts from the Central Andes, according to Dostal *et al.* (1977).

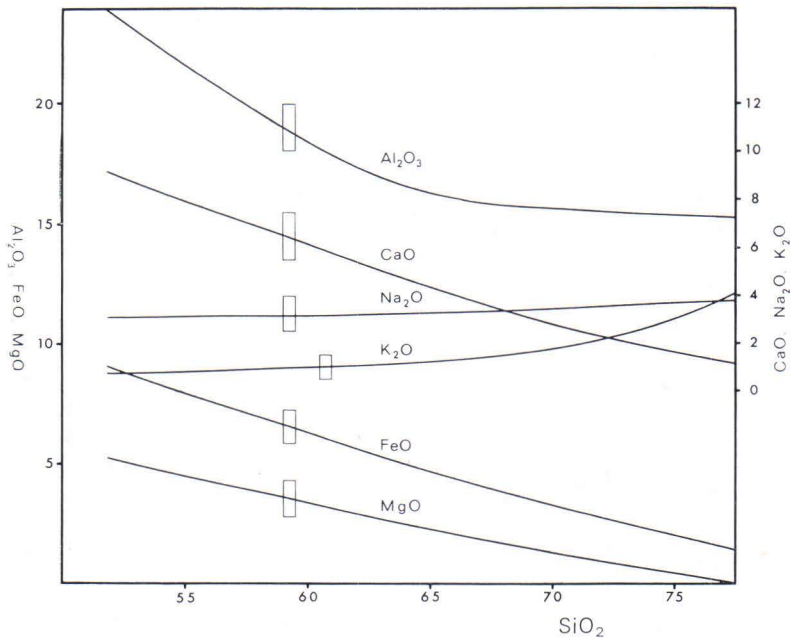

Fig. 7. Harker diagram of the intermediate and acid gneisses of the granulite complex. Bars denote maximum deviation from the trend lines.

Intermediate hypersthene gneiss, hornblende–pyroxene gneisses and garnet–biotite gneisses (andesites—dacites): In chemical composition, the gneisses belonging to this group are highly variable (Table 8). However, the compositions are closely related to each other and vary regularly with the SiO_2 content as shown by the Harker diagram of Fig. 7.

In contrast to the hornblende gneisses of the West Inari schist zone, the rocks are calc-alkaline in terms of the Alk–F–M diagram (Fig. 4). All gneisses have high Al_2O_3 contents and Na_2O ist fairly constant, at least in the intermediate and acid members of the sequence. Rocks of similar composition occur in the calc-alkaline andesite—dacite—rhyolite series of the continental margins (Taylor 1969, Jakeš and White 1972) and also in the old greenstone belts (Baragar and Goodwin 1969).

The calc-alkaline volcanic rocks of the Central Andes (Dostal *et al.* 1977) are very similar, not only in respect to the major elements but also to the trace element abundances and REE distribution patterns (see below).

Table 8

Chemical composition of intermediate hypersthene gneisses and garnet-biotite gneisses.

	83 I	72 I	128 I	J 7 I
SiO_2	61.27	59.23	64.14	64.96
Al_2O_3	17.92	19.29	16.89	16.32
TiO_2	0.93	0.39	0.93	0.99
Fe_2O_3	2.50	0.64	2.06	0.93
FeO	3.76	4.90	4.24	3.45
MnO	0.066	0.078	0.076	0.049
MgO	3.32	3.92	2.91	2.66
CaO	5.97	5.95	3.37	3.45
Na_2O	3.56	3.36	3.03	3.13
K_2O	0.64	0.94	1.25	1.89
P_2O_5	0.133	0.129	0.012	0.053
$H_2O + CO_2$	0.47	0.62	1.17	1.46
	100.54	99.45	100.09	99.34

83 I. Hypersthene-plagioclase gneiss
72 I. Garnet-hypersthene-plagioclase gneiss
128 I, J 7 I. Garnet-biotite gneisses

Garnet gneisses (rhyodacites, rhyolites): The rocks comprise two groups which both have very high SiO_2 contents but different Na_2O/K_2O ratios (Table 9). The Harker diagram of Fig. 7 shows that they are chemically related to the andesitic hypersthene gneisses and dacitic garnet-

Table 9
Chemical composition of garnet gneisses.

	1.		2.
	a	b	
SiO_2	75.50	77.14	74.51 ±2.97
Al_2O_3	16.02	12.29	13.46 ±1.42
TiO_2	0.03	0.10	0.14 ±0.13
Fe_2O_3	0.23	0.89	0.51 ±0.40
FeO	0.02	0.46	0.86 ±0.30
MnO	0.005	0.030	0.023±0.015
MgO	0.08	0.10	0.41 ±0.34
CaO	1.74	1.13	0.96 ±0.29
Na_2O	3.16	3.40	2.50 ±0.43
K_2O	3.00	3.98	5.96 ±1.04
P_2O_5	0.082	0.010	0.070±0.061
$H_2O + CO_2$	0.56	0.70	0.61 ±0.18

1. Rhyodacitic samples 154 I (a), 130 I (b)
2. Average of the rhyolitic samples 46 I, 47 I, 76 I, 143 I, 148 I.

biotite gneisses of the granulite complex, and factor analysis (Shaw 1972) demonstrates also an igneous parentage. The rocks possibly represent the highest differentiated members of the calc-alkaline rock series of the granulite complex.

However, rocks of such compositions are not commonly encountered in the calc-alkaline orogenic series of the continental margins, e.g. the andesite and rhyolite formations of the Central Andes (Pichler and Zeil 1972, Kussmaul *et al.* 1977). Nevertheless, obsidians and pitchstones which occur less abundantly in the calc-alkaline volcanic rock sequences have compositions similar to the garnet gneisses (e.g. Hörmann and Pichler 1980). The fact that rocks of this composition are present in such enormous quantities is unusual. Goodwin (1977) estimated the abundance of similar rocks in the old greenstone belts of the Canadian shield as about 15 percent.

Similar rocks are also found in the West Inari schist zone, where they occur as quartz–feldspar gneisses.

Hypersthene gneisses (greywackes) and *garnet–biotite gneisses* (subgreywackes), *garnet–cordierite–sillimanite gneisses* (subgreywackes), *garnet gneisses* (arkoses and quartzites): The metasedimentary rocks were identified either by the alk/si diagram (Bilål 1978) or by factor analysis (Shaw 1972). About 50 percent of the samples studied discriminated as metasediments. They are characterized by lower sodium and calcium contents, higher SiO_2 contents and higher K_2O/Na_2O ratios than those of comparable rocks of magmatic source. These trends are incompatible with an anatectic origin of the rocks. The cordierite-bearing gneisses often contain accessory graphite, which might give additional evidence for their sedimentary origin (Eskola 1952).

Table 10
Chemical composition of metasedimentary rocks.

	1.	2.	3.	4.
SiO_2	56.10	60.40 ±2.76	65.11 ±3.90	66.68 ±3.05
Al_2O_3	19.44	16.27 ±1.22	17.13 ±1.53	17.46 ±2.16
TiO_2	0.79	0.67 ±0.22	0.73 ±0.16	0.35 ±0.24
Fe_2O_3	1.19	2.03 ±0.23	1.62 ±0.64	1.09 ±0.86
FeO	5.83	5.22 ±0.69	4.88 ±0.75	4.62 ±2.27
MnO	0.117	0.124±0.008	0.088±0.031	0.064±0.056
MgO	4.85	4.32 ±1.09	2.81 ±0.52	3.15 ±0.72
CaO	8.32	5.51 ±0.58	2.07 ±1.86	0.97 ±0.53
Na_2O	1.43	2.57 ±1.00	2.03 ±0.94	1.36 ±0.38
K_2O	0.93	2.05 ±1.36	2.48 ±1.52	3.08 ±0.35
P_2O_5	0.078	0.146±0.077	0.058±0.047	0.058±0.027
$H_2O + CO_2$	0.83	0.31 ±0.06	0.76 ±0.38	1.04 ±0.44
	99.91			

1. Basic hypersthene gneiss 59 I (greywacke).
2. Average of the intermediate hypersthene gneisses (greywackes) 93 II, J 1 I, J 12 I.
3. Average of garnet-biotite gneisses (subgreywackes) 59 II, 62 I, 65 I, 91 I, 93 I, 128 I.
4. Average of garnet-cordierite-sillimanite gneisses (subgreywackes) 89 I, 158 I, 158 II, 161 I.

Table 11
Chemical composition of metasedimentary rocks.

	1.	2.
SiO_2	76.21 ±2.93	79.35 ±3.06
Al_2O_3	12.07 ±1.79	10.27 ±1.36
TiO_2	0.39 ±0.10	0.30 ±0.10
Fe_2O_3	1.01 ±0.39	0.87 ±0.38
FeO	2.58 ±1.27	1.80 ±1.08
MnO	0.043±0.015	0.051±0.017
MgO	1.25 ±0.42	1.12 ±0.56
CaO	1.25 ±0.46	2.85 ±1.60
Na_2O	1.95 ±0.67	1.91 ±0.22
K_2O	2.37 ±0.75	0.52 ±0.27
P_2O_5	0.059±0.016	0.052±0.038
$H_2O + CO_2$	0.46 ±0.16	0.97 ±0.48

1. Average of garnet gneisses (arkoses and quartzites) 70 II, 71 I, 150 I, 156 I, 169 I, J 5 II.
2. Average of garnet gneisses (arkoses and quartzites) 63 I, 65 III, 69 II, J 3 I.

The basic and intermediate greywackes and subgreywackes are chemically related to the andesitic rocks of the granulite complex, the arkoses and quarzites to the dacitic and rhyolitic.

The compositions of the main metasedimentary rock types are shown in Tables 10 and 11.

Trace element composition

Basic hypersthene gneisses (high-alumina basalt): The gneisses of this group have trace element compositions similar to that of calc-alkaline basalts of the volcanic orogenic rock series. The main characteristics are high Ba, Sr and REE abundances and low Ni and Cr contents (Table 12). Compared to the average high-alumina basalt of Taylor (1969) and Jakeš and White (1972), the contents of the large-ion-lithophile elements (Ba, Sr, La, Ce, Th, U) are higher by a factor of about 2. This is also a property of the basalts and basaltic andesites of the Central Andes (Dostal *et al.* 1977). The REE distribution patterns are characterized by moderate fractionation of the HREE and stronger enrichment of the LREE (Hörmann and Schock 1980). In their REE spectra the basic hypersthene gneisses are closely related with the other gneisses of the granulite complex (see below) but differ from the tholeiitic amphibolites of the West Inari schist zone.

Intermediate hypersthene gneisses, hornblende–pyroxene gneisses, garnet–biotite gneisses (andesites—dacites) and *garnet gneisses* (dacites—rhyolites): The gneisses have the trace element contents of the Andean-type calc-alkaline andesite—dacite—rhyolite series (Taylor 1969, Jakeš and White 1972, Dostal *et al.* 1977, Hörmann and Pichler 1980). The Rb and Ba contents of the gneisses increase with increasing K_2O content (Fig. 5). The K/Rb ratios, the most abundant values of which are 200—300 (ranging from 100—600), are similar to that of calc-alkaline volcanic rocks (Hörmann and Pichler 1980). Therefore, it is assumed that the Rb abundances reflect the low Rb contents of the source rocks rather than indicating significant removal of Rb by fluids during granulite facies metamorphism as suggested by Heier (1960) and Lambert and Heier (1968) for other granulite terrains.

All rocks of this group have similar REE distribution patterns. The HREE are concentrated by factors 5—30 and the LREE by factors 50—300 compared with chondrites. The La_N/Yb_N ratios are 10—30 and Eu anomalies, if present, are positive (Hörmann and Schock 1980). This strong fractionation of the REE is commonly found in Andean-type andesites (Taylor 1969, Dostal *et al.* 1977) and also in volcanic rocks of the old greenstone belts (e.g. Condie and Baragar 1974).

The contents of the ferromagnesian elements Ni, Cr, V are low and correlate with the MgO contents (Fig. 6).

Despite of these similarities with the calc-alkaline volcanic rock series, there are also some important differences. Th is only weakly correlated with K_2O, and there is no correlation between U and K_2O (Fig. 5). It is presumed that U, and to a lesser extent also Th, were partially removed from the gneisses during the metamorphic process. This U and Th depletion

Table 12
Average trace element content (in ppm) of rocks of the granulite complex.

	1.	2.	3.	4.	5.	6.	7.	8.
Li	9.9	9.5	4.1	4.8	9.3	9.5	7.6	4.8
Rb	9.2	50	42	134	49	64	66	42
Ba	263	517	540	870	616	806	846	518
Sr	347	381	173	139	266	261	218	141
Ni	15	17	1	3	34	28	49	12
Cr	47	50	3	8	103	101	70	61
V	116	79	28	15	110	86	73	41
La	17	17	17	25	25	18	22	21
Ce	44	47	39	30	37	47	34	53
Y	25	12	10	56	43	20	34	23
Th	2.7	4.2	1.7	7.9	5.0	5.2	6.4	6.8
U	1.1	0.8	1.2	1.1	0.8	0.7	1.4	0.8

1. 5 hypersthene gneisses (high alumina basalt).
2. 20 intermediate hypersthene gneisses and garnet-biotite gneisses (andesite-dacite).
3. 2 garnet gneisses (rhyodacite).
4. 5 garnet gneisses (rhyolite).
5. 5 basic hypersthene gneisses (greywacke).
6. 14 intermediate hypersthene gneisses and garnet-biotite gneisses (greywacke).
7. 5 garnet-cordierite-sillimanite gneisses (subgreywacke).
8. 15 garnet gneisses (arkoses and quartzites).

The standard deviation of the values ranges from 10—30 per cent.

in high-grade gneisses was discussed in detail by Heier (1962) and Heier and Adams (1964) and is observed in many granulite terrains.

Hypersthene gneisses and garnet–biotite gneisses (greywackes), *garnet–cordierite–sillimanite gneisses* (subgreywackes), *garnet gneisses* (arkoses, quartzites): The results of the trace element studies (Table 12) indicate that rocks of sedimentary and magmatic origin of the granulite complex cannot be distinguished by means of their trace element contents. The REE distribution patterns of both rock groups are also similar (Hörmann and Schock 1980).

Differences do occur with respect to the trace element-major element relationships. The correlations of Rb and Ba with K_2O is less pronounced in the metasedimentary gneisses (Fig. 5), and there is no correlation of Ni and Cr with MgO in these rocks.

METAMORPHIC ZONES AND EPISODES

The crystalline rocks of the area investigated have been metamorphosed under different conditions: Whereas the rocks of the West Inari schist zone and the granite gneiss complex correspond to amphibolite facies metamorphism, those of the granulite complex have to be assigned to granulite facies. The transition of the two facies occurs within the two marginal zones of the granulite complex.

The following discussion of the mineralogical development in the rocks of the profile pursues two objectives:

(a) to establish regional changes of metamorphic conditions within the individual rock units

b) to find out the changes in mineral assemblages with time and the relationship between crystallization and deformation.

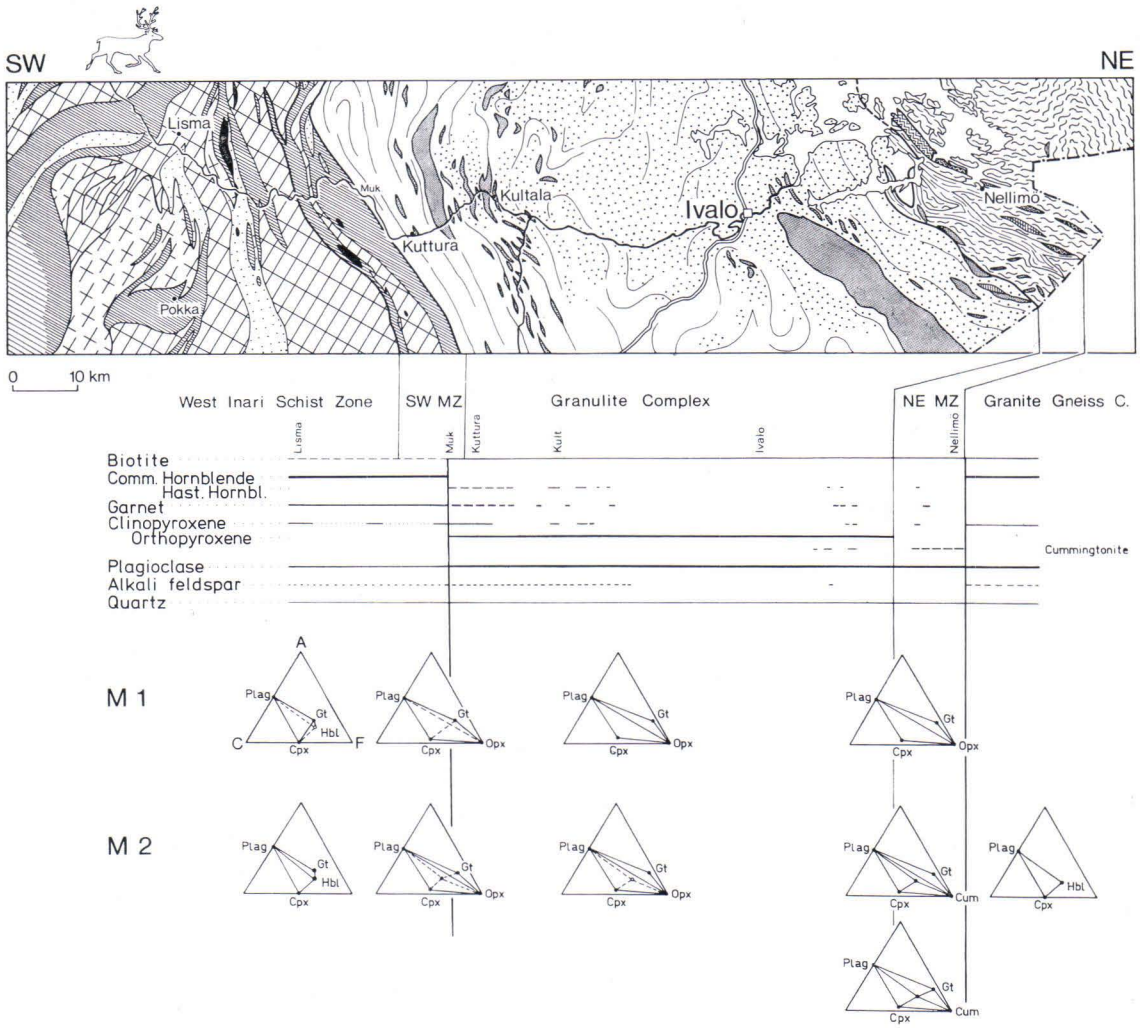

Fig. 8. Mineral content and its regional variation in hornblende–pyroxene rocks along the Ivalojoki—Inarijärvi profile. Sample localities (Fig. 2) have been projected in the direction of the regional strike. Rock signatures in the geological map are explained in Fig. 1. Mineral assemblages of the two metamorphic stages M1 and M2 are presented in ACF projections. The lowermost ACF diagram (northeastern marginal zone) is assigned to a late stage of M2.

For this purpose we will treat the hornblende- and pyroxene-bearing rocks on the one hand and the quartz–feldspar gneisses and garnet gneisses on the other separately. The complete mineral assemblages of the samples are given in the Appendix.

In the *hornblende–pyroxene rocks* four zones characterized by their different mineralogy can be distinguished (Fig. 8):

1) In the West Inari schist zone and the main part of the southwestern marginal zone these rocks typically contain common hornblende, plagioclase (An 30—50), garnet and clinopyroxene. In a single occurrence 15 km south of Repojoki (sample 23 IV) staurolite has been found in a fine-grained garnet-bearing amphibolite. Rare opaques are ilmenite, magnetite, and sulfides.

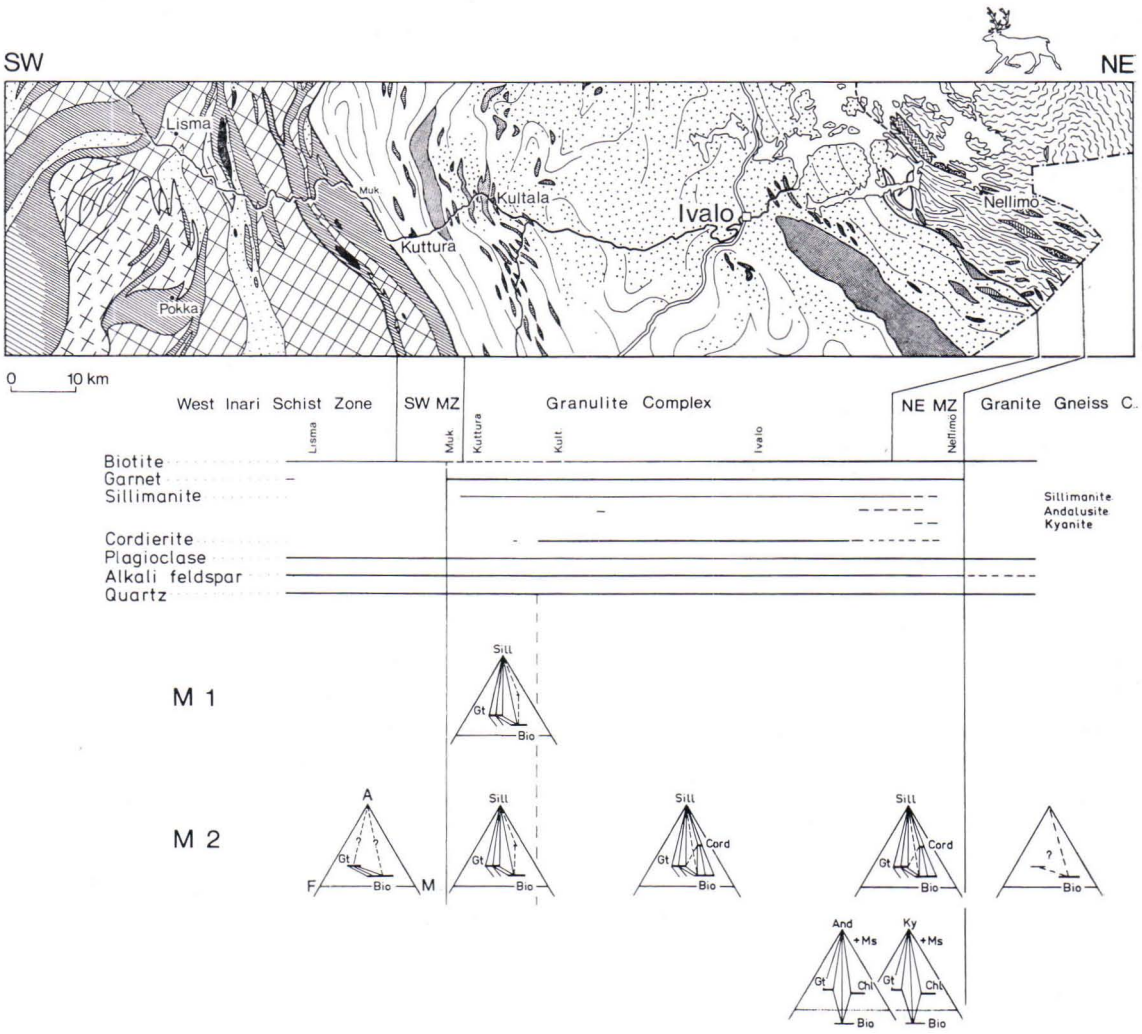

Fig. 9. Mineral content and its regional variation in quartz–feldspar gneisses and garnet gneisses along the Ivalojoki—Inarijärvi profile. Sample localities (Fig. 2) have been projected in the direction of the regional strike. Rock signatures in the geological map are explained in Fig. 1. Mineral assemblages of the two metamorphic stages M1 and M2 are presented in AFM projections from quartz and K-feldspar. The two lowermost AFM diagrams (northeastern marginal zone) are muscovite projections referring to a late stage of M2.

2) Within the granulite complex these rocks contain hypersthene, plagioclase (An 40—100) and biotite, in addition to occasional hastingsitic hornblende, clinopyroxene and garnet. Widespread ore minerals are complex ilmenite–hematite intergrowths, magnetite, pyrite and pyrrhotite.

3) In the northeastern part of the granulite complex and the northeastern marginal zone retrograde formation of cummingtonite and anthophyllite is observed.

4) Within the granite gneiss complex the basic rocks typically contain hornblende, plagioclase (An 30—50) and sometimes clinopyroxene. Opaques are ilmenite, pyrrhotite, and pyrite.

The southwestern marginal zone adjacent to the granulite complex (at Mukkapalo) contains both amphibolites and hornblende gneisses

similar to those of the West Inari schist zone, as well as hypersthene-bearing hornblende–clinopyroxene gneisses, indicating a gradual transition between the amphibolite facies and granulite facies rocks. In the northeastern marginal zone the hypersthene-bearing rocks are replaced by amphibolites again suggesting that the conditions of the amphibolite facies are attained again at the transition to the granite gneiss complex.

Similarly, a metamorphic sequence can be established from the mineralogical development in the *quartz–feldspar gneisses* and *garnet gneisses* of the profile (Fig. 9):

1) The gneisses of the West Inari schist zone and the main part of the southwestern marginal zone exhibit the simple mineralogy plagioclase (An 02—25), microcline, quartz and biotite besides occasional garnet. Sulfides are typically absent, ilmenite and magnetite are rare.

2) Gneisses in the southwestern part of the granulite complex contain garnet, biotite, plagioclase (An 25—40), orthoclase, quartz and, as a new phase, sillimanite. Rare opaques are rutile, ilmenite and pyrite. The fabric is characterized by platy quartz.

3) In the central and northeastern part of the granulite complex anatectic gneisses with garnet, cordierite, biotite, plagioclase (An 20—40), orthoclase, quartz, sillimanite, and rare hercynite are exposed. The ore mineral assemblage typically contains appreciable amounts of pyrrhotite besides pyrite, ilmenite and rutile. Graphite may be present. Approaching the granite gneiss complex in the northeast the modal amount of biotite increases and cordierite disappears. Secondary andalusite has been found in the rocks of the northeastern part of the granulite complex, whereas in the northeastern marginal zone late kyanite occurs in some of the garnet gneisses besides sillimanite and andalusite.

4) The quartz–feldspar gneisses of the granite gneiss complex are characterized by the simple mineralogy plagioclase (An 15—25), quartz, biotite besides some microcline. Hornblende-bearing varieties are widespread.

Regional and temporal development of mineral assemblages

A polyphase metamorphism of the rocks is evident from the textural relationships of the minerals. In the granulite complex and the West Inari schist zone at least two high-grade stages of crystallization can be distinguished; these will be named M1 and M2 in the following.

The early stage M1 was largely synkinematic, leading to the formation of intensely folded and sheared rocks. The deformation might be related to the overthrusting of the granulite complex onto the West Inari schist zone. The platy quartz textures of the granulitic garnet gneisses were formed during this episode.

The later phase of crystallization, M2, on the other hand, was mainly postkinematic, i.e. it took place under essentially static conditions. The rocks recrystallized and coarsened and the regional anatexis, which is particularly distinct in the central and northeastern parts of the granulite complex, led to deorientation of the former granulitic fabric thus producing rather massive rocks. In the granite gneiss complex only a high-grade postkinematic stage of crystallization can be recognized which might be related to the M2 stage in the granulite complex.

In the following only the development of the typical assemblages in space and time will be discussed. Mineral compositions and their changes mentioned here will be described in more detail in the section on mineral chemistry.

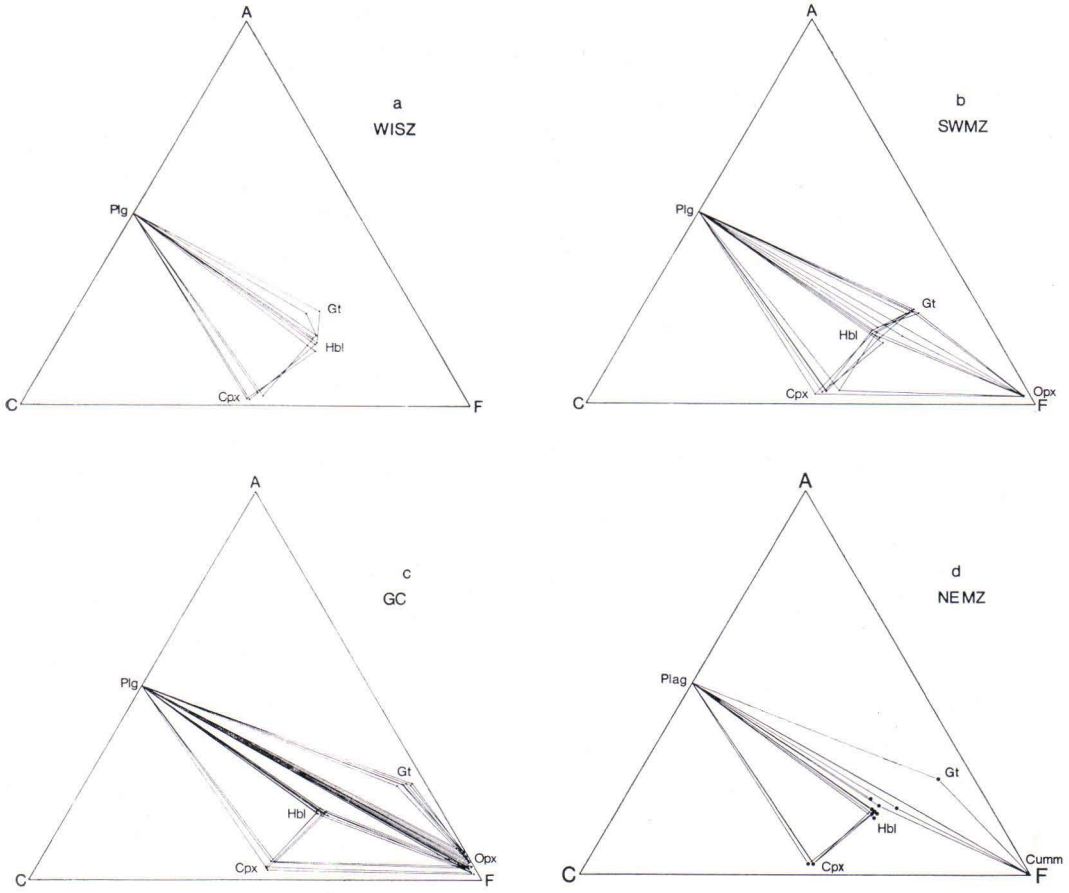

Fig. 10 a-d. ACF projections of minerals coexisting during M2 in a) amphibolites of the West Inari schist zone, b) pyroxene-hornblende-bearing rocks of the southwestern marginal zone, c) hypersthene-plagioclase rocks of the granulite complex. Further details on the orthopyroxene chemistry are given in Fig. 21. Due to either Mg/Fe fractionation or variable activity of water the phases plagioclase, hornblende, clinopyroxene and orthopyroxene form a four-phase volume. d) Amphibolites of the northeastern marginal zone.

Hornblende- and pyroxene-bearing rocks

In the *West Inari schist zone* metabasites typically formed the assemblage hornblende + garnet + clinopyroxene + plagioclase + quartz ± microcline during M1 (cf. Fig. 8). The mineral pair garnet–clinopyroxene was no longer compatible during M2: The idioblastic garnet grains are now separated from the clinopyroxene-bearing matrix by rims of hornblende + plagioclase (Fig. 14) indicating a reaction

clinopyroxene + garnet + H_2O ⇆ hornblende + plagioclase (An-component).

Such a reaction will proceed to the right on increase of water pressure or on decrease of temperature. M2 thus corresponds either to higher water pressures than M1 or to lower temperatures. As a consequence of the newly established tie-line hornblende-plagioclase there appear the frequently encountered assemblages hornblende + plagioclase + garnet + quartz, hornblende + plagioclase + clinopyroxene ± quartz and hornblende + plagioclase ± quartz

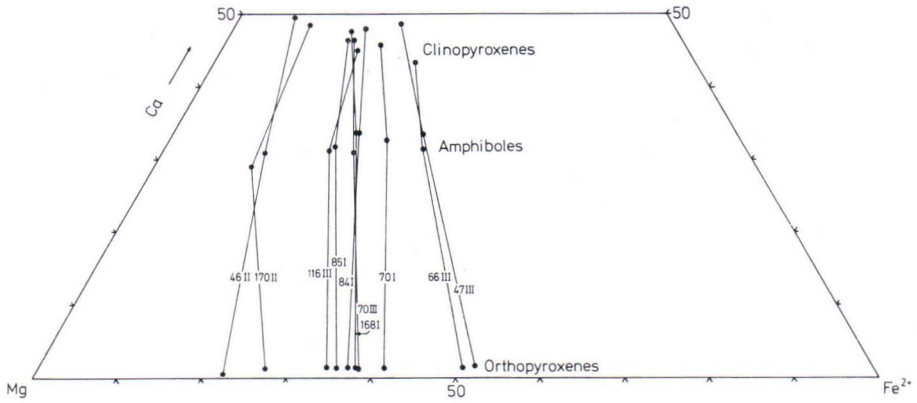

Fig. 11. Projection of orthopyroxene, clinopyroxene and hornblende analyses into the system $MgSiO_3$–$FeSiO_3$–$CaSiO_3$. For discussion see text.

(Fig. 8). In a single thin section all three newly formed assemblages can be observed to occur in a mosaic-type equilibrium. The compatibility relations during M2 constructed from the mineral compositions given in the following section are summarized in Fig. 10 a.

In rocks containing calcite-bearing layers garnet + clinopyroxene + hornblende + plagioclase + quartz exhibit grain contacts. It can be assumed that by the presence of CO_2 in the gas phase the water fugacity was lowered, thus stabilizing the assemblage garnet + clinopyroxene even during M2.

In the *southwestern marginal zone* M1 is similarly characterized by the assemblage hornblende + garnet + clinopyroxene + plagioclase. During M2 complex assemblages result by the appearance of orthopyroxene, a shift of garnet composition towards almandine–pyrope as well as recrystallization and growth of hornblende. Nevertheless, the garnet-clinopyroxene tie-line remained stable in some rocks even during M2 which here might be due to the generally higher X_{CO_2} of the intergranular fluid (see below). The crossing tie-lines shown in Fig. 10 b are probably due to Mg/Fe^{2+} fractionation between coexisting phases ($X^{Fe}_{Gt} > X^{Fe}_{Hbl} > X^{Fe}_{Opx} > X^{Fe}_{Cpx}$).

In the *granulite complex* metabasic and intermediate rocks crystallized during M1 into the assemblages hypersthene + plagioclase + biotite + quartz, hypersthene + clinopyroxene + plagioclase + biotite + quartz, and hypersthene + garnet + plagioclase + biotite + quartz ± orthoclase (Fig. 8). In some layers of the rock sequence a hastingsitic hornblende grew postkinematically during M2. Using the mineral compositions, the following reaction can be formulated

clinopyroxene + orthopyroxene + biotite + plagioclase + hemoilmenite + H_2O ⇆ hornblende + quartz

Formation of hornblende will thus be favoured either by an increase in water fugacity or by a deficit in silica. The role of biotite and hemoilmenite in this reaction is only minor, because the hornblende plots close to the tie-line between orthopyroxene and clinopyroxene in a Ca–Mg–Fe projection (Fig. 11).

The following assemblages with hornblende are typical of M2 in these rocks (Figs. 8 and 10c): hypersthene + plagioclase + biotite + quartz ± orthoclase, hypersthene + clinopyroxene + plagioclase + biotite.

The paragenesis orthopyroxene + plagioclase + garnet remained stable during M2 but the compositions of the minerals reequilibrated. The garnets are richer in almandine + pyrope component compared to those from the southwestern marginal zone.

In the *northeastern part of the granulite complex* and the *northeastern marginal zone* the hypersthene-bearing rocks suffered greater changes leading to a complete destruction of M1 assemblages in the northeastern marginal zone. The assemblages during M2 are plagioclase + hornblende + cummingtonite + biotite + quartz, plagioclase + hornblende + anthophyllite + biotite + quartz, plagioclase + garnet + cummingtonite + biotite + quartz and plagioclase + hornblende + clinopyroxene + biotite + quartz (Figs. 8 and 10d). During a late episode at lower grades than M2 orthopyroxene was first corroded by cummingtonite or anthophyllite which were later largely or completely replaced by common hornblende. During this stage the typical parageneses are hornblende + plagioclase + biotite + quartz ± K-feldspar, hornblende + clinopyroxene + plagioclase ± quartz ± biotite, and hornblende + garnet + plagioclase + biotite + quartz (Fig. 8).

In the *granite gneiss complex* the metabasites exhibit only two postkinematic assemblages: hornblende + biotite + plagioclase + quartz ± microcline and hornblende + clinopyroxene + plagioclase ± quartz, which may be assigned to M2 (Fig. 8).

Quartz-feldspar gneisses and garnet gneisses

The quartz-feldspar rocks of the *West Inari schist zone* and of the main part of the *southwestern marginal zone* do not exhibit evidence of polyphase metamorphism. The assemblages recrystallized postkinematically and, therefore, may be related to M2. These are plagioclase + microcline + quartz + biotite and plagioclase + microcline + quartz + biotite + garnet (Fig. 9).

No aluminium silicates have been encountered, probably due to chemical restrictions. However, Eskola (1952) mentions kyanite- and staurolite-bearing schists from the southeastern part of the West Inari schist zone near Korvatunturi.

In the garnet gneisses of the *granulite complex* both textures and assemblages point towards a polyphase crystallization. The early synkinematic stage M1 is still largely preserved in the southwestern part where banded, intensely sheared granulitic garnet gneisses with platy quartz texture are typical. Additional textural features attributed to M1 are the preferred orientation of sillimanite and biotite parallel to the schistosity. Nevertheless, some recrystallization under static conditions (M2) is indicated by the polygonal granoblastic texture of the feldspars and original platy quartz growing with amoeboid grain boundaries. In these rocks M2 did not lead to a change in mineral assemblages, although it probably affected the composition of the coexisting minerals. The assemblages observed are (Figs. 9, 12a):

garnet + biotite + sillimanite + orthoclase + plagioclase + quartz
garnet + biotite + orthoclase + plagioclase + quartz
garnet ± sillimanite + orthoclase + plagioclase + quartz
garnet + biotite ± sillimanite + plagioclase + quartz
biotite ± orthoclase + plagioclase + quartz
sillimanite + orthoclase + plagioclase + quartz

In the central and northeastern part the granulitic garnet gneisses of M1 suffered strong anatexis during the postkinematic M2 stage. Coarse-grained and schlieric to massive cordierite-bearing anatexites were formed. The appearance of cordierite in this part of the granulite complex is due to the specific composition of the rocks (lower $CaO/(CaO+FeO+MgO)$ and lower $K_2O/(K_2O+FeO+MgO)$ ratios, Fig. 13, and incorporation of a large part of the FeO into sulfides) and thus does not define an isograd. The textural relationships indicate that cordierite

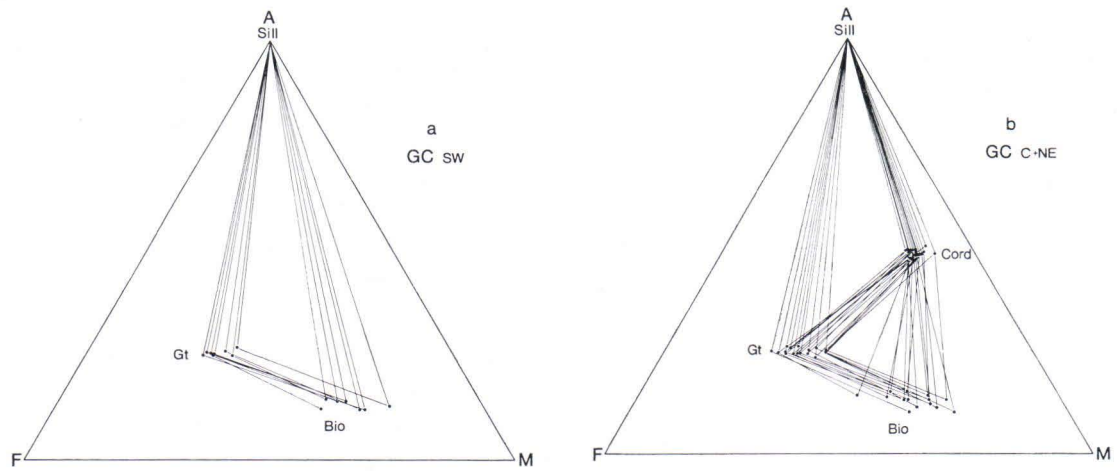

Fig. 12 a, b. AFM projections from K-feldspar and quartz of minerals coexisting during M2 in a) garnet gneisses of the southwestern part of the granulite complex and b) garnet-cordierite gneisses of the central and northeastern part of the granulite complex. For plotting the biotite compositions a $K(Mg, Fe^{2+})\ Ti\ \square\ AlSi_3O_{10}\ (OH)_2$ component with X_{Mg} equal to the bulk X_{Mg} has been subtracted.

grew under static conditions (M2), in general in equilibrium with garnet, biotite, sillimanite, orthoclase, plagioclase, quartz. From this assemblage a reaction

biotite + sillimanite + quartz $\leftrightarrows$ cordierite + K-feldspar + garnet + H_2O

might be deduced (Lee and Holdaway 1977). However, the actual relationships are expected to be more complex, since also plagioclase, a melt, sulfides and a complex gas phase may have been involved.

The observed cordierite-bearing assemblages (all including plagioclase and quartz) with grain contacts are (Figs. 9, 12b):

garnet + biotite + cordierite + sillimanite + orthoclase
garnet + biotite + cordierite + sillimanite
garnet + biotite + cordierite
garnet + cordierite + sillimanite + orthoclase
garnet + biotite ± cordierite ± sillimanite + orthoclase + hercynite

In the anatexites and their late pegmatitic moblization products of the northeastern part of the granulite complex (between Inari and Ivalo) andalusite may be encountered. It coexists with chlorite, white mica, carbonate, and quartz and replaces garnet and mainly cordierite. Some of the andalusite is certainly formed by hydrous decomposition of cordierite (Lal 1969). These processes correspond to a late event at temperatures much lower than those of M2, and might be simultaneous to the formation of cummingtonite in the mafic rocks.

The quartz-feldspar gneisses of the *northeastern marginal zone* exhibit parageneses similar to those of the northeastern part of the granulite complex (Fig. 9):

biotite + garnet + plagioclase + quartz
biotite + sillimanite + plagioclase + K-feldspar + quartz
biotite + garnet + sillimanite + plagioclase + quartz
garnet + cordierite + sillimanite + biotite + plagioclase + quartz

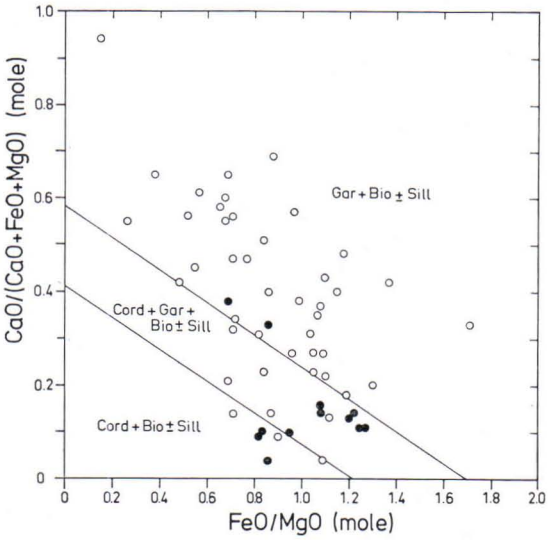

Fig. 13. Dependence of mineral assemblage on CaO/(CaO + MgO + FeO) and FeO/MgO ratio of the bulk rock, uncorrected for sulfide. The limits given are from Wynne-Edwards and Hay (1963). Circles: garnet gneisses; dots: garnet-cordierite gneisses.

The sporadic occurrence of late kyanite and andalusite suggests that during retrogression the PT-path passed in the vicinity of the Al_2SiO_5 triple point. On the other hand, the simple biotite gneisses with the assemblage biotite + plagioclase + quartz resemble the migmatic gneisses of the granite gneiss complex.

In the *granite gneiss complex* the banded migmatic gneisses are characterized by the absence of garnet, cordierite and aluminium silicates. Hornblende- and biotite-bearing gneisses with the assemblage plagioclase + biotite + hornblende + quartz predominate. Hornblende-free gneisses with the parageneses plagioclase + biotite + quartz and plagioclase + microcline + biotite + quartz are rare in the profile studied.

MINERAL CHEMISTRY

The following section deals only with the occurrence, textural relationship and composition of important mineral phases formed during high-grade metamorphism. Accessories such as sphene, spinel, opaques, graphite and late retrograde alteration products such as white mica, chlorite, epidote, prehnite, carbonates will not be treated here. Studies on fluid inclusions in quartz and the regional development of quartz fabrics will be presented in separate publications.

Only selected analyses can be given here. The complete set of data is available on request.

Amphiboles

Occurrence and textural relationships

Ca-amphiboles are widespread in the amphibolites, garnet amphibolites and hornblende gneisses of the *West Inari schist zone*. In the amphibolites and hornblende gneisses the hornblendes have grown synkinematically; they are xenoblastic to hypidioblastic prismatic and often well oriented parallel to the banding and schistosity. Late recrystallization under static conditions is also evident. In the garnet amphibolites reaction rims consisting of hornblende + plagioclase separate garnet from clinopyroxene (Fig. 14) indicate that the amphiboles are at least in part a late, postkinematic product of crystallization.

In the *granulite complex* amphiboles occur only in subordinate amounts in bands and streaks of the clinopyroxene-bearing hypersthene–plagio-

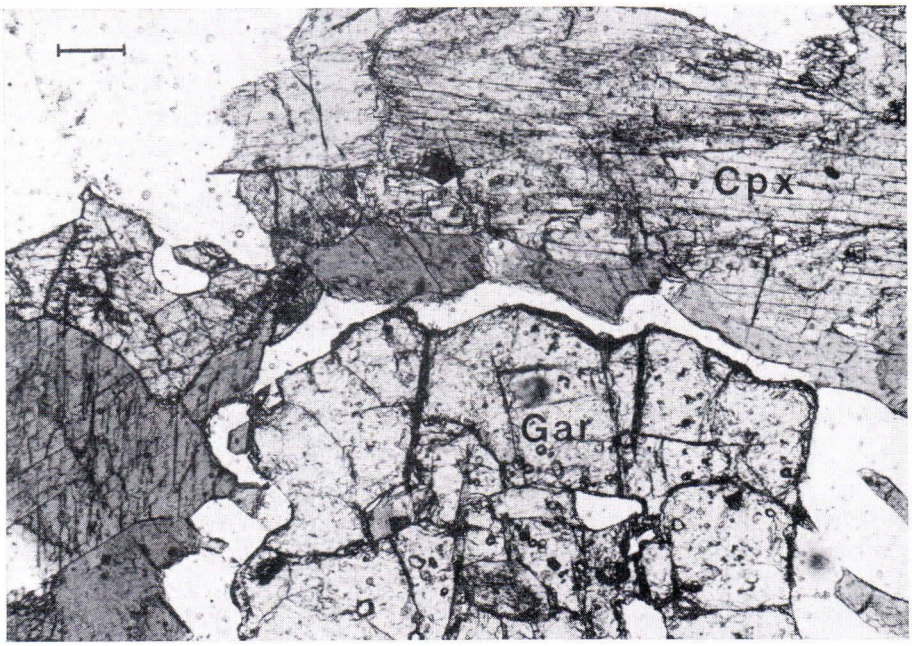

Fig. 14. Reaction rim consisting of hornblende and plagioclase, separating clinopyroxene (upper part) and garnet (lower part). Sample 18 II, garnet amphibolite from the West Inari schist zone. The length of the bar corresponds to 0.1 mm.

clase rocks free from quartz but amphibole becomes more important in the marginal zones of the granulite complex where rocks transitional to the metabasites of the adjoining rock units are exposed.

Amphiboles from the granulite complex and its marginal zones form, in general, xenoblastic, amoeboid grains elongated in the direction of the lineation of the rock. During their growth these amphiboles have replaced and rimmed pyroxenes and opaques (ilmenohematite). They contain corroded inclusions of these minerals, biotite and plagioclase (Fig. 15). Although these textural relationships prove a late formation of the amphibole, this mineral was obviously in equilibrium with the entire former mineral assemblage, since sharp grain contacts are developed throughout.

In the *northeastern part of the granulite complex* and the *northeastern marginal zone* (cf. Fig. 8) cummingtonite and anthophyllite occur besides Ca-amphiboles as retrograde products growing at the expense of orthopyroxene. Cummingtonite sometimes forms thin overgrowths on hypersthene or occurs as large xenoblasts which may, in turn, be corroded and overgrown by common hornblende. Anthophyllite occurs locally in some bronzite–plagioclase rocks where it replaces orthopyroxene and forms fibrous aggregates. The retrograde formation of either anthophyllite or cummingtonite is controlled by the composition of the parent orthopyroxene.

Ca-amphiboles are again widespread in the amphibolites and migmatic gneisses of the *granite gneiss complex*. The textural relationships show that they grew under syn- to postkinematic conditions.

Chemistry

The most significant chemical parameters of the amphiboles are displayed in Figs. 16—18, selected analyses are given in Table 13. Besides

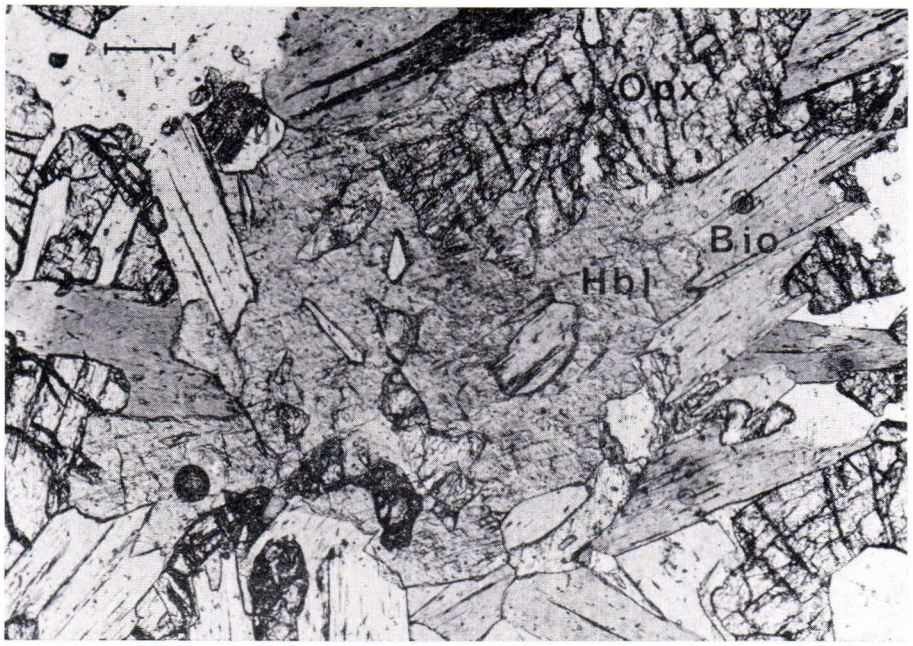

Fig. 15. Amoeboidal replacement of hypersthene by hornblende and biotite. Sample 100 I, hornblende-biotite-orthopyroxene-plagioclase gneiss, central part of the granulite complex. The length of the bar corresponds to 0.1 mm.

the dependence of amphibole composition on mineral assemblage and bulk rock chemistry (Fig. 16a) characteristic compositional variations also occur along the profile suggesting changes in metamorphic conditions.

In the *West Inari schist zone* Fe concentrations in amphiboles decrease from microcline gneisses to plagioclase gneisses to amphibolites (Fig. 17). The Al^{VI} contents increase and the alkali contents decrease in this order.

The amphiboles from the orthopyroxene–plagioclase rocks of the *granulite complex* exhibit similar Fe contents as those from amphibolites of the West Inari schist zone, but are distinct by their very low Al^{VI} contents (Fig. 17). Besides, they are characterized by higher K, Al^{IV}, Fe^{3+} and Ti concentrations (Fig. 18 a-d). Their composition is close to that of the end member hastingsite, and they will be termed hastingsitic hornblende in the following. On the other hand, amphiboles from the West Inari schist zone vary from common hornblende to tschermakitic hornblendes.

Amphiboles from the amphibolites of the *marginal zones of the granulite complex* and of the *granite gneiss complex* are in general transitional between common hornblende and hastingsitic hornblende.

The changes in amphibole composition from common hornblende in the West Inari schist zone to hastingsitic hornblende in the granulite complex can be explained by the following scheme of coupled substitutions:

	common hornblende		hastingsitic hornblende
Z position	$0.3\ Si^{4+}$	$\longleftrightarrow$	$0.3\ Al^{3+}$
Y position	$0.3\ Al^{3+}$	$\longleftrightarrow$	$0.2\ Fe^{3+} + 0.1\ Ti^{4+}$
A position	$0.2\ \square$	$\longleftrightarrow$	$0.2\ K^{+}$
net substitution	$0.3\ Si^{4+}$	$\longleftrightarrow$	$0.2\ Fe^{3+} + 0.1\ Ti^{4+} + 0.2\ K^{+}$

Table 13

Microprobe analyses and structural formulae of Ca-amphiboles. Geological units, rock types, some of the coexisting minerals and sample numbers are indicated in the top rows.

	West Inari Schist Zone					SWMZ		Granulite Complex			NEMZ			Granite Gneiss Complex			
	Amphibolites					Amphibolites		Hyp-Plag Rocks			Amphibolites			Amphibolites			
	Gt, Cpx 1 LI	Cpx 4 I	Gt, Cpx 18 II	Cpx 27 I	Corun 14 I	Opx 43 IV	Gt 67 I	Cpx, Opx 70 I	Opx J 12 I	Cpx, Opx 116 III	174 II	Cpx 219 I	Cpx 460 II	Gt, Cpx, Cumm 458 II	Cpx 464 II	465 II	470 II
SiO_2	43.10	45.20	44.75	44.83	45.68	42.75	40.93	41.92	42.45	42.05	42.84	42.36	42.39	42.00	40.84	40.20	44.56
TiO_2	1.36	1.27	0.99	0.92	0.05	1.43	1.22	2.54	2.14	2.35	1.13	2.20	0.99	1.77	1.77	1.91	0.36
Al_2O_3	12.00	10.26	11.05	10.67	15.32	10.18	11.95	11.38	10.65	11.15	11.41	10.52	10.30	10.57	9.93	10.67	9.83
Cr_2O_3	0.05	0.07	0.05	0.03	0.03	0.00	0.02	0.07	0.06	0.00	0.00	0.02	0.00	0.00	0.04	0.03	0.10
[a]Fe_2O_3	3.40	2.00	2.98	3.16		5.20	5.64	4.37	4.77	4.72	6.11	3.86					
[a]FeO	15.21	11.58	11.80	12.83	5.10	17.63	15.79	11.85	9.84	9.40	13.15	16.32	18.52	19.79	20.82	21.56	13.67
MnO	0.12	0.21	0.04	0.24	0.07	0.25	0.27	0.15	0.19	0.10	0.44	0.42	0.31	0.25	0.37	0.33	0.25
MgO	8.53	12.03	11.85	10.88	16.32	8.70	8.08	10.78	12.05	13.10	9.26	7.56	9.21	8.00	7.74	6.32	12.55
CaO	11.15	12.30	11.60	11.77	12.46	8.82	11.00	11.75	11.25	11.52	10.94	11.16	11.84	10.95	11.19	11.15	12.12
K_2O	0.38	0.79	1.00	0.73	0.15	0.52	1.27	1.82	1.86	2.00	0.70	0.79	0.88	0.84	1.42	1.47	1.04
Na_2O	1.39	0.93	1.44	1.43	0.89	2.00	1.73	1.54	1.44	1.75	1.34	1.78	1.29	1.57	1.51	1.49	1.13
Total	96.69	96.64	97.55	97.49	96.07	97.48	97.90	98.17	96.70	98.14	97.32	96.99	95.73	95.74	95.63	95.13	95.61
Number of ions on the basis of 46 cation valences																	
Si	6.504	6.700	6.597	6.649	6.505	6.505	6.236	6.256	6.366	6.222	6.437	6.475	6.506	6.469	6.394	6.339	6.686
Al	1.496	1.300	1.403	1.351	1.495	1.495	1.764	1.744	1.634	1.778	1.563	1.525	1.494	1.531	1.616	1.661	1.314
Al	0.638	0.493	0.517	0.514	1.077	0.331	0.382	0.258	0.248	0.167	0.457	0.371	0.369	0.388	0.214	0.322	0.425
Ti	0.154	0.142	0.110	0.103	0.005	0.164	0.140	0.285	0.241	0.261	0.128	0.253	0.114	0.205	0.208	0.226	0.041
Cr	0.006	0.008	0.006	0.003	0.003	0.000	0.002	0.008	0.007	0.000	0.000	0.002	0.000	0.000	0.005	0.000	0.012
Fe^{3+}	0.386	0.223	0.331	0.353		0.595	0.646	0.491	0.538	0.525	0.691	0.444	0.430	0.460	0.490	0.520	0.310
Fe^{2+}	1.919	1.435	1.454	1.591	0.607	2.243	2.011	1.478	1.234	1.163	1.652	2.086	1.940	2.080	2.220	2.320	1.400
Mn	0.015	0.026	0.011	0.030	0.008	0.032	0.035	0.019	0.024	0.013	0.056	0.054	0.040	0.033	0.049	0.044	0.032
Mg	1.918	2.657	2.603	2.404	3.463	1.973	1.834	2.397	2.693	2.888	2.073	1.722	2.106	1.836	1.803	1.485	2.806
Ca	1.803	1.953	1.832	1.870	1.901	1.438	1.796	1.878	1.807	1.826	1.761	1.828	1.947	1.807	1.874	1.884	1.948
K	0.073	0.149	0.188	0.138	0.027	0.101	0.247	0.346	0.365	0.377	0.134	0.154	0.172	0.165	0.283	0.296	0.199
Na	0.407	0.267	0.411	0.411	0.246	0.590	0.511	0.445	0.418	0.502	0.390	0.527	0.384	0.469	0.457	0.455	0.329
X_{Mg}	0.50	0.65	0.64	0.60	0.85	0.47	0.48	0.62	0.69	0.71	0.56	0.45	0.52	0.47	0.45	0.39	0.67

[a] Fe_2O_3 and FeO determined by wet chemical analysis, except samples 14I, 460II, 458II, 464II, 465II, 470II, where FeO represents total iron. For the latter samples Fe^{3+} and Fe^{2+} in the structural formulae has been inferred from the ore assemblage

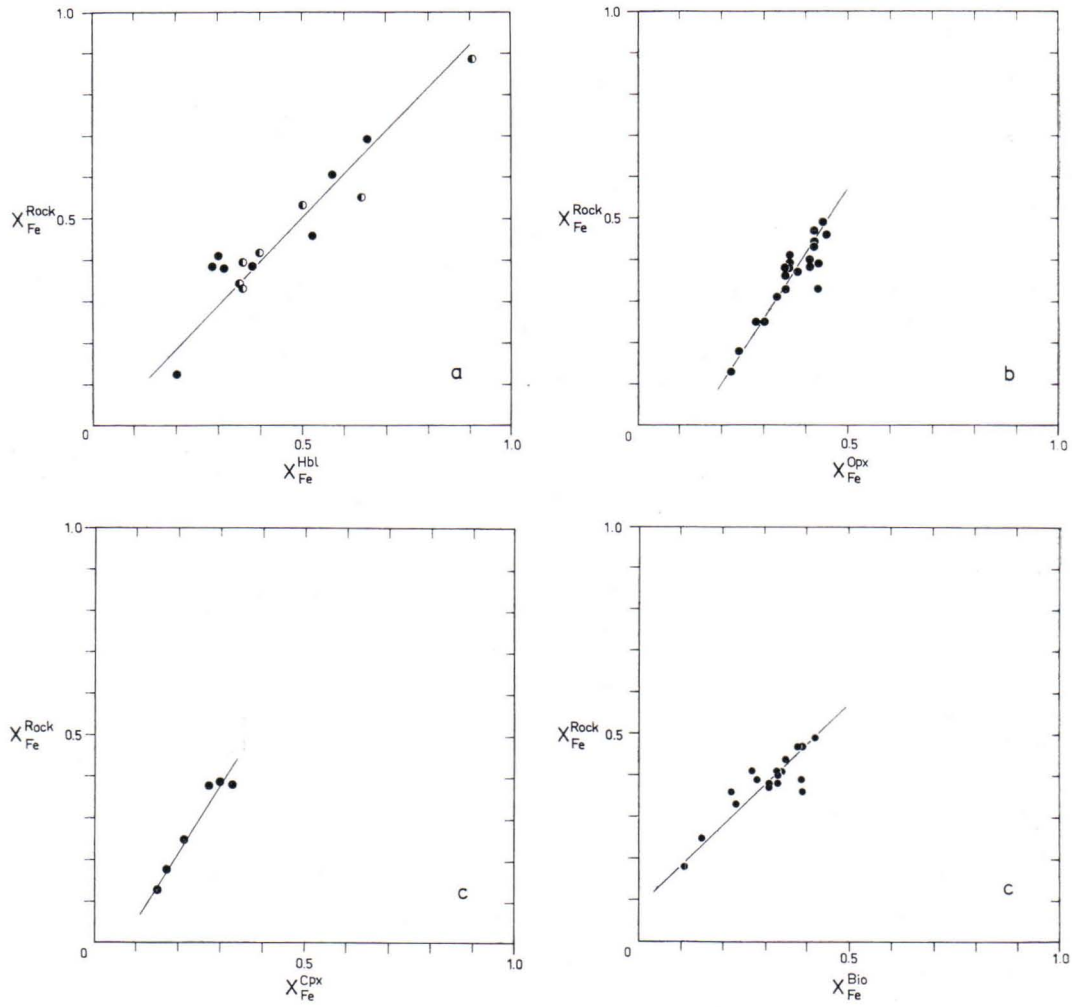

Fig. 16 a-d. Relation between bulk rock X_{Fe}(= FeO/(FeO + MgO) and X_{Fe} of hornblende (a), orthopyroxene (b), clinopyroxene (c) and biotite (d) in rocks from the West Inari schist zone (half-filled circles) and hypersthene-plagioclase rocks of the granulite complex and its marginal zones (solid dots).

Obviously the average cation radius in all positions is larger in the hastingsitic hornblende compared to the common hornblende, which may tentatively be related to higher temperature or lower pressure conditions during the formation of the hastingsitic hornblendes.

The Fe^{3+} contents of the hornblendes are controlled by the oxygen fugacity which may be deduced from the ore mineral assemblage. Hematite–ilmenite–magnetite assemblages in most of the orthopyroxene-bearing rocks indicate rather high and buffered f_{O_2}. Amphiboles in these rocks consequently have a high Fe^{3+}/Fe^{2+} ratio (Table 13). On the other hand, the amphibolites of the West Inari schist zone do not contain iron oxides. Due to the unbuffered and probably low f_{O_2} amphiboles with varying but low Fe^{3+}/Fe^{2+} ratios were formed.

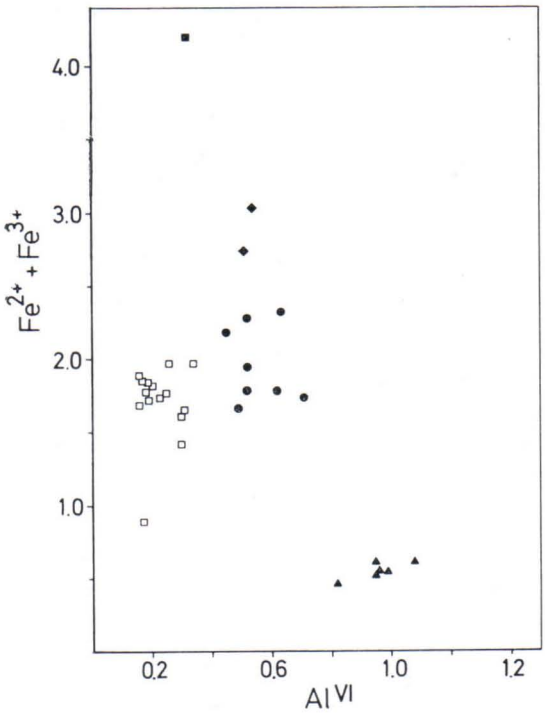

Fig. 17. Relation between total iron and Al^{VI} in amphiboles from the West Inari schist zone (solid symbols), and the granulite complex (open symbols). Dots: amphibolites, diamonds: hornblende-plagioclase gneisses, squares: hornblende-microcline gneisses and hornblende-hypersthene-plagioclase gneisses, respectively, triangles: corundum-bearing amphibolites from Paaraskalla.

Table 14

Microprobe analyses and structural formulae of cummingtonite (220II) and anthophyllite (222III).

	NEMZ Gt-Cumm-Plag rock 220 II	GC Bio-Anth-Plag rock 222 III
SiO_2	51.80	55.61
TiO_2	0.08	0.06
Al_2O_3	2.20	0.98
Cr_2O_3	0.00	0.06
[a]FeO	25.37	19.44
MnO	0.30	0.31
MgO	14.27	21.17
CaO	0.85	0.45
K_2O	tr.	tr.
Na_2O	0.16	0.02
Total	95.03	98.10
Number of ions on the basis of 46 cation valences		
Si	7.869	7.911
Al	0.131	0.089
Al	0.263	0.075
Ti	0.009	0.006
Cr	0.000	0.007
Fe[a]	3.222	2.312
Mn	0.039	0.037
Mg	3.230	4.488
Ca	0.138	0.069
K	0.000	0.000
Na	0.047	0.006
X_{Mg}	0.50	0.66

[a] total iron as FeO

Analyses of the Mg–Fe amphiboles cummingtonite and anthophyllite (from the Inarijärvi region) are given in Table 14. A Mössbauer investigation of the anthophyllite showed the total absence of any ferric iron and a high degree of ordering of Fe^{2+} and Mg between the M4 site and the combined M123 sites. From the area ratio in the Mössbauer spectrum the following structural formula is calculated:

$$\underset{A}{Na_{0.01}Ca_{0.04}}\ \underset{M4}{(Ca_{0.03}Mg_{0.28}Fe^{2+}_{1.65}Mn_{0.04})}\ (Mg_{4.21}$$
$$Fe^{2+}_{0.67}Cr_{0.01}Ti_{0.01}Al_{0.07})\ \underset{Z}{(Si_{7.91}Al_{0.09})}O_{22}(OH)_2$$
$$\text{M1, M2, M3}$$

The ordering parameter $K = (X^{Fe}_{M123} \cdot X^{Mg}_{M4}) / (X^{Fe}_{M4} \cdot X^{Mg}_{M123}) = 0.0270$ indicates a low cut-off temperature for the ordering process and thus a low cooling rate, as would be expected in a regional metamorphic terrain (Seifert and Virgo 1975).

Regional development of amphibole chemistry

Amphiboles from amphibolites and orthopyroxene–plagioclase rocks show systematic compositional changes along the profile investigated (Fig. 19). Within the West Inari schist zone the alkali content and the ratio $(Al^{IV} + Na + K)/Si$ increases from SW to NE in hornblendes from the amphibolites, whereas the Al^{VI}/Al^{IV} ratio decreases markedly in this direction. The composition of these hornblendes thus continuously approaches that of the hastingsitic hornblendes typically found in the granulite complex. The differences in the average compo-

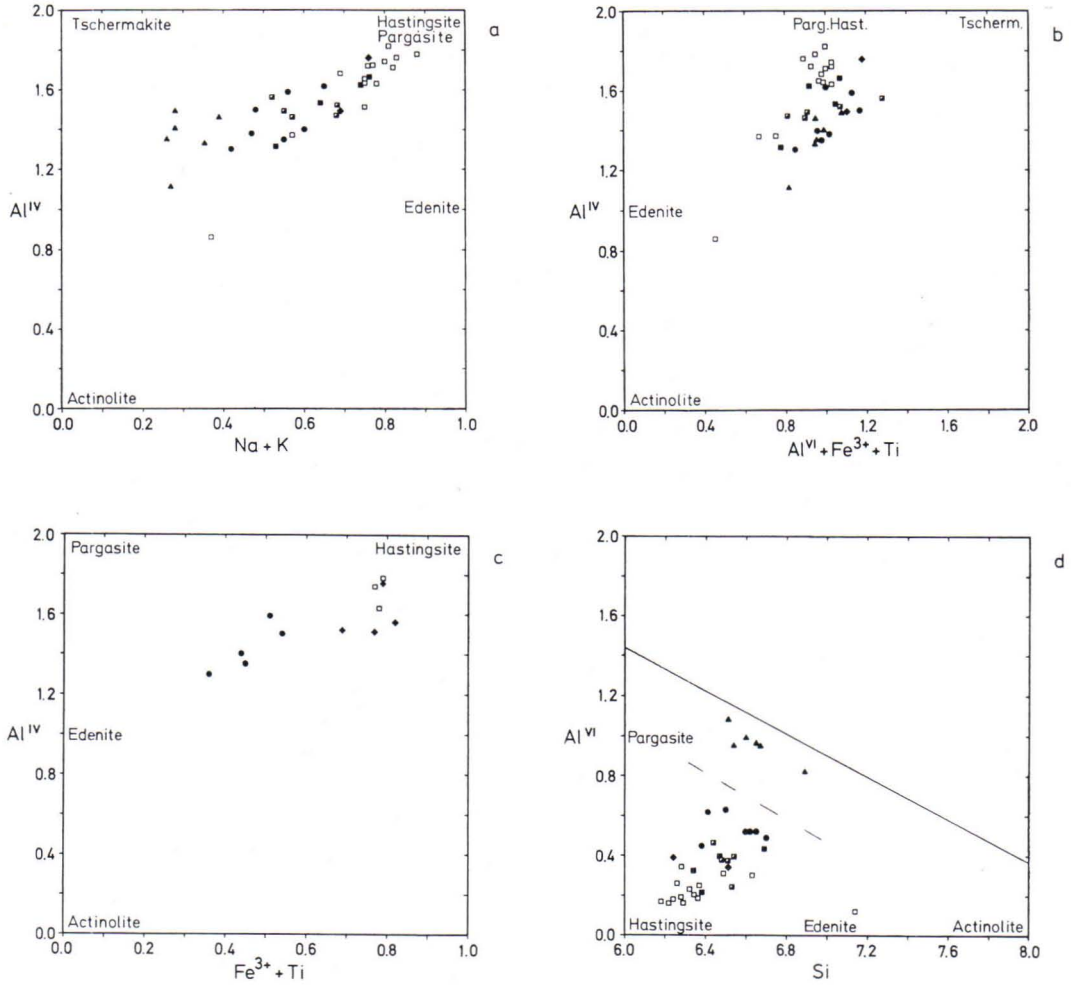

Fig. 18 a-d. Selected compositional parameters of amphiboles, expressed as number of atoms per 23 oxygens. Solid dots: amphibolites from the West Inari schist zone, diamonds: amphibolites from the southwestern marginal zone, triangles: corundum-bearing amphibolites from Paaraskalla, open squares: hypersthene-bearing rocks from the granulite complex, half-filled squares: amphibolites from the northeastern marginal zone, filled squares: amphibolites from the granite gneiss complex. In Fig. 5 d the solid line represents the maximum possible Al^{VI} contents in amphiboles according to Leake (1965), the broken line indicates maximum Al^{VI} contents for amphiboles formed at pressures up to 5 kbar (Raase 1974).

sitons of hornblendes from the amphibolites of the West Inari schist zone on the one side and the orthopyroxene gneisses of the granulite complex on the other (see above) are certainly not due to the different assemblages: In the southwestern marginal zone both rock types show nearly identical amphibole compositions transitional between those of the granulite complex proper and the West Inari schist zone.

Due to the lack of hornblende-bearing rocks in the central part of the granulite complex these trends in amphibole composition cannot be traced here. However, amphiboles from the northeastern part show a decrease in alkali and

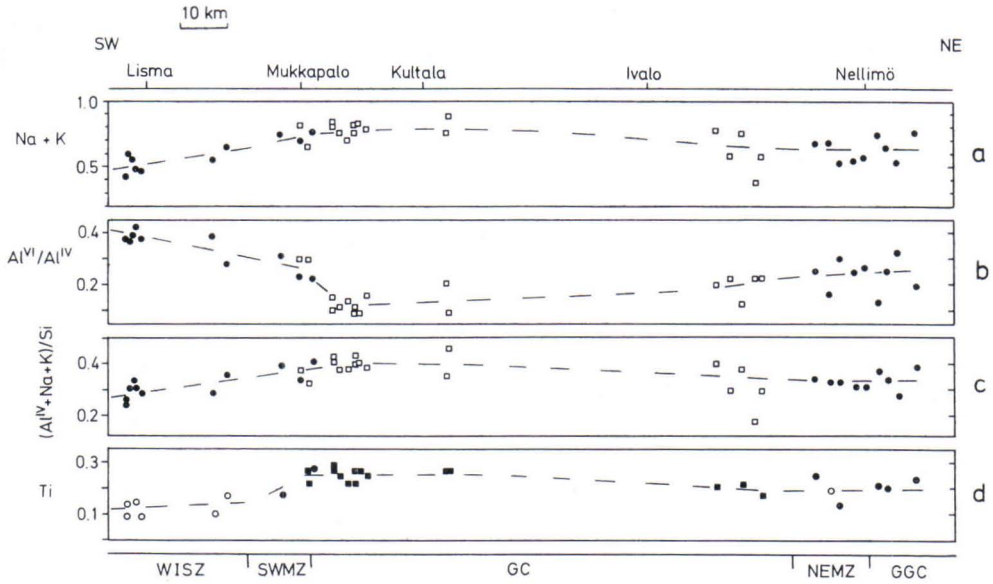

Fig. 19. Regional development of the chemical composition of amphiboles. Profiles a-c: amphibolites (dots), hypersthene-bearing rocks (squares). Profile d: amphibolites with sphene (circles), amphibolites with ilmenite (dots) and hypersthene-bearing rocks with ilmenite (filled squares). For discussion see text.

Ti contents, a lower $(Al^{IV} + Na + K)/Si$ ratio and a higher Al^{VI}/Al^{IV} ratio compared to the western part of the granulite complex. These trends continue without break through the northeastern marginal zone into the granite gneiss complex (Fig. 19).

Orthopyroxene

Occurrence and textural relationships

In the *West Inari schist zone* orthopyroxene is restricted to ultramafic rocks, whereas in the granulite complex it is an important constituent of basic to intermediate rocks. Only rarely it occurs there in light gneisses devoid of garnet and hornblende.

Orthopyroxene-bearing ultramafic rocks of the West Inari schist zone have been described by Mikkola and Sahama (1936). In the profile studied the following assemblages containing relic olivine have been encountered:

orthopyroxene + chlorite + serpentine + talc + carbonate

orthopyroxene + Ca-amphibole + chlorite + serpentine + talc + carbonate ± spinel

orthopyroxene + Ca-amphibole + chlorite + talc

In the *granulite complex* by far the most frequent assemblage is hypersthene + plagioclase (An54 ±20) + biotite.

To a lesser extent the assemblages

hypersthene + plagioclase (An62±20) + biotite + hornblende + clinopyroxene

hypersthene + plagioclase (An60±20) + biotite + hornblende

hypersthene + plagioclase (An43±6) + biotite + garnet

are developed. In all assemblages quartz and K-feldspar may be present. No parageneses of orthopyroxene with cordierite or sillimanite have been found.

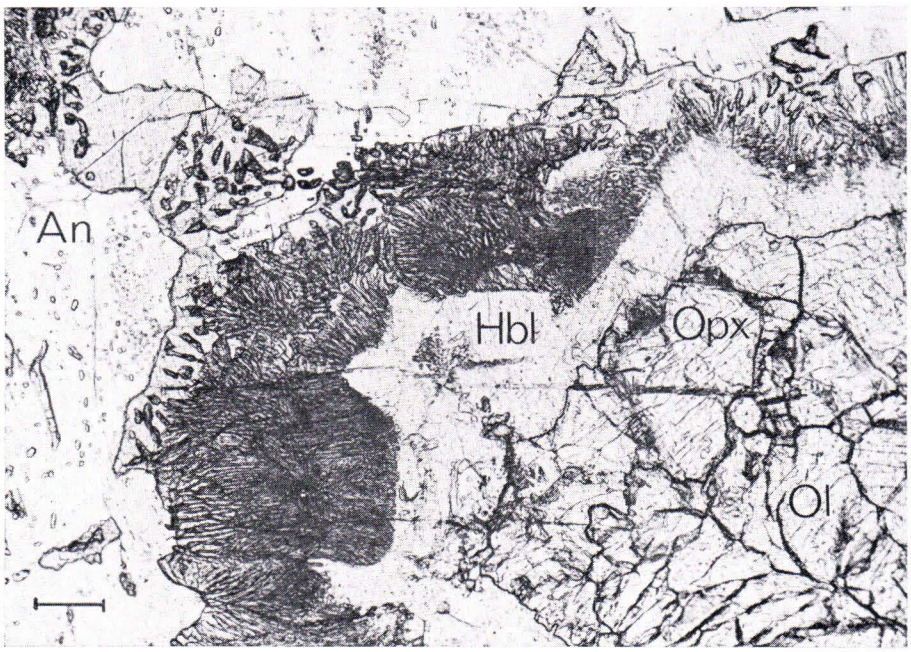

Fig. 20. Corona texture around olivine in a metatroctolite from Mukkapalo, southwestern marginal zone (locality 46, see text). The length of the bar corresponds to 0.1 mm.

In the *southwestern marginal zone* rocks transitional between the hypersthene rocks of the granulite complex and the garnet amphibolites of the West Inari schist zone are exposed. They contain orthopyroxene in association with clinopyroxene, amphibole, plagioclase, and garnet. However, garnet and orthopyroxene only occur in separate layers of the rock and do not form grain contacts. — Besides small lenses of bronzite felses a troctolitic gabbro with typical corona textures (cf. Gardner and Robins 1974, Lasnier 1977) occurs in the southwestern marginal zone near Mukkapalo: Olivine crystals set in an anorthite matrix are rimmed by bronzite which is again surrounded by a symplectitic intergrowth of clinopyroxene + hercynitic spinel. On both sides of this symplectite zone an amphibole rim can be developed in an advanced stage of replacement (Fig. 20). Rarely garnet grows as an outermost zone. In some rock types the previous corona structures are obliterated by the formation of abundant amphibole, partly separated from the anorthite by discountinuous rims of garnet which may contain blebs of spinel.

In the basic to intermediate rocks of the granulite complex orthopyroxene forms xenomorphic to hypidiomorphic mostly short prismatic grains which are randomly oriented in the massive rock types but aligned parallel to the foliation in the gneissic types. Orthopyroxene is locally enclosed and replaced by hastingsitic hornblende grown in a postkinematic stage of crystallization. On the other hand, in the northeastern part of the granulite complex replacement occurs by cummingtonite or anthophyllite. Talc and serpentine are formed from orthopyroxene in rocks which have suffered diaphthoresis.

Composition

The orthopyroxenes vary in composition from bronzite to Fe-rich hypersthene. Table 15 gives a selection of analyses of orthopyroxenes from the granulite complex.

Table 15

Microprobe analyses and structural formulae of orthopyroxenes from the southwestern marginal zone and the granulite complex.

	SWMZ		Granulite Complex														
	Hbl-Pyx Rocks		Hyp-Gar-Plag Gneisses				Hyp-Plag Rocks					Hyp-Cpx-Hbl-Plag Gneisses					
	47 III	66 II	72 I	95 I	140 III	203 II	59 II	83 I	125 I	141 I	J 1 I	70 I	100 I	116 III	168 I	170 II	J 12 I
SiO_2	50.45	50.90	51.77	48.40	49.70	49.35	50.10	49.36	48.14	51.40	50.66	51.70	54.20	52.83	51.63	53.92	52.45
TiO_2	0.07	0.10	0.12	0.15	0.11	0.08	0.14	0.10	0.15	0.20	0.10	0.09	0.05	0.13	0.11	0.11	0.09
Al_2O_3	1.00	1.00	3.21	4.62	3.51	5.19	2.47	3.85	6.86	2.45	2.97	1.47	1.33	1.60	1.55	1.06	1.61
Cr_2O_3	0.02	0.04	0.06	0.02	0.01	0.03	0.03	0.02	0.02	0.00	0.06	0.02	0.15	0.00	0.06	0.10	0.00
FeO[a]	30.45	31.24	20.07	27.18	22.97	25.90	25.55	22.92	24.18	22.50	27.48	25.93	16.00	22.23	23.70	17.84	22.28
MnO	0.66	0.52	0.24	0.34	0.17	0.61	0.47	0.29	0.29	0.56	0.50	0.52	0.37	0.31	0.38	0.31	0.75
MgO	15.15	16.01	23.07	18.12	21.17	19.05	19.75	20.86	19.68	22.05	18.16	19.65	27.10	22.05	20.73	25.36	21.75
CaO	0.77	0.67	0.21	0.24	0.13	0.10	0.24	0.21	0.11	0.38	0.40	0.61	0.46	0.66	0.67	0.65	0.73
Total	98.57	100.48	98.75	99.07	97.77	100.31	98.75	97.61	99.43	99.54	100.33	99.99	99.66	99.81	98.83	99.35	99.66
Ox[b]	0.040	0.042	0.060	0.080	0.057	0.085	0.037	0.064	0.124	0.028	0.063	0.046	0.020	0.066	0.060	0.027	0.020
Number of ions on the basis of 12 cation valences																	
Si	1.985	1.968	1.926	1.857	1.895	1.861	1.917	1.884	1.807	1.916	1.920	1.954	1.963	1.960	1.953	1.975	1.960
Al	0.015	0.032	0.074	0.143	0.105	0.139	0.083	0.116	0.193	0.084	0.080	0.046	0.037	0.040	0.047	0.025	0.040
Al	0.031	0.014	0.067	0.066	0.053	0.092	0.028	0.057	0.111	0.024	0.053	0.019	0.020	0.030	0.022	0.021	0.031
Ti	0.002	0.003	0.003	0.004	0.003	0.002	0.004	0.003	0.004	0.006	0.003	0.003	0.001	0.003	0.003	0.003	0.003
Cr	0.001	0.001	0.002	0.001	0.001	0.001	0.001	0.001	0.001	0.000	0.002	0.001	0.004	0.000	0.002	0.003	0.000
Fe^{3+}	0.036	0.038	0.034	0.069	0.041	0.062	0.030	0.054	0.094	0.020	0.045	0.038	0.010	0.045	0.045	0.013	0.014
Fe^{2+}	0.957	0.963	0.583	0.803	0.691	0.739	0.787	0.679	0.665	0.681	0.826	0.082	0.475	0.644	0.705	0.533	0.683
Mn	0.022	0.017	0.008	0.011	0.005	0.019	0.015	0.009	0.009	0.018	0.016	0.017	0.011	0.010	0.012	0.010	0.024
Mg	0.888	0.922	1.279	1.036	1.020	1.070	1.126	1.187	1.101	1.250	1.026	1.107	1.462	1.219	1.169	1.384	1.211
Ca	0.032	0.028	0.008	0.010	0.005	0.004	0.010	0.009	0.004	0.015	0.016	0.025	0.018	0.026	0.027	0.026	0.029
X_{Mg}	0.48	0.49	0.64	0.56	0.64	0.59	0.59	0.64	0.62	0.65	0.62	0.59	0.75	0.65	0.62	0.72	0.64

[a] total iron as FeO; [b] the molecular ratio $Fe^{3+}/(Fe^{3+} + Fe^{2+}) = Ox$ has been obtained from Mössbauer effect measurements or estimated from the ore assemblage (samples: 47III, 66II, 72I, 203II, 168I, 170II).

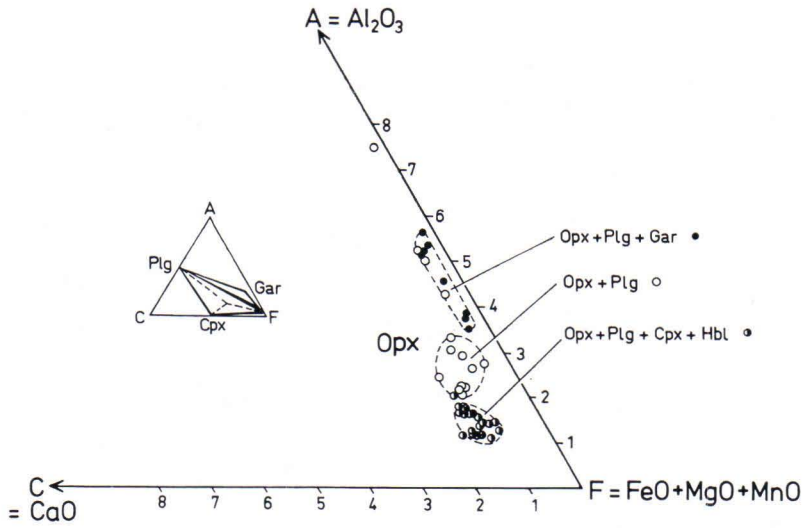

Fig. 21. Chemical composition of orthopyroxenes from the granulite complex in the ACF projection, and its dependence on mineral assemblage (cf. inset and text).

The Fe content of the orthopyroxenes is controlled both by the bulk rock chemistry (Fig. 16b) and the coexisting ore assemblage stressing the role of oxygen and sulfur fugacities. The most Fe-rich hypersthenes ($X_{Fe} = Fe^{2+}/(Fe^{2+} + Mg) = 0.45—0.35$), which are also characterized by elevated Fe^{3+} contents (0.04 to 0.07 Fe^{3+} p.f.u.), occur in oxidized rocks with the ore mineral assemblage ilmenite + hematite + magnetite + pyrite ($X_{Fe}^{rock} \approx 0.35$, $Ox^{rock} = Fe^{3+}/(Fe^{3+} + Fe^{2+}) \approx 0.30$). Hypersthenes from more reduced rocks with ilmenite, pyrite, pyrrhotite ($X_{Fe}^{rock} \approx 0.4$, $Ox^{rock} \approx 0.16$) are lower in X_{Fe} (0.43—0.33) because here a larger proportion of Fe^{2+} is fixed as sulfide. A rather low oxygen fugacity is reflected by the low Fe^{3+} contents of the orthopyroxenes, which ranges from 0.02 to 0.04 Fe^{3+} p.f.u. Orthopyroxenes with $X_{Fe} = 0.35—0.22$ are restricted to iron-poor rocks ($X_{Fe}^{rock} \approx 0.2$, $Ox^{rock} \approx 0.16$) devoid of iron ore minerals. Consequently, the Fe^{3+} in these orthopyroxenes amounts to only 0.01 Fe^{3+} p.f.u.

The Al contents vary greatly from 0.04 to 0.30 Al p.f.u. (Table 15, Fig. 21) and strongly depend on the mineral assemblage. In general, the highest Al contents (0.15—0.24) are encountered in the assemblage with garnet and plagioclase, whereas the lowest Al values (0.04—0.07 Al p.f.u.) are found in orthopyroxenes coexisting with clinopyroxene, hornblende and plagioclase. Orthopyroxene coexisting with plagioclase only exhibits intermediate values (0.08—0.13) but a few samples plot towards higher Al contents.

The Ca contents are low and also related to the various assemblages (Fig. 21, Table 15). The highest values are encountered in orthopyroxenes coexisting with clinopyroxene and hornblende (0.030—0.023 Ca p.f.u.), the lowest values (0.010—0.004) in those coexisting with garnet. No dependence on the An content of the coexisting plagioclase has been observed.

Since the concentrations of Ca, Ti, Cr, Mn and Na are very low, the chemical variation of the orthopyroxenes can be described by the substitutions $Mg^{2+} \leftrightarrows Fe^{2+}$ and $2(Al, Fe^{3+}) \leftrightarrows (Mg, Fe^{2+}) + Si$.

Regional development of orthopyroxene chemistry

In orthopyroxenes coexisting with garnet and plagioclase a characteristic variation in Al content along the profile can be observed (Fig. 22). It

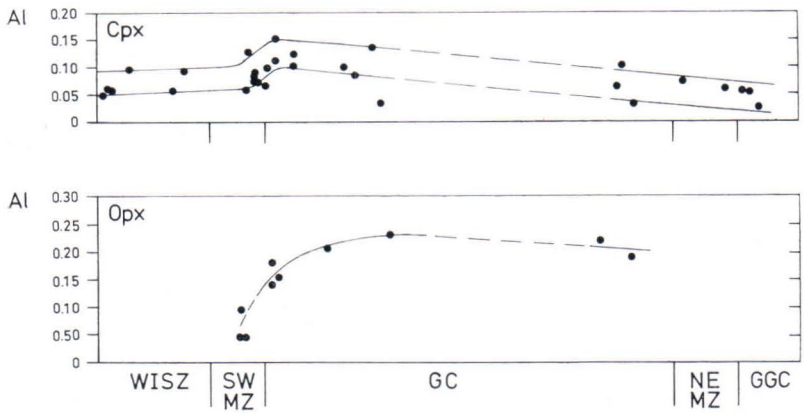

Fig. 22. Regional variation of alumina content (atoms per 6 oxygens) in pyroxenes. For orthopyroxenes, only its assemblage with garnet is considered.

increases from 0.10 Al in the southwestern marginal zone to 0.24 in the central part of the granulite complex. Concomitantly the grossularite component in the garnet decreases from 9 to 4 mole per cent. These trends indicate a systematic variation in pressure — temperature conditions (see section on metamorphic conditions). Other trends are not obvious, probably due to the strong dependence of orthopyroxene composition on bulk rock chemistry and oxygen and sulfur fugacities.

Clinopyroxene

Occurrence and textural relationships

Clinopyroxene forms a minor but characteristic constituent of the amphibolites and hornblende gneisses of the West Inari schist zone and the granite gneiss complex. Within the granulite complex clinopyroxene is restricted to the hornblende-bearing hypersthene–plagioclase gneisses and rare pyroxenites. The textural relationships prove that clinopyroxene has formed in all the rock types as an early mostly synkinematic phase. During this stage of crystallization (M1) clinopyroxene coexisted with garnet in the amphibolites of the West Inari schist zone and the southwestern marginal zone but during the subsequent postkinematic recrystallization (M2) of the rocks it was separated from garnet by a reaction rim consisting of hornblende + plagioclase (Fig. 14). Late postkinematic corrosion of clinopyroxene by hastingsitic hornblende is observed in the hypersthene–plagioclase rocks of the granulite complex.

Composition

Representative microprobe analyses of clinopyroxenes are presented in Table 16.

The Fe content of clinopyroxene (ranging from $X_{Fe} = 0.90$ to 0.16) depends strongly on bulk rock chemistry (Fig. 16 c) but is also controlled by the coexisting ore assemblage (cf. Appendix). Fe-poorest clinopyroxenes ($X_{Fe} < 0.20$) occur in pyroxenitic rocks from the granulite complex whereas the Fe-richest ($X_{Fe} > 0.70$) have been found in amphibolites from the southwestern marginal zone near Mukkapalo.

Ferric iron contents determined by Mössbauer spectroscopy or estimated according to the method proposed by Hamm and Vieten (1971) amount to about 10 % of total iron. Calculation of end member components which is strongly affected by analytical errors shows that most of the ferric iron is present as acmite component.

Al contents are rather low (0.050—0.100 p.f.u.) in clinopyroxenes from the West Inari schist zone and the granite gneiss complex

Table 16

Microprobe analyses and structural formulae of clinopyroxenes.

	West Inari Schist Zone				SWMZ				Granulite Complex					NEMZ			GGC	
	Amphibolites				Hbl-Gar-Pyx Rocks				Hyp-Cpx-Hbl-Plag Gneisses					Amphibolites			Amphibolites	
	1 LI	4 I	18 II	27 I	43 I	47 III	48 I	66 II	70 I	100 I	116 III	168 I	170 II	219 I	458 II	460 II	464 II	470 II
SiO_2	50.90	53.08	52.68	52.55	47.18	51.34	48.15	51.23	50.80	52.65	51.50	51.37	53.28	50.53	50.18	50.73	50.38	52.36
TiO_2	0.11	0.09	0.14	0.07	0.37	0.14	0.20	0.23	0.43	0.14	0.40	0.26	0.13	0.23	0.11	0.10	0.18	0.04
Al_2O_3	1.34	1.14	2.22	1.24	2.48	1.30	1.38	1.97	3.36	2.23	3.07	2.31	1.03	1.61	1.40	1.65	1.50	0.74
Cr_2O_3	0.07	0.00	0.03	0.00	0.00	0.02	0.00	0.05	0.00	0.29	0.00	0.09	0.11	0.00	0.00	0.00	0.02	0.07
FeO[a]	11.90	8.36	8.72	9.12	26.92	11.90	21.92	14.86	11.20	5.67	10.20	9.13	5.67	14.55	15.75	11.58	13.31	8.19
MnO	0.14	0.28	0.16	0.28	0.32	0.28	0.62	0.25	0.00	0.19	0.16	0.15	0.14	0.64	0.36	0.46	0.52	0.32
MgO	11.40	13.40	13.10	12.50	1.56	10.58	4.38	10.99	11.70	15.30	13.00	13.05	14.94	9.49	8.92	10.86	9.84	12.98
CaO	21.40	24.13	21.84	23.05	21.47	22.47	20.30	20.07	20.80	22.90	20.90	22.54	23.47	21.71	21.82	22.98	21.73	24.01
K_2O	0.03	0.00	0.02	0.00	0.02	0.01	0.00	0.00	0.01	0.00	0.01	0.00	0.00	0.00	0.00	0.00	0.01	0.01
Na_2O	0.46	0.26	0.54	0.41	0.42	0.33	1.15	0.41	0.49	0.21	0.85	0.45	0.17	0.37	0.37	0.53	0.66	0.35
Total	97.75	100.74	99.45	99.22	100.74	98.37	98.10	100.06	98.79	99.58	100.09	99.35	98.94	99.13	98.91	98.89	98.15	99.07
Ox[b]	0.091	0.097	0.099	0.021	0.084	0.091	0.082	0.091	0.101	0.046	0.138	0.087	0.091	0.085	0.090	0.094	0.095	0.100
Number of ions on the basis of 12 cation valences																		
Si	1.966	1.967	1.966	1.983	1.903	1.974	1.951	1.948	1.926	1.946	1.921	1.933	1.981	1.953	1.954	1.947	1.957	1.975
Al	0.034	0.033	0.034	0.017	0.097	0.026	0.049	0.052	0.074	0.054	0.079	0.067	0.019	0.047	0.046	0.053	0.043	0.025
Al	0.027	0.017	0.064	0.038	0.021	0.033	0.017	0.036	0.076	0.043	0.056	0.035	0.026	0.026	0.018	0.022	0.026	0.008
Ti	0.003	0.003	0.004	0.002	0.011	0.004	0.006	0.007	0.012	0.004	0.011	0.007	0.004	0.007	0.003	0.003	0.005	0.001
Cr	0.002	0.000	0.001	0.000	0.000	0.001	0.000	0.002	0.000	0.008	0.000	0.003	0.003	0.000	0.000	0.000	0.001	0.002
Fe^{3+}	0.035	0.025	0.027	0.006	0.076	0.035	0.061	0.043	0.036	0.008	0.044	0.025	0.016	0.040	0.046	0.035	0.041	0.026
Fe^{2+}	0.349	0.234	0.246	0.280	0.833	0.348	0.682	0.429	0.319	0.168	0.274	0.262	0.160	0.430	0.467	0.337	0.392	0.233
Mn	0.005	0.009	0.005	0.009	0.011	0.009	0.021	0.008	0.000	0.006	0.005	0.005	0.004	0.021	0.012	0.015	0.017	0.010
Mg	0.656	0.740	0.728	0.703	0.094	0.606	0.264	0.623	0.661	0.842	0.722	0.732	0.828	0.547	0.518	0.621	0.570	0.730
Ca	0.886	0.958	0.873	0.932	0.928	0.926	0.881	0.817	0.845	0.907	0.835	0.909	0.935	0.899	0.910	0.945	0.905	0.970
K	0.001	0.000	0.001	0.000	0.001	0.000	0.000	0.000	0.000	0.000	0.000	0.000	0.000	0.000	0.000	0.000	0.000	0.000
Na	0.034	0.019	0.039	0.030	0.033	0.025	0.090	0.030	0.036	0.015	0.061	0.033	0.012	0.028	0.028	0.039	0.050	0.026
X_{Mg}	0.65	0.76	0.75	0.72	0.10	0.64	0.28	0.59	0.67	0.83	0.73	0.74	0.84	0.56	0.52	0.65	0.59	0.76

[a] total iron as FeO; [b] the molecular ratio $Fe^{3+}/(Fe^{3+} + Fe^{2+}) = Ox$ has been obtained from Mössbauer effect measurements (samples: 27I, 43I, 48I, 70I, 100I, 116III, 168I) or estimated from the ore assemblage.

but significantly higher (0.080—0.150 p.f.u.) in clinopyroxenes from the southwestern marginal zone and the granulite complex.

Since the entire Al^{VI}, Ti, Cr and part of the Fe^{3+} is needed to balance Al^{IV}, all Al may be assigned to a Tschermak's component.

Na contents depend on the Na content of the rock and its oxidation state. The positive correlation between the Na and the Fe^{3+} contents of the clinopyroxenes confirms that most of the Na is incorporated into the clinopyroxene solid solution as an acmite component (ranging from 1 to 10 mole per cent).

Regional development of clinopyroxene chemistry

Systematic changes in clinopyroxene composition along the profile are observed only with respect to its Al and Ti contents (Figs. 22 and 28). Low values of Al and Ti are characteristic for clinopyroxenes of the West Inari schist zone. Within the granulite complex the Al and Ti contents of clinopyroxene are higher. They increase within the southwestern marginal zone, attain maximum values in the southwestern part of the granulite complex and decrease slightly towards the northeastern marginal zone and the granite gneiss complex. This compositional trend may reflect a regional variation in temperature, because, at least in the model system $CaO-MgO-Al_2O_3-SiO_2$, high temperature favours the incorporation of a $CaAl_2SiO_6$ component into the clinopyroxene (Clark *et al.* 1962).

Garnet

Occurrence and textural relationships

Garnet is a common constituent of the amphibolites and hornblende gneisses of the West Inari schist zone and of the garnet–biotite, sillimanite–garnet–biotite, and sillimanite–garnet–cordierite gneisses of the granulite complex. Only rarely it has been found in the hypersthene-plagioclase gneisses of the granulite complex. In the rocks of the granite gneiss complex garnet is extremely rare.

In the amphibolitic rocks of the West Inari schist zone garnet forms roundish poikiloblasts distributed homogeneously in a nematoblastic to granoblastic matrix. Garnet of the clinopyroxene-bearing amphibolites is now often separated from clinopyroxene by a younger reaction zone consisting of hornblende and plagioclase (Fig. 14), indicating that in these rocks garnet + clinopyroxene were no longer in equilibrium during the postkinematic stage of recrystallization (M2). As discussed in the section on amphiboles, garnet + clinopyroxene remained, however, stable where X_{CO_2} was high.

In the gneisses of the granulite complex garnet occurs as porphyroblasts aligned in streaks and bands and is set in a granoblastic matrix consisting of quartz and feldspars. An early formation of garnet during M1 is indicated by small inclusions of quartz, feldspars, and fibrolitic sillimanite in the core of the garnet grains. The sillimanite needles are sometimes well oriented and define a relic schistosity. The garnet porphyroblasts are strongly corroded by quartz and feldspars. The lack of any deformation texture in these corrosion zones proves their formation during high-grade recrystallization and anatexis (M2).

In the high-grade migmatites of the northeastern part of the granulite complex garnet is sometimes replaced by cordierite + quartz symplectites and by myrmekitic intergrowths of plagioclase + quartz. Such replacement textures have been discussed by Henry (1974). They form in a complex, two-stage process initiated by a reactive intergranular fluid phase (see section on cordierite).

Table 17a

Microprobe analyses and structural formulae of garnets from amphibolites and hypersthene-plagioclase gneisses.

	WISZ				SWMZ			Granulite Complex				NEMZ	
	Gar Amphibolites				Gar-Hbl-Pyx Rocks			Gar-Hyp-Plag Gneisses				Gar-Cumm Amphibolites	
	1 LI		18 II		47 III	66 II	67 I	72 I	95 I	140 III	203 II	220 II	458 II
	core	rim	core	rim									
SiO_2	37.75	37.70	39.00	39.10	38.18	37.90	37.75	38.40	38.99	38.50	39.24	38.22	37.37
TiO_2	0.10	0.08	0.03	0.05	0.04	0.07	0.05	0.05	0.07	0.02	0.03	0.01	0.02
Al_2O_3	20.37	20.40	21.05	21.05	20.87	21.19	20.48	21.50	21.49	21.30	21.43	21.34	20.70
Cr_2O_3	0.05	0.04	0.03	0.04	0.04	0.03	0.01	0.03	0.07	0.02	0.03	0.00	0.00
FeO[a]	25.18	24.45	22.15	22.90	27.55	28.37	28.53	25.30	22.55	27.70	27.25	31.35	28.01
MnO	1.49	1.95	1.26	1.16	1.56	1.20	2.00	0.55	0.66	0.95	0.95	0.91	1.74
MgO	2.65	2.55	5.50	4.82	3.82	4.37	4.25	9.98	11.12	8.25	8.47	4.13	3.26
CaO	11.45	11.85	10.65	9.80	7.15	7.47	6.89	2.11	2.57	2.40	1.67	3.66	7.73
Total	99.04	99.02	99.67	98.92	99.21	100.60	99.96	97.52	99.14	97.92	99.07	99.62	98.83
Number of ions on the basis of 48 cation valences													
Si	6.030	6.023	6.059	6.119	6.069	5.958	5.998	6.042	6.018	5.997	6.066	6.065	6.003
Al						0.042	0.002			0.003			
Al	3.835	3.842	3.855	3.883	3.912	3.885	3.333	3.925	3.924	3.955	3.905	3.992	3.920
Ti	0.012	0.010	0.004	0.006	0.005	0.008	0.006	0.008	0.002	0.006	0.003	0.001	0.002
Cr	0.006	0.005	0.004	0.005	0.005	0.004	0.001	0.009	0.002	0.004	0.004	0.000	0.000
Fe[a]	3.363	3.266	2.877	2.996	3.662	3.729	3.790	2.921	3.620	3.303	3.522	4.159	3.762
Mn	0.202	0.264	0.166	0.154	0.210	0.160	0.269	0.087	0.126	0.073	0.250	0.122	0.237
Mg	0.631	0.607	1.273	1.124	0.904	1.024	1.006	2.567	1.922	2.322	1.951	0.977	0.780
Ca	1.959	2.028	1.772	1.643	1.205	1.258	1.173	0.426	0.402	0.353	0.277	0.622	1.330
X_{Mg}	0.16	0.16	0.31	0.27	0.20	0.22	0.21	0.47	0.35	0.41	0.36	0.19	0.17

[a] total iron as FeO

Alteration of garnet to chlorite is rare and restricted to zones which have suffered diaphthoresis.

Composition

The chemical composition of the garnets has been determined by the microprobe and, in addition, from the lattice constant and refractive index (Winchell 1958). The latter method also gives dependable results because the concentrations of the spessartite and andradite components are very low. A selection of microprobe analyses is given in Table 17, all analyses are represented in terms of end members in Fig. 23.

Garnet of all rock types exhibit almandine contents in the range 50—70 mole per cent. The variation can be related to changes in bulk rock chemistry and the specific ore and silicate mineral assemblages: Almandine-rich garnets typically occur in Fe-rich rocks devoid of ore minerals (e.g. amphibolites of the West Inari schist zone) or in rocks with magnetite, hematite and ilmenite (e.g. garnet–hypersthene–plagioclase gneisses of the granulite complex, see Appendix). Garnets poorer in almandine are characteristic of Fe-poor rocks (e.g. the light garnet–quartz–feldspar gneisses of the granulite complex) but also of more Fe-rich rocks bearing sulfides (e.g. sillimanite–garnet–cordierite gneisses of the granulite complex). Pyrite and pyrrhotite captured significant amounts of Fe in these rocks.

The pyrope, grossularite and spessartite contents of the garnets vary significantly with the rock type and metamorphic zone (Fig. 23, Table 17):

Table 17b
Microprobe analyses and structural formulae of garnets from gneisses.

	WISZ			Granulite Complex												NEMZ
	Qz-Fsp Gneisses			Sill-Gar Gneisses					Sill-Gar-Cord Gneisses					Gar Gneisses			Gar-Cord Gneiss
	6 I	8 II	31 I	65 I	69 III	76 II	96 I	223 I	89 I	110 III	158 I	161 I	169 I	70 II	I 7 I	111 I	424 II
SiO_2	37.47	36.35	37.38	38.84	38.40	39.23	39.81	38.40	38.26	38.25	38.03	37.33	37.95	40.15	39.60	39.73	37.80
TiO_2	0.08	0.00	0.03	0.01	0.02	0.04	0.02	0.02	0.04	0.06	0.09	0.06	0.08	0.06	0.07	0.08	0.05
Al_2O_3	20.47	20.97	20.05	22.53	22.61	22.53	22.59	22.33	21.20	22.50	21.27	21.03	22.10	22.53	22.29	21.86	22.00
Cr_2O_3	0.00	0.00	0.00	0.02	0.06	0.09	0.04	0.03	0.09	0.04	0.05	0.07	0.06	0.10	0.06	0.06	0.07
FeO[a]	25.50	32.75	24.35	29.04	27.16	29.60	24.93	29.01	27.74	26.30	29.80	30.10	26.40	29.18	30.75	29.74	32.20
MnO	3.92	1.71	5.73	0.34	0.30	0.26	0.28	0.35	0.46	0.29	0.29	0.33	0.30	0.33	0.60	0.64	0.87
MgO	2.89	3.19	1.60	8.86	9.15	8.20	9.54	8.39	10.96	11.65	9.06	8.31	11.45	8.91	8.01	6.90	5.90
CaO	8.11	1.27	10.31	1.11	1.27	1.22	1.15	0.90	1.30	1.07	0.83	0.86	1.00	1.26	1.37	3.08	1.00
Total	98.44	96.24	99.45	100.75	98.97	101.17	98.36	99.43	100.05	100.16	99.42	98.09	99.34	102.52	102.75	102.09	99.89
Number of ions on the basis of 48 cation valences																	
Si	6.040	6.028	6.025	5.956	5.952	6.002	6.118	5.970	5.906	5.845	5.949	5.942	5.853	6.036	6.000	6.062	5.960
Al				0.044	0.048			0.030	0.094	0.155	0.051	0.058	0.147				0.040
Al	3.889	4.099	3.809	4.028	4.083	4.059	4.092	4.062	3.763	3.890	3.872	3.889	3.870	3.992	3.981	3.932	4.049
Ti	0.009	0.000	0.004	0.001	0.002	0.005	0.002	0.002	0.005	0.010	0.011	0.007	0.009	0.007	0.008	0.009	0.006
Cr	0.000	0.000	0.000	0.002	0.007	0.011	0.005	0.004	0.011	0.005	0.006	0.009	0.007	0.012	0.007	0.007	0.009
Fe[a]	3.437	4.541	3.281	3.723	3.520	3.782	3.203	3.771	3.580	3.360	3.898	4.006	3.404	3.668	3.895	3.794	4.245
Mn	0.535	0.240	0.782	0.044	0.039	0.034	0.036	0.046	0.060	0.040	0.038	0.044	0.039	0.042	0.077	0.083	0.116
Mg	0.694	0.788	0.384	2.024	2.113	1.867	2.185	1.944	2.521	2.650	2.112	1.971	2.631	1.996	1.808	1.569	1.386
Ca	1.401	0.226	1.780	0.182	0.211	0.200	0.189	0.150	0.215	0.180	0.139	0.147	0.165	0.203	0.222	0.503	0.169
X_{Mg}	0.17	0.15	0.10	0.35	0.38	0.33	0.41	0.34	0.41	0.44	0.35	0.33	0.44	0.35	0.32	0.29	0.25

[a] total iron as FeO

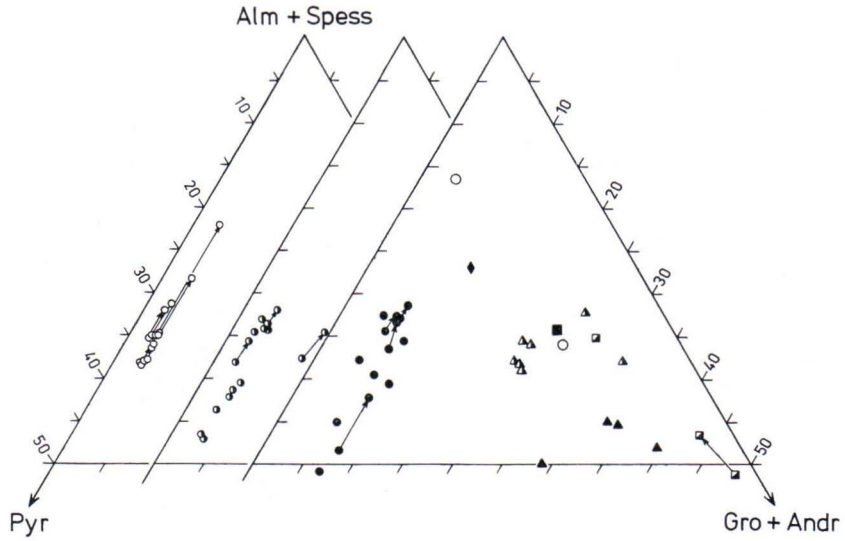

Fig. 23. Plot of garnet compositions in terms of end members. For the sake of clarity the data are presented in three separate triangles. Strong compositional zoning is indicated by the arrows pointing to the rim composition. Small open circles: sillimanite-garnet gneisses (granulite complex), half-filled circles: sillimanite-garnet-cordierite gneisses (granulite complex), dots: hypersthene-bearing rocks (granulite complex), large open circles: quartz-feldspar gneisses (West Inari schist zone), solid triangles: amphibolites and hornblende gneisses (West Inari schist zone), half-filled triangles: metabasites (southwestern and northeastern marginal zones), solid diamond: cummingtonite-bearing amphibolite (northeastern marginal zone), half-filled squares: hornblende-clinopyroxene rocks (granulite complex), solid square: amphibolite (granite gneiss complex).

High but variable grossularite contents (from 20 to 50 mole per cent) characterize the garnets of the amphibolites from the West Inari schist zone, whereas garnets from the rocks of the granulite complex exhibit generally very low and highly constant values: 2—3 mole per cent in the light sillimanite–garnet gneisses, 2.5—4 % in the sillimanite–garnet–cordierite gneisses and 4.5—9 % in the garnet–hypersthene gneisses. Garnets of the hornblende- and clinopyroxene-bearing gneisses of the southwestern marginal zone are transitional with respect to their grossularite content (about 20 mole per cent). The highest grossularite contents (up to 50 mole per cent) have been encountered in garnet from clinopyroxene–hornblende gneisses of the granulite complex.

The pyrope concentrations in the garnets of the amphibolites of the West Inari schist zone are rather low (7—20 mole per cent), but they become markedly higher in rocks of the granulite complex: 20—36 % in the garnet–quartz–feldspar gneisses, 28—43 % in the sillimanite–garnet–cordierite gneisses and 25—45 % in the garnet–hypersthene–plagioclase gneisses. Because in garnets from the granulite complex the concentrations of grossularite and spessartite are low, the pyrope contents are inversely related to the almandine contents.

The spessartite content is positively correlated to the MnO content of the rocks. Rather high and variable contents (from 3 to 14 mole per cent) have been encountered in garnets from the West Inari schist zone and the southwestern marginal zone, whereas garnets from the granulite complex are significantly lower in spessartite component (0.45—0.80 mole per cent in garnet–quartz–feldspar gneisses, 0.5—

1.5 % in sillimanite–garnet–cordierite gneisses and 1.5—5 % in garnet–hypersthene–plagioclase gneisses).

A semiquantitative estimate of the andradite component can be obtained from the occupancy of the Y position by Al. Garnets from the amphibolites of the West Inari schist zone exhibit values around 4 mole per cent, whereas those from the granulite complex attain some 1.5 per cent andradite component only. This figure is also supported by Mössbauer spectroscopic studies.

Zoning

Microprobe scans show that the bulk of the garnet grains is virtually unzoned with respect to the concentrations of Fe, Mg, Mn, and Ca. Only the outermost rims may exhibit a slight zoning.

In the garnets from the amphibolites of the West Inari schist zone Fe and Mg increase, and Ca and Mn decrease towards the edge. This trend corresponds to the regional changes in bulk garnet chemistry towards the granulite complex and might thus reflect the prograde paragenetic changes.

Garnets from hypersthene–plagioclase gneisses of the granulite complex show slightly increasing Fe and Mn contents and decreasing Mg and Ca contents in the outermost rims.

A different pattern of zonation is observed in garnets from all types of garnet gneisses of the granulite complex: Mn contents remain constant, Mg decreases, Fe and Ca increase towards the edge. This zoning is more pronounced at the contacts with cordierite and biotite grains, which then are also zoned, but with opposite trends.

The Fe–Mg zoning in the outer rims of garnets from the granulite complex can be described by Fe–Mg exchange reactions between garnet and the coexisting phases biotite, cordierite, and orthopyroxene. The thermodynamic models developed for these equilibria (see section on metamorphic conditions) indicate that the rims formed at lower temperatures compared to the bulk garnet. The zoning thus represents a retrograde effect. Similarly, the changes in Ca contents may be related to retrograde reequilibration by the divariant reactions discussed in more detail in the section on metamorphic conditions:

anorthite $\leftrightarrows$ grossularite + sillimanite + quartz (garnet gneisses)

enstatite + anorthite $\leftrightarrows$ $CaMg_2$ garnet + quartz (garnet–hypersthene–plagioclase gneisses).

According to Ghent (1976) the first-mentioned reaction, which is applicable to the garnet gneisses only, shifts towards higher grossularite contents in the garnet with decreasing temperature or increasing pressure. Based on molar volumes, an inverse effect is expected for the second reaction (cf. Wells 1979). Thus, both the increase of grossularite component towards the edge of garnets coexisting with plagioclase, sillimanite and quartz, and its decrease in garnets coexisting with plagioclase, orthopyroxene and quartz are consistent with a formation during falling temperatures.

Regional development of composition

In the garnets of the metabasic rocks distinct compositional changes occur along the profile. Towards the northeast the grossularite component decreases and the pyrope component increases (cf. Fig. 10): 32 Gross/10—20 Pyr (garnet amphibolites of the West Inari schist zone) → 22 Gross/17 Pyr (garnet–pyroxene–hornblende gneisses of the southwestern marginal zone) → 4—8 Gross/30—40 Pyr (garnet–hypersthene–plagioclase gneisses of the granulite complex). These changes are obviously related to the paragenetic changes and may be explained by continuous reactions involving garnet, plagioclase, amphibole, and garnet, plagioclase, orthopyroxene (Figs. 8 and 10). By the formation of plagioclases richer in An component the garnets change towards compositions poor in grossularite.

Besides, systematic though less pronounced compositional changes also occur along the profile within specific mineral assemblages. They are not related to bulk rock chemistry and, therefore, reflect regional variations in pressure and temperature of metamorphism, and the activities of the volatile species.

In rocks with the assemblage hypersthene + plagioclase + quartz the grossularite contents decrease from 7 % at Mukkapalo to some 4 % at Inarijärvi.

The pyrope contents of garnet in the sillimanite–garnet–cordierite gneisses of the granulite complex decrease from about 38 % near Kultala to 30 % at Inarijärvi.

The evaluation of these compositional changes of garnet by thermodynamic models will be presented in the section on metamorphic conditions. Only the data are described here.

Cordierite

Occurrence and textural relationships

Cordierite occurs only in the medium- to coarse-grained sillimanite–garnet–biotite gneisses and anatexites of the central and northeastern part of the granulite complex (Meriläinen 1976; see Figs. 1 and 9). It is thus restricted to a region which underwent an intense anatexis during the postkinematic stage of the Karelian metamorphism (M2). Platy quartz textures which characterize the cordierite-free garnet gneisses in the southwestern part of the granulite complex have been destroyed almost completely here by the mobilization and recrystallization.

Massive anatexites particularly rich in cordierite are well exposed along the road Sodankylä—Karigasniemi (E4, some 3 km S of Ivalo, near Ukonjärvi, and between Inari and Kaamanen) as well as along the road Inari—Kittilä 11 km SW of Inari.

The conspicuous translucent lilac blue cordierites form streaks and schlieren or may also occur as individual xenoblasts up to 1 cm in diameter dispersed in the matrix. In thin section it is easily recognized by the characteristic lamellar twinning and the yellow pleochroic haloes around inclusions of zircon.

Cordierite grew mainly in layers rich in biotite and sillimanite, corroding and including biotite, sillimanite and garnet, whilst K-feldspar, plagioclase and quartz recrystallized. The textural relations prove a late, postkinematic formation (M2) in an early stage of anatexis.

Cordierite + quartz symplectites replace plagioclase, biotite and garnet in the strongly mobilized anatexites occurring near the southwestern shores of Inarijärvi. Similar textures have been described by Henry (1974) from garnet-cordierite gneisses of southern Norway. Concomitant with the formation of cordierite + quartz symplectites biotite and garnet are replaced by quartz and plagioclase, often in myrmekitic intergrowths. Following Henry (1974) these textures can be basically explained by the following local equilibria

$$\text{plagioclase} + (\text{Fe, Mg})_{\text{fluid}} \leftrightarrows \text{cordierite} + \text{quartz} + (\text{Na, Ca, K})_{\text{fluid}}$$

$$\text{garnet} + (\text{Na, Ca, K, Si})_{\text{fluid}} \leftrightarrows \text{plagioclase} + (\text{Fe, Mg})_{\text{fluid}}$$

An active intergranular fluid phase thus mainly transported alkalies, Fe and Mg. However, the cycle given above is certainly not closed with respect to the Fe/Mg ratio. It is, therefore, assumed that biotite and ore minerals (mainly pyrrhotite) also participated.

During a late stage cordierite is replaced by fine-grained aggregates of white mica and chlorite. These pinites generally are restricted to grain edges or fractures but seem to increase in amount towards the granite gneiss complex in the northeast. These observations may tentatively

be interpreted by water fugacities increasing towards the northeast during the cooling stage at temperatures around 500°C (Seifert and Schreyer 1970).

Composition and structural state

The cordierites are of rather uniform, Mg-rich composition with 20—26 mole per cent Fe-cordierite component (cf. Fig. 12 b). The Mn-cordierite end member is extremely low (below 0.2 %) and the cordierites may be represented by the binary join Mg-cordierite–Fe-cordierite. Table 18 gives representative analyses, in addition to those reported by v. Doetinchem (1977).

The cordierite crystals are in general homogeneous, occasionally a retrograde rim poorer in Fe-cordierite component is developed at the contacts with garnet grains.

Cordierite can incorporate cations as well as molecular species into the channels of the structure. These account for the about 0.01 Na p.f.u. observed in the analyses, and for the CO_2 and H_2O contents (Table 18). Experimental data reported by Johannes and Schreyer (1977, 1979) indicate that the $X_{CO_2} = CO_2/(CO_2 + H_2O)$ in cordierites reflects the ratio of these species in the coexisting fluid. The gravimetric analysis for H_2O and CO_2 (Riley 1958) on very pure concentrates of cordierite (less than 1—2 % pinite and mica) resulted in high absolute gas contents and X_{CO_2} values in the range 0.17 to 0.40 (Table 18). Using the diagram given by Johannes and Schreyer (1977) for 600°C and 5 kbar this would correspond to a composition of the fluid phase with X_{CO_2} ranging from 0.35 to 0.85. However, because the closing temperature for the H_2O–CO_2 exchange process between cordierite and fluid is unknown to date, and because the fractionation will be temperature-dependent, the data by Johannes and Schreyer (1977, 1979) cannot be applied strictly. Nevertheless we conclude that the intergranular fluid was rather high in CO_2 during the cooling process. A CO_2-rich intergranular fluid during the peak of static crystallization (M2) is also evident from fluid inclusions of CO_2 in the quartz grains coexisting with cordierite (Klatt, pers. comm. 1978).

It should be pointed out that gravimetric CO_2 and H_2O determinations on these cordier-

Table 18

Microprobe analyses and structural formulae of cordierites. The lower table gives gravimetric analyses of water and carbon dioxide and the distortion index Δ (Miyashiro 1957). Samples arranged according to their position in the section studied (cf. Fig. 2).

	Granulite Complex					NEMZ
	Sill-Gar-Cord Gneisses					
	89 I	110 III	158 I	161 I	169 I	424 II
SiO_2 ...	47.20	47.65	48.15	47.33	47.30	46.92
Al_2O_3 ..	32.40	32.15	31.60	31.83	32.20	31.30
FeO[a] ...	4.95	5.03	5.33	6.19	5.40	6.52
MnO ...	0.04	00.01	0.02	0.03	0.00	0.08
MgO ...	10.85	10.83	10.09	9.83	10.80	8.99
Na_2O ..	0.07	0.08	0.08	0.06	0.20	0.23
Total ...	95.51	95.75	95.27	95.27	95.90	94.04
Number of ions on the basis of 36 cation valences						
Si	4.937	4.971	5.044	4.985	4.940	5.018
Al	1.063	1.029	0.956	1.015	1.060	0.982
Al	2.931	2.924	2.950	2.936	2.904	2.963
Fe[a]	0.433	0.439	0.467	0.545	0.472	0.583
Mn	0.004	0.001	0.002	0.002	0.000	0.007
Mg	1.691	1.683	1.576	1.551	1.681	1.433
Na	0.014	0.011	0.016	0.008	0.040	0.048
X_{Mg} ...	0.80	0.79	0.77	0.74	0.78	0.71

[a] total iron as FeO

	wt. %		molar ratio	Δ
	H_2O	CO_2	$H_2O/(H_2O+CO_2)$	
89 V	0.81	1.30	0.60	0.26
93 IV	0.91	0.84	0.73	0.26
204 I	1.15	0.91	0.75	0.26
198 III	1.08	0.99	0.73	0.27
158 I	1.15	1.20	0.70	0.25
158 II	1.13	1.12	0.72	0.27
158 IV	1.07	0.97	0.73	0.27
164 I	0.82	0.90	0.70	0.26
161 II	1.11	0.79	0.77	0.26
196 III	1.19	0.97	0.75	0.26
205 I	1.37	1.11	0.75	0.28
195 I	1.42	0.76	0.82	0.28
194 II	1.33	0.94	0.78	0.27
194 III	1.27	1.24	0.71	0.29
215 I	2.29	1.15	0.83	0.26

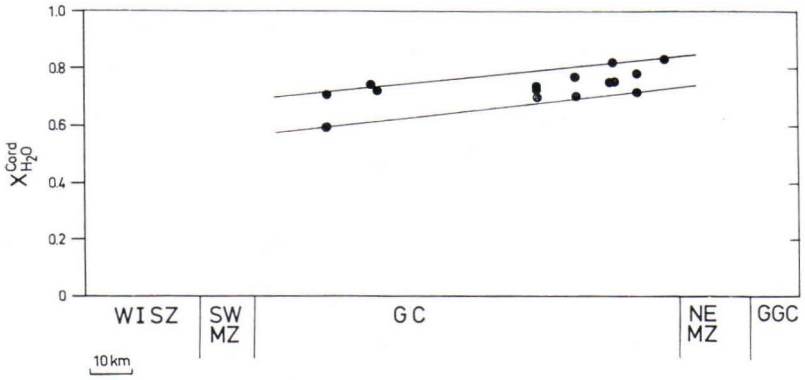

Fig. 24. Regional variation of X_{H_2O} (= $H_2O/(H_2O + CO_2)$ in mole proportions) in the fluid enclosed in the channels of the cordierite structure.

ites may be fallacious: It has been observed by microprobe on Be-coated samples that the cordierites investigated sometimes contain minute inclusions of graphite in addition to the CO_2 enclosed in the channels of the structure. Since the graphite can be oxidized by the water released, the analytic CO_2 values might be too high. Therefore, an infrared spectroscopic technique is in preparation.

The distortion index Δ (Miyashiro 1957) which describes the deviation of the cordierite structure from hexagonal symmetry, varies between 0.25 and 0.29 and probably increases systematically towards the northeast. This might be due to the H_2O contents which also increase in this direction (see below) and would support the relationships between H_2O content and distortion index postulated by Stout (1975), although the effect of CO_2 is unknown. For a comprehensive review of the interpretation of Δ values the interested reader is referred to the papers by Langer and Schreyer (1969, 1976).

Regional development of composition

Along the profile studied the composition of the cordierite varies only slightly. The $X_{Fe}^{cordierite}$ values increase from 0.23 near Kultala to 0.25 near Inarijärvi. Since cordierite is always in contact with garnet, biotite, sillimanite, K-feldspar and quartz, its X_{Fe} should only depend on P_{total}, P_{H_2O}, and temperature (Holdaway and Lee 1977). The petrological analysis of the Fe–Mg distribution between cordierite, garnet and biotite (see section on metamorphic conditions) may, however, be complicated by the incorporation of components such as Ca into garnet, Fe^{3+} and Ti into biotite, and Na into the K-feldspar (cf. v. Doetinchem 1977).

The general increase of X_{H_2O} in cordierites towards the northeastern parts of the granulite complex points to an increased water fugacity in the intergranular fluid (Fig. 24). Hence, the regional variation of cordierite composition in terms of the Fe and Mg end members may be attributed to a varying activity of water.

Biotite

Occurrence and textural relationships

Biotite can occur in all rock types of the profile investigated as a minor to major constituent.

Its modal amount is very low in the quartz–feldspar gneisses and amphibolites of the West Inari schist zone but is generally higher in intermediate to basic hypersthene–plagioclase rocks of the granulite complex. Here it can be replaced by late hornblende and the recrystallizing quartz–feldspar matrix.

In the fine-grained and distinctly foliated garnet gneisses of the southwestern part of the granulite complex biotite is enriched in streaks,

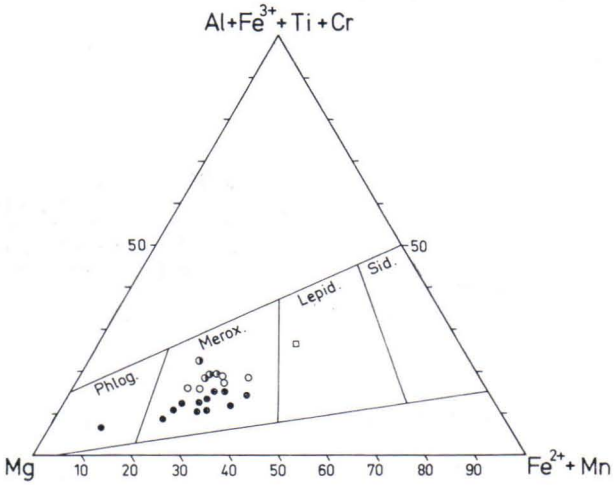

Fig. 25. Biotite compositions in a Mg—(Fe^{2+} + Mn)—(Al + Fe^{3+} + Ti + Cr) projection (Tröger 1971). Dots: hypersthene-plagioclase rocks (granulite complex), open circles: sillimanite-garnet gneisses (granulite complex), half-filled circles: sillimanite-garnet-cordierite gneisses (granulite complex), square: quartz-feldspar gneiss (West Inari schist zone).

whereas garnet occurs mainly in the light quartz–feldspar-rich bands. The formation of garnet proceeded by prograde decomposition of biotite according to the at least divariant reaction

biotite + sillimanite + quartz ⇆ garnet + K-feldspar + H_2O.

The banding may be explained by one or several of the following processes: local differences in water fugacity, primary differences in bulk rock chemistry leading to an early consumption of one of the reactant phases (e.g. quartz), or metamorphic segregation induced by the deformation.

In the coarse-grained foliated to massive garnet gneisses and sillimanite–garnet–cordierite gneisses of the northeastern part of the granulite complex biotite, garnet, cordierite, and sillimanite form dark coloured streaks and schlieren. The modal amount of biotite in these rock types is highly variable but increases markedly towards the northeastern marginal zone and the granite gneiss complex. Concomitantly the amounts of cordierite and garnet decrease. Thus, the modal amounts of the phases may be controlled by the equilibrium

biotite + sillimanite + quartz ⇆ cordierite + garnet + K-feldspar + H_2O

which, under constant temperature and total pressure, is shifted to the left hand side with increasing water fugacity (Holdaway and Lee 1977).

In the high-grade anatexites at Inarijärvi biotite may be replaced by vermicular quartz and K-feldspar.

The textural relationships of biotite prove that it was a stable phase during the synkinematic stage of metamorphism (M1) both in the West Inari schist zone and in the granulite complex, since it defines the foliation and schistosity of the rocks. Especially in the central and northeastern part of the granulite complex biotite recrystallized during the postkinematic anatectic stage (M2), lost its preferred orientation and formed coarse flakes in the anatectic mobilizates.

Composition

Biotites vary in composition from phlogopite to lepidomelane (Fig. 25), most samples plotting in the field of meroxene (Tröger 1971). Representative analyses are given in Table 19.

The composition of the biotites critically hinges on bulk rock chemistry (Fig. 16d), silicate and ore mineral assemblage and position of the sample within the profile studied.

Table 19a

Microprobe analyses and structural formulae of biotites from hypersthene-plagioclase rocks of the granulite complex.

	WISZ			Granulite Complex												
	Qz-Fsp Gneisses			Sill-Gar Gneisses					Sill-Gar-Cord Gneisses					Gar Gneisses		
	6 I	8 II	31 I	65 I	69 III	76 II	96 I	223 I	89 I	110 III	158 I	161 I	169 I	70 II	J 7 I	111 I
SiO_2	36.70	34.87	37.20	36.04	37.80	35.55	36.49	37.25	36.60	36.00	36.50	35.43	35.75	34.69	37.80	37.11
TiO_2	2.54	1.99	3.20	5.34	5.73	5.05	5.60	5.03	5.14	5.88	4.88	5.52	5.40	5.43	5.37	4.51
Al_2O_3	16.17	16.60	15.30	16.11	15.75	16.62	15.02	16.44	15.40	14.70	15.60	15.10	16.15	14.74	15.55	14.88
Cr_2O_3	0.00	0.00	0.00	0.07	0.13	0.15	0.07	0.06	0.14	0.09	0.12	0.16	0.10	0.38	0.03	0.04
FeO[a]	18.67	21.93	22.80	13.17	12.32	12.99	8.96	13.65	11.60	12.47	16.15	14.55	14.60	17.03	13.46	13.12
MnO	0.34	0.12	0.32	0.00	0.00	0.00	0.00	0.00	0.02	0.01	0.05	0.03	0.02	0.00	0.00	0.00
MgO	9.90	8.07	7.04	13.47	13.60	13.92	15.11	13.37	15.55	14.33	11.45	12.85	12.75	13.34	13.68	14.86
CaO	0.00	0.01	0.06	0.00	0.00	0.05	0.02	0.00	0.00	0.00	0.00	0.02	0.03	0.10	0.00	0.00
K_2O	9.50	8.49	9.47	9.36	9.18	9.60	9.76	9.27	7.91	9.53	9.44	9.42	9.10	9.28	9.93	9.08
Na_2O	0.03	0.00	0.10	0.11	0.15	0.07	0.21	0.04	0.13	0.15	0.18	0.08	0.30	0.13	0.07	0.09
Total	93.85	92.08	95.49	93.67	94.66	94.00	91.24	95.11	92.49	93.16	94.37	93.16	94.20	95.12	95.89	93.69
Ox[b]	0.180	0.233	0.233	0.137	0.207	0.130	0.133	0.089	0.116	0.133	0.133	0.177	0.132	0.133	0.128	0.066
Number of ions on the basis of 44 cation valences																
Si	5.609	5.483	5.663	5.403	5.550	5.317	5.534	5.504	5.395	5.438	5.509	5.330	5.367	5.254	5.510	5.476
Al	2.391	2.517	2.337	2.597	2.450	2.683	2.466	2.496	2.605	2.562	2.491	2.670	2.633	2.631	2.490	2.524
Al	0.522	0.560	0.409	0.250	0.276	0.247	0.219	0.367	0.071	0.055	0.284	0.007	0.225		0.182	0.064
Cr	0.000	0.000	0.000	0.008	0.015	0.018	0.008	0.007	0.016	0.011	0.014	0.019	0.012	0.045	0.003	0.005
Ti	0.292	0.235	0.366	0.602	0.632	0.568	0.638	0.559	0.570	0.668	0.554	0.624	0.609	0.618	0.588	0.500
Fe^{3+}	0.429	0.665	0.676	0.230	0.313	0.217	0.170	0.148	0.203	0.209	0.271	0.364	0.243	0.287	0.227	0.129
Fe^{2+}	1.956	2.191	2.226	1.443	1.198	1.448	0.966	1.523	1.547	1.366	1.767	1.698	1.603	1.869	1.546	1.829
Mn	0.044	0.016	0.041	0.000	0.000	0.000	0.000	0.000	0.002	0.001	0.006	0.004	0.003	0.000	0.000	0.000
Mg	2.225	1.891	1.597	3.009	2.975	3.10 -	3.145	2.944	3.416	3.225	2.575	2.880	2.852	3.010	2.971	3.268
Ca	0.000	0.002	0.010	0.000	0.000	0.008	0.003	0.000	0.000	0.000	0.000	0.003	0.005	0.016	0.000	0.000
K	1.852	1.703	1.839	1.790	1.719	1.831	1.888	1.747	1.487	1.836	1.817	1.808	1.743	1.793	1.846	1.709
Na	0.009	0.000	0.030	0.032	0.043	0.020	0.062	0.011	0.037	0.044	0.053	0.023	0.087	0.038	0.020	0.026
X_{Mg}	0.54	0.46	0.42	0.68	0.71	0.68	0.78	0.66	0.69	0.70	0.59	0.63	0.64	0.58	0.72	0.64

[a] total iron as FeO; [b] the molecular ratio $Fe^{3+}/(Fe^{3+} + Fe^{2+}) = Ox$ has been determined by wet chemical analysis, or estimated from the ore assemblage (samples: 6I, 31I, 70II, 110III, 158I, 169I).

Table 19b
Microprobe analyses and structural formulae of biotites from gneisses.

	Granulite Complex													
	Hyp-Gar-Plag Gneisses				Hyp-Plag Rocks					Hyp-Cpx-Hbl-Plag Gneisses				
	72 I	95 I	140 III	203 II	59 II	83 I	125 I	141 I	J 1 I	70 I	100 I	116 III	170 II	I 12 I
SiO_2	38.05	35.70	36.90	36.92	35.90	34.50	36.23	37.50	36.20	36.64	38.70	36.65	38.80	37.10
TiO_2	5.42	5.93	4.62	4.14	4.31	5.31	5.10	3.97	5.13	4.83	2.12	3.65	4.88	5.59
Al_2O_3	13.75	13.27	13.60	16.14	14.30	14.77	14.23	14.00	13.70	14.48	13.50	13.50	13.25	13.55
Cr_2O_3	0.11	0.05	0.04	0.00	0.08	0.03	0.04	0.00	0.09	0.03	0.37	0.09	0.49	0.06
FeO[a]	11.15	16.70	10.56	14.07	14.10	15.43	13.40	9.96	15.50	13.79	5.60	13.85	8.89	14.30
MnO	0.03	0.11	0.00	0.12	0.06	0.02	0.02	0.18	0.06	0.03	0.02	0.01	0.02	0.10
MgO	16.05	12.20	16.65	14.20	15.30	12.73	15.33	18.25	13.40	15.00	22.00	15.50	18.84	14.90
CaO	0.00	0.00	0.00	0.00	0.00	0.00	0.00	0.00	0.03	0.00	0.50	0.04	0.00	0.01
K_2O	9.99	9.58	9.64	9.77	9.12	9.39	9.53	9.29	9.61	9.16	10.00	9.68	9.45	9.82
Na_2O	0.04	0.10	0.00	0.11	0.28	0.14	0.00	0.12	0.01	0.18	0.18	0.10	0.10	0.06
Total	94.59	93.64	92.01	95.47	93.45	92.32	93.88	93.27	93.73	94.14	92.99	93.07	94.72	95.49
Ox[b]	0.108	0.098	0.118	0.115	0.158	0.163	0.158	0.129	0.102	0.128	0.219	0.146	0.101	0.203
Number of ions on the basis of 44 cation valences														
Si	5.534	5.465	5.520	5.464	5.376	5.337	5.406	5.529	5.481	5.503	5.649	5.576	5.634	5.486
Al	2.357	2.395	2.398	2.536	2.524	2.663	2.503	2.433	2.445	2.497	2.323	2.421	2.268	2.362
Al				0.280		0.030				0.066				
Cr	0.013	0.006	0.005	0.000	0.010	0.004	0.005		0.011	0.004	0.043	0.011	0.056	0.007
Ti	0.593	0.682	0.520	0.461	0.485	0.617	0.572	0.440	0.584	0.545	0.233	0.417	0.533	0.621
Fe^{3+}	0.182	0.221	0.188	0.200	0.314	0.325	0.288	0.181	0.215	0.215	0.171	0.258	0.117	0.369
Fe^{2+}	1.505	2.025	1.404	1.541	1.673	1.675	1.533	1.220	1.899	1.467	0.610	1.504	1.038	1.448
Mn	0.004	0.014	0.000	0.015	0.008	0.003	0.003	0.022	0.008	0.004	0.002	0.001	0.002	0.013
Mg	3.478	2.783	3.711	3.132	3.414	2.934	3.408	4.009	3.023	3.357	4.785	3.514	4.076	3.283
Ca	0.000	0.000	0.000	0.000	0.000	0.000	0.000	0.000	0.005	0.000	0.078	0.007	0.000	0.002
K	1.853	1.871	1.839	1.845	1.742	1.853	1.814	1.747	1.856	1.755	1.862	1.879	1.750	1.852
Na	0.011	0.030	0.000	0.030	0.081	0.042	0.000	0.034	0.003	0.052	0.051	0.030	0.028	0.017
X_{Mg}	0.70	0.58	0.73	0.67	0.67	0.64	0.69	0.77	0.61	0.70	0.89	0.70	0.80	0.68

[a] total iron as FeO; [b] the molecular ratio $Fe^{3+}/(Fe^{3+} + Fe^{2+}) = Ox$ has been determined by wet chemical analysis or estimated from the ore assemblage (samples: 70I, 116III, 203II)

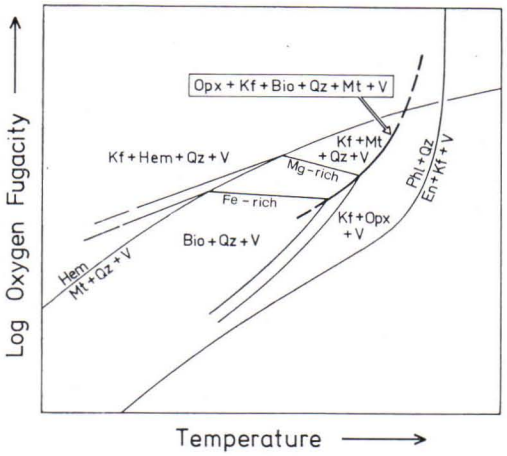

Fig. 26. Schematic isobaric stability diagram of biotite solid solution according to Wones and Eugster (1965). Along the isobarically univariant curve orthopyroxene + K-feldspar + biotite + quartz + magnetite + vapour biotites decrease in X_{Fe} with increasing temperature and log fO_2

Fe-rich biotites ($X_{Fe} > 0.5$) only occur in the quartz–feldspar gneisses and hornblende–clinopyroxene gneisses of the West Inari schist zone, which have sphene as excess Ti-phase. These biotites are distinguished from those from the granulite complex by their high Al^{VI} and Fe^{3+} but low Ti contents (Table 19).

Biotites from hypersthene–plagioclase rocks of the granulite complex vary from $X_{Fe} = 0.11$ to $X_{Fe} = 0.42$ due to large variation in bulk rock chemistry. Phlogopites ($X_{Fe} < 0.2$) are restricted to the rare ultramafic rock types. The X_{Fe} of both biotites and bulk rocks is generally controlled by oxygen fugacity, which is reflected in the specific ore mineral assemblage: If rocks with equal silicate assemblage are considered, biotites from ilmenite + magnetite -bearing rocks have higher X_{Fe} than those from rocks without oxidic ore phases but with sulfides (see Appendix). In terms of the log f_{O_2}—T stability relations derived by Wones and Eugster (1965, Fig. 12) the decrease in X_{Fe} with decreasing f_{O_2} can be explained by the instability of Fe-rich biotites at low f_{O_2} provided the oxygen fugacity is below that controlled by the assemblage biotite + sanidine + magnetite + quartz + orthopyroxene + gas (Fig. 26). Total Al contents are low and mainly incorporated into the tetrahedral layer. Charge balance between octahedral and tetrahedral layer is achieved by the incorporation of Fe^{3+}, Ti^{4+} and Cr^{3+} into the former. Ti contents are high in these biotites which always coexist with hematite-ilmenite solid solution as an excess Ti phase. They attain values up to 0.7 Ti p.f.u. which represents the upper limit encountered in biotites of similar paragenetic rock types (Sobolev 1972). The correlation between the contents of the individual cations (Fig. 27) suggests that Ti is introduced into the octahedral layer by two different substitutions

$$Si + Al^{VI} \leftrightarrows Al^{IV} + Ti \text{ and}$$
$$2\,(Mg,\ Fe^{2+}) \leftrightarrows \square + Ti$$

A structural explanation for the negative correlation between Mg on the one side and Ti and Al^{IV} on the other, which is obvious from Fig. 27, has been proposed by Guidotti *et al.* (1977).

Biotites from sillimanite–garnet gneisses and sillimanite–garnet–cordierite gneisses of the granulite complex are Al-rich meroxenes with X_{Fe} ranging from 0.42 to 0.28 (Table 19). In addition to the effects of rock bulk composition the X_{Fe} of the biotite is also influenced by the presence or absence of sulfides: The sulfide-bearing garnet–cordierite gneisses have biotites slightly richer in Mg, because part of the Fe^{2+} available is bounded to the sulfides.

Compared to the biotites of the hypersthene-bearing rocks the Al contents of these biotites are higher, particularly in the sillimanite-garnet gneisses. Since excess Al^{IV} (excess relative to ideal phlogopite–annite) roughly equals $Al^{VI} + Fe^{3+}$, a substitution

$$Si + (Mg,\ Fe^{2+}) \leftrightarrows (Al^{VI},\ Fe^{3+}) + Al^{IV}$$

can be assumed.

The Ti contents are of a similar magnitude as in the biotites of the hypersthene-bearing rocks. Excess Ti phases are rutile (in the sillimanite–garnet gneisses) and rutile and/or ilmenite in the

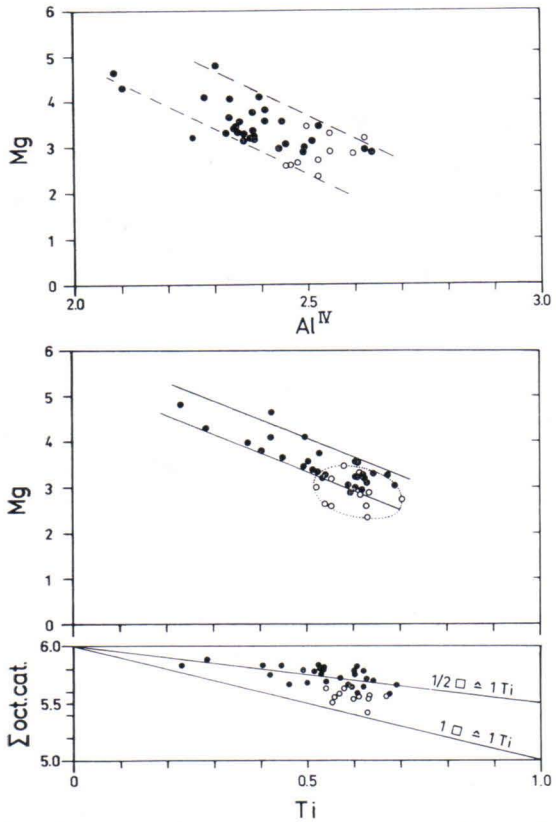

Fig. 27. Correlation between Al^{IV} and Mg (top), Mg and Ti (middle), and octahedral occupancy and Ti (bottom) in biotites from hypersthene-plagioclase rocks (dots) and garnet gneisses (circles). For discussion see text.

garnet–cordierite gneisses. Ti is essentially incorporated into the biotite by a substitution 2 (Mg, Fe^{2+}) ⇆ □ + Ti.

Regional development of composition

The Ti contents of the biotites show a systematic variation along the profile (Fig. 28): Within the West Inari schist zone a continuous increase from 0.23 to 0.45 Ti p.f.u. is recognized when the granulite complex is approached. This trend leads without break to the very high Ti contents (up to 0.7 Ti p.f.u.) encountered in the biotites of the southwestern part of the granulite complex. Within the granulite complex a slight decrease in Ti towards the northeast is probable but not documented well enough.

It is generally accepted that the Ti content of biotite coexisting with an excess Ti phase is essentially determined by temperature (cf. Engel and Engel 1960, Kwak 1968, Sobolev 1972, Guidotti *et al.* 1977). According to Sobolev (1972) an increase in metamorphic grade from amphibolite to granulite facies leads, on the average, to an increase in Ti from 0.24 to 0.41 Ti p.f.u. in biotites from micaschists and gneisses and from 0.25 to 0.49 Ti p.f.u. in biotites from metabasites, respectively.

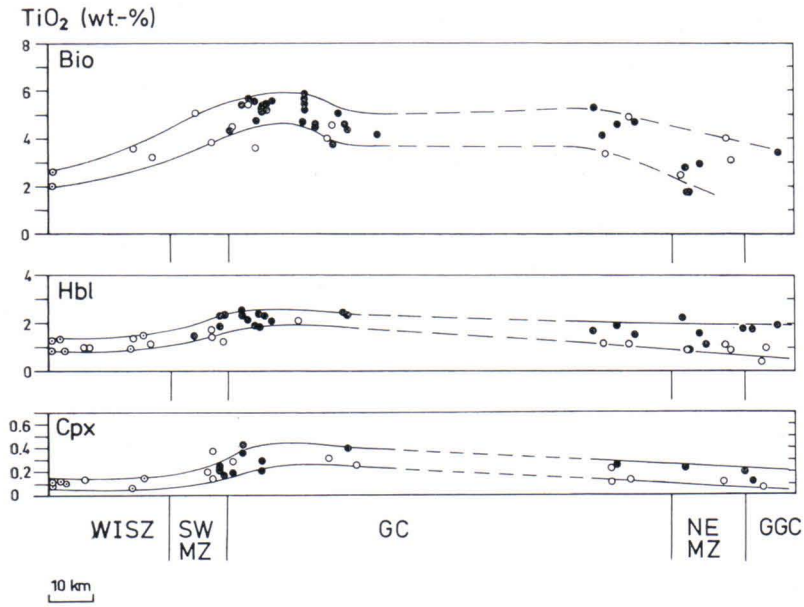

Fig. 28. Regional variation of TiO_2 contents in biotites, hornblendes, and clinopyroxenes. Minerals coexisting with ilmenite (dots), with sphene (centered circles), without Ti minerals (open circles). Note the maximum in TiO_2 contents in the southwestern part of the granulite complex.

Although this trend is also reflected in the data of the profile studied (low Ti contents in biotites from the amphibolite facies rocks of the West Inari schist zone — high Ti contents in biotites from rocks of the granulite complex) it is obvious from the data given in Table 19 and the Appendix that both X_{Fe} of the biotite and the kind of excess Ti phase present influence the Ti content of the biotite as well.

The regional variations in Mg, Al^{IV} and Al^{VI} contents cannot be related to metamorphic grade directly because they critically depend on bulk composition, oxidation ratio and mineral assemblage.

Plagioclase

Occurence and textural relationships

Plagioclase is an essential constituent in the metabasites and gneisses of the West Inari schist zone and the granulite complex being, however, subordinate in amount with respect to alkali feldspar in the garnet–cordierite gneisses and the sillimanite-rich garnet–biotite gneisses.

In the amphibolites of the West Inari schist zone and the marginal zones of the granulite complex plagioclase occurs in the form of xenoblastic grains with subordinate lamellar twinning. In the quartz–feldspar gneisses hypidiomorphic plagioclases are found in addition which exhibit abundant lamellar twinning, occasionally antiperthitic exsolution and normal zoning, possibly suggesting a magmatic origin of the rocks. At the contacts with K-feldspar grains myrmekitic intergrowths are often developed.

In the granulite complex plagioclase mostly forms xenoblastic grains of the granoblastic matrix. They are in general twinned according to the albite law, only in the bytownites and anorthites of some hypersthene–plagioclase rocks the pericline law and complex twinning predominates. Coarse antiperthitic exsolution and myrmekitic intergrowths are frequent.

Retrograde alteration in tectonized zones (e.g. 5 km NE of Kuttura, and in the north-eastern marginal zone) led to the formation of scapolite, epidote, and sericite from plagioclase.

Anorthite content

Determinative methods: The anorthite content has been measured optically by the universal stage from the extinction angle normal to [100] (Rittmann 1929, revised diagram given by Burri *et al.* 1967) and by the Tsuboi (1934) method (diagram taken from Morse 1968). For comparison and for a determination of the K-feldspar content about 50 samples have been analyzed by the microprobe, too. The latter data agree within $\pm$ 3 mole per cent anorthite content with the results of the Tsuboi method. On the other hand, systematically high An contents (+ 5 %) are obtained from the extinction method in the range An 40-60. These discrepancies are probably related to the dependence of the extinction angle on the structural state of the plagioclases: X-ray powder data (see below) indicate that plagioclases of this compositional range are not completely ordered.

Dependence on assemblage and bulk rock chemistry: The An contents of the plagioclases exhibit a marked dependence on the chemical composition of the host rocks and the mineral assemblage. Fig. 29 shows that the An contents are mostly controlled by the $Na_2O/(CaO + Na_2O)$ ratio of the host rock. However, because the plagioclase is not the only Ca- and Na-bearing mineral in these rocks, a dependence on the mineral assemblage can be expected (Fig. 30). In the West Inari schist zone the An contents of plagioclases in the quartz-feldspar gneisses and amphibolites fall into the welldefined ranges An 0—An 25 and An 25—An 60, respectively. In the granulite complex the anorthite contents of the plagioclases from sillimanite-garnet gneisses and garnet–cordierite gneisses define a distinct maximum at An 29, whereas for the

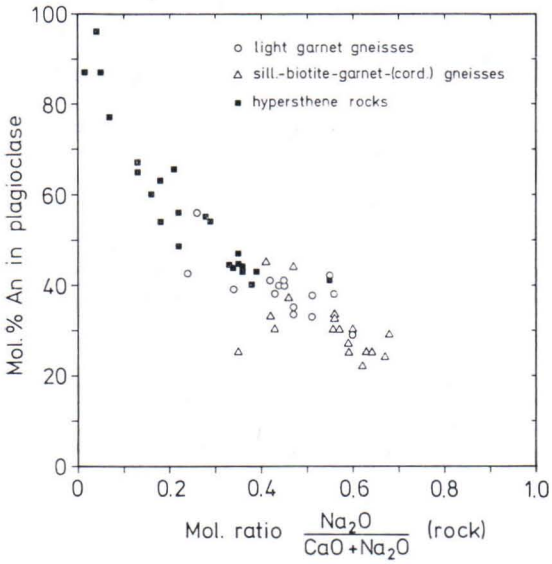

Fig. 29. Dependence of anorthite content in plagioclase on the $Na_2O/(Na_2O + CaO)$ ratio of the bulk rock in the granulite complex.

light garnet gneisses and garnet–biotite gneisses a skew frequency histogram with a maximum at An 35 is obtained. All these garnet gneisses are thus characterized by a rather small variation in plagioclase composition in the range An 20—An 40.

On the other hand, plagioclases from the hypersthene-bearing rocks show a wide variation from about An 30 to An 95, which does not hinge critically on the particular mineral assemblage. Only in the garnet–orthopyroxene–plagioclase rocks An contents are restricted to 40—50 %. Plagioclases with An 60 to An 80 are comparatively rare and, when present, always strongly zoned and exsolved. The width and spacing of the lamellae vary systematically with the composition of the plagioclase grain. The range in which exsolution could be observed by the microscope closely corresponds to the Huttenlocher miscibility gap (Nissen 1974, Smith 1974).

Zoning: In the West Inari schist zone plagioclases from amphibolites are frequently inversely zoned. The An contents generally increase from An 35—An 40 in the core to An 40—An 50 at the rim, probably due to the continous reaction

clinopyroxene + garnet + $H_2O \leftrightarrows$ hornblende + anorthite

(cf. Fig. 14). Occasionally an outermost Ab-rich rim (about An 30) is developed. It can be assigned to a diaphthoretic episode. Similarly, plagioclase (about An 20) of the light biotite- or hornblende-bearing gneisses has albitic rims (An 0—An 8).

Plagioclases from rocks of the granulite complex with compositions in the ranges An 20—An 55 and An 80—An 100 are either homogeneous or only weakly zoned, but display reverse zoning in the range An 55—An 80. In these plagioclases the core compositions vary from An 55 to An 65 and the rims from An 75 to An 90. Zones with compositions between An 60 and An 80 are exsolved (Fig. 30).

Regional development of An contents: Due to the strong dependence of An contents on bulk rock chemistry any regional variation of pressure and temperature along the profile might not be evident from the plagioclase compositions. However, trends may show up if plagioclases of rocks with similar composition are considered. Systematic changes are observed in rocks of basaltic composition: In the amphibolites of the West Inari schist zone the An contents of the plagioclases are close to 40 %, whereas the chemically similar hypersthene-bearing rocks of the granulite complex have anorthite contents in the range 55—80 %. The abrupt increase of An contents which occurs within the southwestern marginal zone can be related to the model reaction

hornblende + garnet $\leftrightarrows$ orthopyroxene + anorthite (in plagioclase) + H_2O

which may be taken to define the limit of the amphibolite versus the granulite facies.

Structural state

The angular separation of the 131—$1\bar{3}1$ X-ray powder diffraction peaks of plagioclases plotted against the An content (Fig. 31) gives an

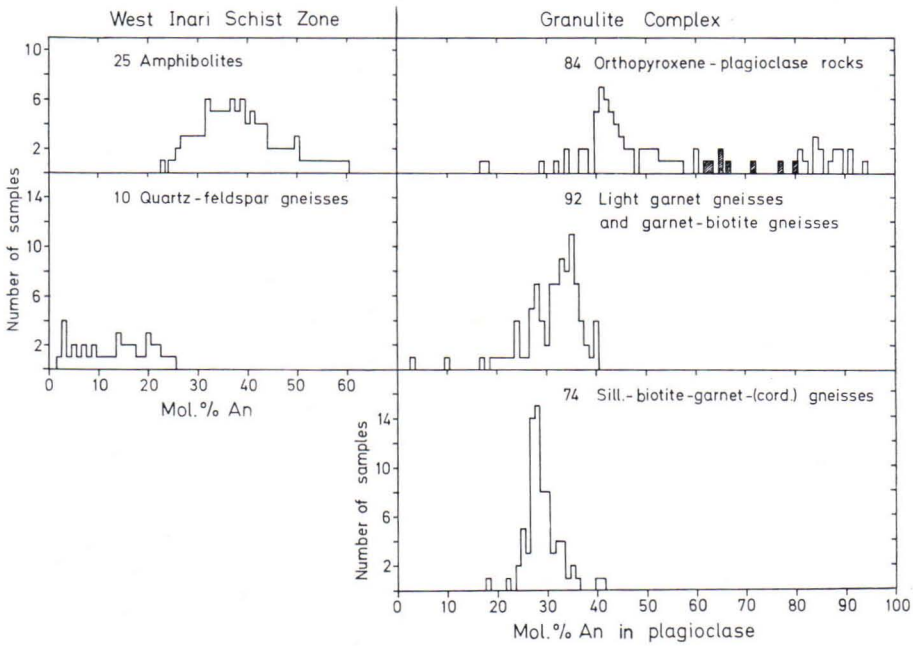

Fig. 30. Frequency distribution of anorthite contents in plagioclase from the different rock types. Hatched areas in the An60—An80 range indicate exsolved plagioclases (cf. text).

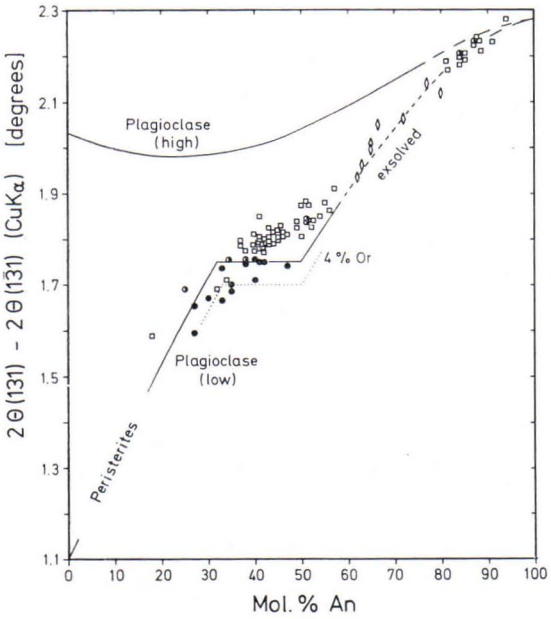

Fig. 31. Angular separation of 131 and $1\bar{3}1$ peaks vs. anorthite content in plagioclases from amphibolites of the West Inari schist zone (dots), amphibolites and metatroctolite of the southwestern marginal zone (half-filled circles), hypersthene-plagioclase rocks of the granulite complex (open squares, and diamonds for exsolved phases). The lines for the different structural states and Or content are taken from Bambauer et al. (1967). Note the deviation of the data points from the plagioclase (low) curve in the range An40—An55.

indication of the Al–Si order in these minerals (Bambauer *et al.* 1967). Plagioclases from rocks of the West Inari schist zone plot close to the curve representing maximum Al–Si order whereas those from the hypersthene-bearing rocks of the granulite complex deviate markedly in the range An 40—An 55 towards less ordered states. These deviations become even larger if

the effect of the K-feldspar component, which is in the order of 2 per cent, is taken into account. Possibly maximum order in these phases could not be achieved during cooling due to the lack of a coexisting hydrous fluid. The relationships could not be clarified in the range An 60—An 80 due to the zonation and exsolution of the plagioclases and in the range An 80—An 100 where the curves of maximum order and maximum disorder approach.

Alkali feldspars

Occurrence and textural relationships

Within the West Inari schist zone and the southwestern marginal zone alkali feldspars are main constituents of the quartz–feldspar gneisses and of the fine-grained hornblende gneiss near Ivalon Matti and form xenoblastic grains of the ground mass. Larger crystalloblasts include and corrode plagioclase and quartz. Replacement by myrmekite is a common feature.

In the granulite complex alkali feldspar occurs in the light garnet gneisses, the sillimanite–garnet–biotite gneisses, garnet–cordierite gneisses but only in some of the hypersthene–plagioclase rocks. It is frequently the main constituent of the granoblastic matrix but can also form porphyroblasts. Grain contacts with garnet, sillimanite, biotite, cordierite and hypersthene indicate equilibrium assemblages with these minerals. In the hypersthene-plagioclase rocks and the garnet–biotite gneisses alkali feldspar is frequently present as patches of antiperthite within the plagioclase.

Structural state

For a characterization of the Al–Si order the optic angle ($2V\alpha$) has been measured in a large number of samples. In addition, the lattice constants have been determined by X-ray powder techniques on 24 selected samples (Table 20).

Optical data: The optic axial angle of alkali feldspars depend both on the structural state and, to a lesser extent, on chemical composition. Because the albite component in the K-feldspar phase of the perthites is low in all rock types studied (3—8 % Ab according to the cell volumina, see below), the optic axial angle mainly reflects the Al–Si order.

According to the regional variation of $2V\alpha$ (Fig. 32) four different zones may be distinguished:

Zone 1: West Inari schist zone and the main part of the southwestern marginal zone (high-grade amphibolite facies) $2V\alpha \approx 80°$.

Zone 2: southwestern part of the granulite complex $2V\alpha = 50—70°$.

Zone 3: central and northeastern part of the granulite complex: $2V\alpha = 60—80°$.

Zone 4: northeastern marginal zone and granite gneiss complex: $2V\alpha = 80—85°$.

In addition to these systematic differences in $2V\alpha$ the alkali feldspars of the individual zones are characterized by the following properties:

Alkali feldspars of zones 1 and 4 show only rare and rather coarse perthite exsolution, marked cross-hatched twinning, and an extinction angle $Z \wedge \perp(010)$ of about 18°. The optical properties classify these K-feldspars as highly ordered microclines.

Alkali feldspars of zone 2 generally exhibit hair perthite and, in larger grains, coarser spindle perthite in addition (cf. Eskola 1952). The extinction $Z \wedge \perp(010)$ varies within a single grain, it ranges from 0—5° and rarely up to 18° in individual diffuse twin lamellae. These alkali feldspars thus closely correspond to microperthitic orthoclase.

In zone 3 alkali feldspars are characterized by rather coarse perthite exsolution lamellae or spindles and a second generation of hair perth-

Table 20
Lattice constants of K feldspars.

	a_0	b_0	c_0	α	β	γ	V
25 I	8.579 (3)	12.964 (1)	7.220 (3)	90.65 (3)	115.95 (2)	87.71 (1)	721.4 (6)
40 I	8.582 (1)	12.962 (1)	7.221 (1)	90.66 (1)	115.94 (1)	87.65 (1)	721.8 (2)
42 I	8.584 (4)	12.965 (2)	7.221 (3)	90.58 (2)	115.98 (2)	87.75 (1)	721.9 (8)
52 I	8.586 (4)	12.966 (3)	7.220 (3)	90.78 (4)	115.98 (2)	87.82 (3)	722.0 (6)
46 I	8.589 (5)	12.957 (3)	7.205 (2)	90.00	116.06 (2)	90.00	721.2 (7)
65 I	8.585 (3)	12.974 (2)	7.205 (2)	90.00	116.03 (2)	90.00	721.1 (6)
62 Ie	8.588 (5)	12.956 (2)	7.213 (3)		115.98 (3)		721.4 (8)
59 I	8.587 (4)	12.971 (3)	7.207 (2)		116.04 (2)		721.2 (6)
71 I	8.582 (3)	12.964 (2)	7.209 (1)		116.04 (1)		720.6 (3)
76 I	8.578 (5)	12.962 (3)	7.213 (2)		116.00 (2)		720.8 (7)
80 I	8.583 (3)	12.979 (3)	7.203 (2)		116.04 (2)		721.1 (4)
89 I	8.577 (2)	12.973 (2)	7.203 (1)		116.03 (1)		720.1 (2)
96 I	8.579 (2)	12.979 (2)	7.204 (2)		116.03 (1)		720.7 (4)
116 I	8.577 (3)	12.981 (2)	7.203 (1)		116.01 (1)		720.7 (4)
150 I	8.582 (3)	12.962 (2)	7.208 (2)		116.04 (2)		720.5 (4)
154 I	8.580 (2)	12.965 (2)	7.213 (1)		116.01 (1)		721.1 (3)
156 I	8.586 (3)	12.965 (2)	7.208 (2)		116.02 (2)		721.1 (4)
169 I	8.576 (6)	12.961 (4)	7.211 (3)		116.01 (2)		720.3 (7)
190 I	8.588 (3)	12.965 (1)	7.209 (2)		116.06 (2)		721.1 (4)
203 II	8.579 (2)	12.968 (2)	7.207 (1)		116.03 (1)		720.6 (3)
211 II	8.585 (5)	12.974 (3)	7.215 (3)		116.01 (3)		722.3 (8)
217 I	8.575 (5)	12.963 (3)	7.212 (2)		116.04 (2)		720.3 (7)
228 I	8.577 (3)	12.969 (2)	7.210 (2)		116.02 (2)		720.6 (4)
232 I	8.571 (2)	12.966 (1)	7.212 (1)		116.04 (1)		720.1 (2)

Cell parameters are given in Å, degrees and cubic Å respectively. The samples come from the West Inari schist zone (25I, 40I, 42I), the southwestern marginal zone (46I, 52I) and the granulite complex (65I-232I). Parenthesized figures represent one standard deviation in units of the figure cited to their immediate left.

ite. A diffuse cross-hatched twinning can be recognized. The extinction angle may vary within individual grains from 0—18°. The alkali feldspars of this zone may thus be termed microperthitic to mesoperthitic intermediate microclines.

The large variation in the optical properties of alkali feldspars of zone 2 and 3 can be related to a dependence of the structural state on rock composition: As shown in Fig. 33 the optic axial angle of alkali feldspars is negatively correlated to the An content of the coexisting

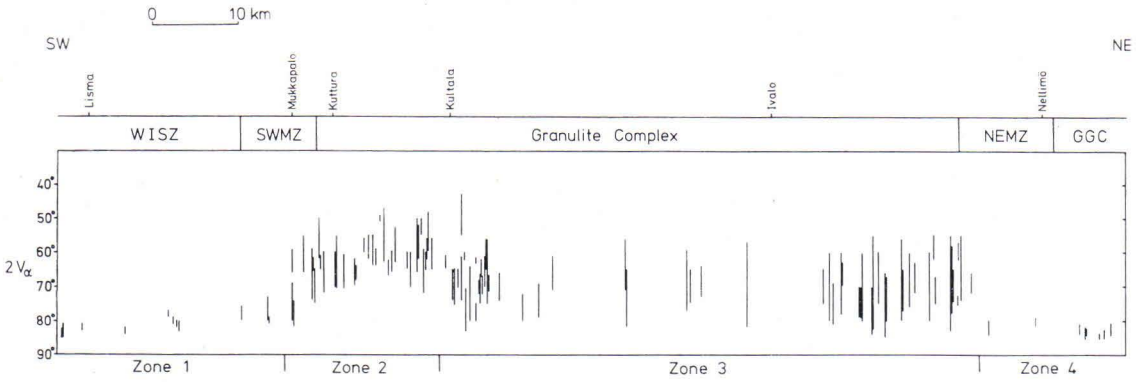

Fig. 32. Regional variation of optical axial angle of K-feldspars. The length of the bar gives the variation encountered within one rock sample. For discussion see text.

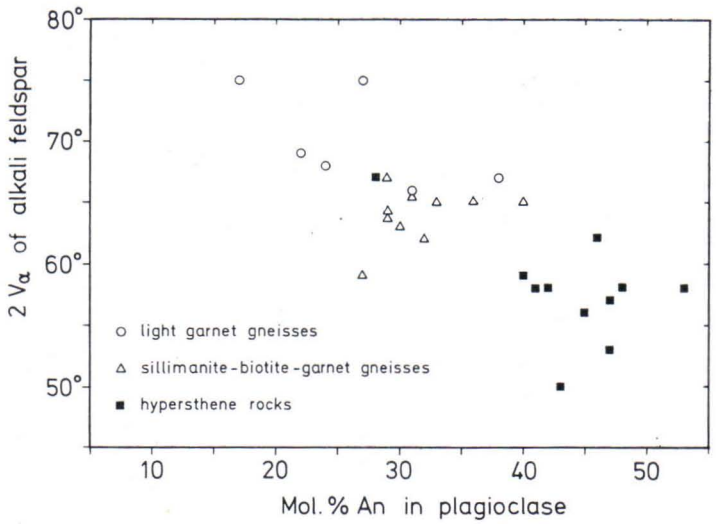

Fig. 33. Correlation between $2V\alpha$ of K-feldspar and anorthite content of the coexisting plagioclase in rocks from the granulite complex.

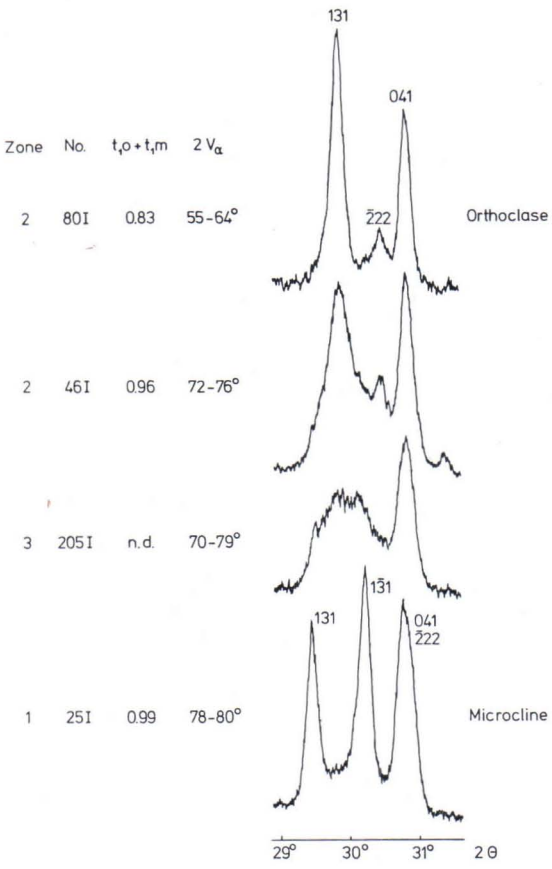

Fig. 34. Sections from the X-ray powder patterns (CuKα) of K-feldspars indicating the different structural states (cf. text).

plagioclase which, in turn, is largely controlled by the rock composition (cf. Fig. 29). The optic axial angle and thus the Al–Si order are the lower the more basic the rocks are. This may be caused by varying alkali/alumina ratios in the coexisting pore fluid which influences the ordering kinetics of alkali feldspars (Martin 1969).

The high Al–Si order encountered in the microclines of the West Inari schist zone, the northeastern marginal zone and the granite gneiss complex (zones 1 and 4) can be related to the wet conditions of the amphibolite facies, although these phases, too, must have passed through an orthoclase structural state as indicated by the cross-hatched twinning.

X-ray data: The triclinicity of alkali feldspars, a measure of Al-Si order, is defined according to Goldsmith and Laves (1954) by $\Delta = 12.5$ $(d_{131}-d_{1\bar{3}1})$. This parameter ranges from 0 (orthoclase, sanidine) to 1 (maximum microcline). Sections of the X-ray powder diffraction patterns are given in Fig. 34 and show the shape of the 131 peaks in four typical samples. Orthoclases with sharp and unsplit or only slightly broadened 131 peaks are encountered in the southwestern part of the granulite complex (zone 2). In the northeastern part of the granulite

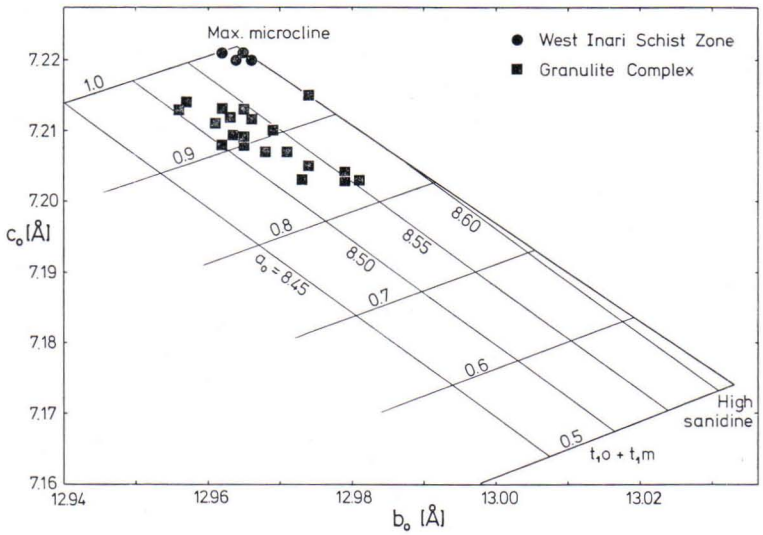

Fig. 35. b_0—c_0 plot of K-feldspars according to Wright and Stewart (1968). The a_0 lines refer to unstrained K-feldspars.

complex (zone 3), however, the 131 peak is strongly broadened. These alkali feldspars, which are also characterized by variable $2V\alpha$ and extinction angles, represent phases transitional between orthoclase and intermediate microcline. The triclinicity varies within a single grain (see above). In the West Inari schist zone (zone 1) the alkali feldspars have sharp and well separated 131–$1\bar{3}1$ peaks with $\Delta = 0.90$—0.98, i.e. very close to maximum microcline.

According to Stewart and Ribbe (1969) and Stewart and Wright (1974) both Al-Si distribution and chemistry of alkali feldspars can be determined from the lattice constants. These have been measured on 24 samples (Table 20). Only insufficient accuracy could, however, be achieved from samples with strongly broadened 131 peaks (cf. sample 205 I, Fig. 34). The data are displayed in the b_0–c_0 plot of Fig. 35 which also gives the theoretical a_0 lattice constant and the Al content of the T_1o and T_1m positions.

Again, samples from the West Inari schist zone plot close to maximum microcline. They are unstrained (the calculated a_0 being close to the a_0 observed, Wright and Stewart 1968) and rich in K-feldspar component (96—97 mole per cent according to the cell volumina). On the other hand, the alkali feldspars from the granulite complex define a band in the b_0–c_0 plot of Fig. 35 with theoretical a_0 values generally between 8.50 and 8.55Å. The actual a_0 lattice constants are, however, 8.57—8.59Å. These differences ($\Delta a_0 = 0.03$—0.08 Å) indicate strained structures (Wright and Stewart 1968) which may be related to semicoherent exsolution of hair perthite. The K-feldspar phase has, according to the cell volumina, 92—95 mole % K-feldspar component, whereas the bulk composition of the perthites is much richer in Ab (18—30 %, see below).

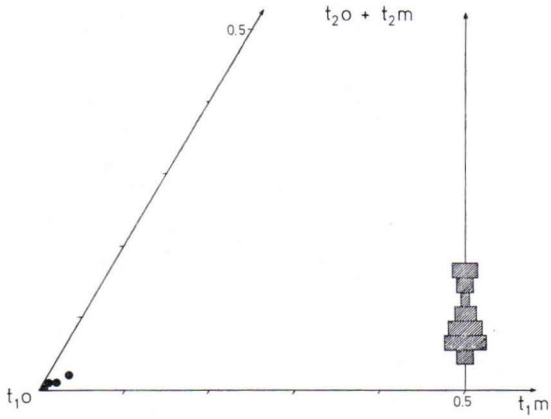

Fig. 36. Site occupancies of the T_1o, $T_2o + T_2m$, and T_1m positions. Boxes refer to samples from zones 2 and 3 (granulite complex), dots to samples from the West Inari schist zone.

Table 21

Bulk composition of K feldspars (from wet chemical analyses) and coexisting plagioclase, distribution coefficient and equilibrium temperatures for 5 kbar according to Stormer (1975) and Powell & Powell (1977).

	Ab in Kf	Or in Kf	An in Kf	An in Plag	$X^{Kf}_{Na} / X^{Plag}_{Na}$	T °C (5 kb) Stormer 1975	T °C (5 kb) Powell & Powell 1977
WISZ							
25 I	7.1	92.5	0.4	12	0.08	405	388
40 I	8.6	91.1	0.3	8	0.09	421	419
SWMZ							
52 I	12.8	85.6	1.6	21	0.16	506	491
46 I	29.8	68.3	1.9	17	0.36	648	623
GC							
59 I	19.4	78.6	2.0	31	0.28	622	601
76 I	19.9	77.8	2.3	29	0.27	618	594
89 I	17.4	80.1	2.5	39	0.29	636	611
150 I	20.3	76.9	2.8	30	0.29	627	597
116 I	19.1	78.0	2.9	33	0.29	628	597
154 I	19.5	77.4	3.1	24	0.26	592	559
156 I	26.2	70.6	3.2	23	0.34	656	612
190 I	24.0	73.1	2.9	29	0.34	663	629
228 I	13.2	84.5	2.3	30	0.19	539	518
169 I	18.6	78.9	2.5	35	0.29	632	606
211 II	22.3	75.1	2.6	28	0.31	644	610
217 I	19.0	79.0	2.0	32	0.28	622	601

The site occupancies of Al in the T_1o, T_1m and $T_2o + T_2m$ positions determined from the lattice constants according to the method proposed by Stewart and Ribbe (1969) are displayed in Fig. 36. It is evident that the microclines of the West Inari schist zone have more than 95 % Al in T_1o. Alkali feldspars from the granulite complex (zones 2 and 3) have 83 to 96 % Al in T_1 positions which, in these monoclinic phases comprise both the T_1o and T_1m positions of the triclinic phases. Most of the samples plot in the range 90—95 % Al in T_1. Despite this strong enrichment these samples are still monoclinic since the 131 peaks are at most only slightly broadened (Fig. 34).

Chemistry

For a determination of the bulk chemistry of the perthitic alkali feldspars these phases have been separated by heavy liquids and analyzed for Na, K and Ca by wet chemical methods. Table 21 gives the Ab, Or, and An contents and, in addition, the An contents of the coexisting plagioclases as determined optically. Alkali feldspars from the West Inari schist zone (zone 1) contain a high Or (83—93 %) and very low An component (0.3—1.6 %) and the coexisting plagioclase has An 08—An 21. On the other hand, in alkali feldspars from the granulite complex (zones 2 and 3) the Or contents are lower (68—85 %) and the An contents higher (1.9—3.2) and plagioclases range from An 17 to An 39. The distribution coefficient $K_D = X^{\text{alkali feldspar}}_{Na} / X^{\text{plagioclase}}_{Na}$ equals 0.29 ± 0.04 in the granulite complex but is much lower (0.08) in samples from the West Inari schist zone. Sample 52I, which comes from the southwestern marginal zone, is transitional between these two groups.

The temperatures derived from the chemistry of the coexisting feldspars (Table 21, Fig. 42) will be discussed in the section on metamorphic conditions.

Scapolite

Occurrence and textural relationships

Scapolite occurs sporadically over the entire profile studied as a late product mainly in the metabasites but very rarely also in quartz–feldspar gneisses. It is clearly a retrograde phase in the amphibolites of the West Inari schist zone. Its coexistence with clinopyroxene and the modal decrease of hornblende and plagioclase in scapolite-bearing veins suggests that scapolite + clinopyroxene was formed from hornblende + plagioclase through addition of a fluid phase rich in CO_2 (see below). Scapolite may belong to the M2 stage of crystallization in the rocks of the southwestern marginal zone and the granulite complex, where it forms mosaic aggregates with sharp contacts to all minerals of the assemblage.

The following assemblages with scapolite (+ plagioclase and quartz) have been encountered:

1. West Inari schist zone: hornblende, clinopyroxene, biotite, epidote, chlorite, calcite (veins in amphibolite)
2. Southwestern marginal zone: clinopyroxene, epidote, chlorite, calcite (veins in hornblende gneiss); hornblende, biotite, clinopyroxene, hypersthene, calcite (in the matrix of hornblende gneiss)
3. Granulite complex: biotite, clinopyroxene, hypersthene, hornblende, epidote, calcite (in the matrix of hypersthene–plagioclase rock); biotite, muscovite, epidote, chlorite (in the matrix of quartz–feldspar gneiss).

Composition

The chemical composition of scapolite is clearly related to its mode of occurrence (Table 22). The Ca/(Ca + Na + K) ratios classify the scapolites as dipyres (Me 39 %) to mizzonites (Me 78 %) (Shaw 1960). Of the anions Cl, F, OH, CO_3 and SO_4 which all can be important in scapolite, only Cl and SO_4 can be determined with sufficient accuracy by microprobe. The low totals indicate that the CO_2 and H_2O contents are high. According to Fig. 37 scapolites poor in Al (i.e. dipyres) are highest in chlorine, i.e. they form a solid solution towards marialite. Mizzonites show SO_3 contents up to 4.3 weight per cent which are among the highest reported so far.

The vein scapolites in the rocks of the West Inari schist zone and the southwestern marginal zone are mizzonites (Me 70—76 %) low in Cl and SO_3. The high deficit in the analytical total can only be explained by high CO_2 contents. In accordance with experimental results (Orville 1975, Goldsmith and Newton 1977, Ellis 1978) the Ca/(Ca + Na) ratio in scapolites is always higher than that of the coexisting plagioclases (Fig. 37b).

Scapolites within the matrix of rocks from the southwestern marginal zone are dipyres (Me 39—51 %) rich in Cl. They may be inhomogeneous but generally also have slightly higher Ca/(Ca + Na) than the coexisting plagioclase. At the grain boundary the plagioclase shows a rim some 20 microns wide lower in An content than the bulk phase.

All scapolites from hypersthene-plagioclase rocks of the granulite complex are SO_3-rich mizzonites (Me 64—78 %). Contrary to the occurrence of scapolites from the southwestern marginal zone the coexisting plagioclase shows no zonation at the contact with scapolite. It is, therefore, assumed, that the scapolites of rocks from the granulite complex formed during M2 and that the plagioclase equilibrated with scapolites, whereas in the southwestern marginal zone even the scapolites in the matrix are retrograde and only the outer rims of the plagioclases achieved equilibrium compositions. The high SO_3 concentrations in scapolites of the granulite complex may be due to an oxidation of primary pyrite, which is often rimmed by secondary magnetite.

Table 22
Microprobe analyses and structural formulae of scapolites.

	WISZ		SWMZ					Granulite Complex			
	Amphibolites		Pyx-Hbl Gneisses				Qz-Fsp Gneiss.	Hyp-Plag Gneisses		Cpx-Hbl Gneisses	
	81 V		63 I		66I		58 III	88 I	74 I	206 I	
	rim	core			rim	core				rim	core
SiO_2	45.9	46.5	46.6	54.2	54.6	50.5	54.7	45.8	46.3	46.4	47.6
TiO_2	—	0.01	—	—	—	—	0.04	0.02	0.05	—	—
Al_2O_3	27.9	27.4	26.7	21.8	22.7	23.8	23.9	25.1	25.8	26.4	25.9
FeO[a]	0.14	0.09	0.19	0.09	0.08	0.11	0.08	0.26	0.25	0.31	0.28
MgO	0.09	0.04	0.06	—	0.01	—	0.29	0.06	0.07	0.10	0.02
CaO	17.6	18.9	17.9	10.5	9.7	13.2	9.9	18.4	17.8	18.4	19.4
Na_2O	4.1	3.3	3.4	7.3	7.7	6.4	7.1	3.2	3.1	3.0	2.7
K_2O	0.08	0.06	0.99	0.67	0.87	0.78	0.95	0.19	0.29	0.50	0.45
SO_3	—	—	—	—	—	—	—	4.2	4.3	0.53	0.92
Cl	0.08	0.07	0.18	2.38	2.36	2.27	2.45	0.08	0.20	0.78	0.32
P_2O_5	0.03	0.07	0.01	—	—	—	0.01	0.03	0.03	—	—
Total	95.92	96.44	96.03	96.94	98.02	97.06	99.42	97.43	98.19	96.42	97.59
Number of ions on the basis of 12(Al, Si)											
Si	6.993	7.084	7.147	8.138	8.054	7.716	7.900	7.289	7.243	7.183	7.311
Al	5.007	4.916	4.848	3.862	3.946	4.284	4.100	4.701	4.757	4.818	4.689
Ti	—	0.001	—	—	—	—	0.004	0.002	0.006	—	—
Fe[a]	0.018	0.012	0.024	0.009	0.009	0.014	0.009	0.035	0.028	0.040	0.036
Mg	0.021	0.009	0.014	—	0.003	—	0.062	0.014	0.019	0.023	0.004
Ca	2.873	3.087	2.957	1.678	1.533	2.158	1.547	3.127	2.979	3.051	3.192
Na	1.201	0.971	0.940	2.129	2.198	1.892	2.006	0.972	0.946	0.893	0.804
K	0.016	0.012	0.195	0.126	0.160	0.147	0.177	0.038	0.056	0.094	0.088
S	—	—	—	—	—	—	—	0.501	0.504	0.062	0.103
Cl	0.018	0.016	0.034	0.604	0.594	0.588	0.589	0.017	0.056	0.206	0.056
P	0.001	0.005	0.001	—	—	—	0.001	0.004	0.004	—	—
mol. % Me[b]	70.1	75.8	72.3	42.7	39.4	51.4	41.5	75.6	74.8	75.6	78.2
mol. % An[c]	64		44		34		37	61	55	92	

[a] total iron as FeO; [b] Me = 100 Ca/(Ca + Na + K); [c] Anorthite content of coexisting plagioclase

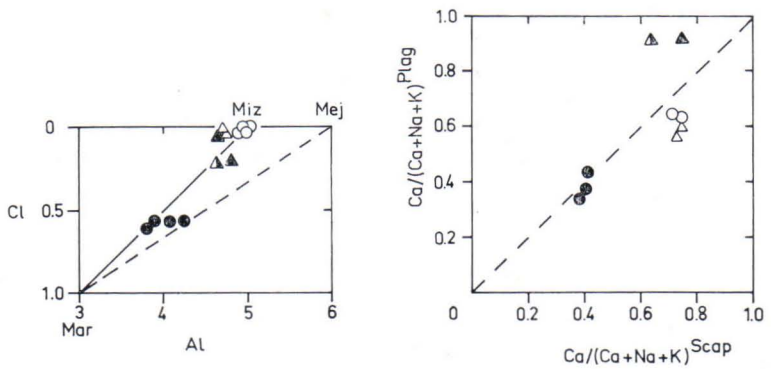

Fig. 37. Relation between Cl and Al contents in scapolites on the basis of Al+Si = 12 (a) and Ca/(Ca + Na + K) ratios in scapolite and plagioclase (b). Miz = mizzonite, Mar = marialite, Mej = mejonite. Dots: southwestern marginal zone, circles: West Inari schist zone, open triangles: hypersthene-plagioclase rocks (granulite complex), solid triangle: clinopyroxene-bearing quartz-feldspar gneiss (granulite complex), half-filled triangle: diaphthoritic quartz-feldspar gneiss (granulite complex).

Aluminium silicates

No aluminium silicates have been encountered in the rocks of the West Inari schist zone and the granite gneiss complex, probably due to the lack of pelitic source rocks. They are, however, widespread in the rocks of the granulite complex and its marginal zones.

Sillimanite

Sillimanite is an important constituent of the garnet–biotite–K-feldspar gneisses and garnet–cordierite gneisses but occurs also in minor amounts in the light garnet gneisses of the granulite complex. It occurs in three different habits which may be related to different stages of metamorphic crystallization:

1. Fibrous sillimanite enclosed in garnet porphyroblasts represents an early stage and often mimics a relic schistosity.
2. Coarse prismatic sillimanite, enriched in biotite-bearing layers and schlieren of the rocks, formed during high-grade synkinematic metamorphism (M1).
3. Corrosion of these prismatic sillimanites mainly by cordierite took place in a late but still high-grade postkinematic phase (M2). This replacement is caused by complex reactions such as

sillimanite + biotite + quartz + S ⇆ cordierite + K-feldspar + pyrrhotite + O_2 + H_2O and
garnet + sillimanite + quartz ⇆ cordierite

The prismatic variety of sillimanite contains low Fe (0.2 to 0.9 weight per cent Fe_2O_3) and Cr (up to 0.2 % Cr_2O_3). Two analyses are reported in Table 23.

Andalusite

The rare occurrence of andalusite is restricted to the central and northeastern parts of the granulite complex and the northeastern marginal zone. It is found locally in garnet–cordierite gneisses and, less frequent, also in the light garnet gneisses and the garnet-biotite gneisses. It is a retrograde product which formed besides

Table 23

Microprobe analyses and structural formulae of aluminium silicates.

	Andalusite				Sillimanite		Kyanite	
	Granulite Complex				GC		NEMZ	
	Garnet-Cordierite Gneisses							
	194 III/1		194 III/2		161 I	169 I	424 II	426 II
	core	rim	core	rim				
SiO_2	36.82	36.59	36.74	36.66	34.80	36.00	36.25	36.17
Al_2O_3	60.66	61.95	59.39	62.60	60.80	60.10	62.12	62.20
Cr_2O_3	0.02	0.02	0.02	0.02	0.20	0.06	0.02	0.13
Fe_2O_3[a]	1.93	0.40	1.79	0.17	0.63	0.89	0.87	0.37
MgO	1.30	0.12	1.59	0.04	0.00	0.02	0.00	0.00
Total	100.73	99.08	99.53	99.49	96.43	97.07	99.26	98.87
Numbers of ions on the basis of 6 cations								
Si	1.978	1.994	1.996	1.988	1.950	2.007	1.974	1.975
Al^{IV}	0.022	0.006	0.004	0.012	2.050	1.993	0.026	0.025
Al^{V}	2.000	2.000	2.000	2.000				
Al^{VI}	1.816	1.973	1.798	1.989	1.964	1.958	3.963	3.979
Cr	0.001	0.001	0.001	0.001	0.009	0.003	0.001	0.006
Fe^{3+}	0.079	0.016	0.073	0.007	0.027	0.037	0.036	0.015
Mg	0.104	0.010	0.128	0.003		0.002		

[a] total iron as Fe_2O_3

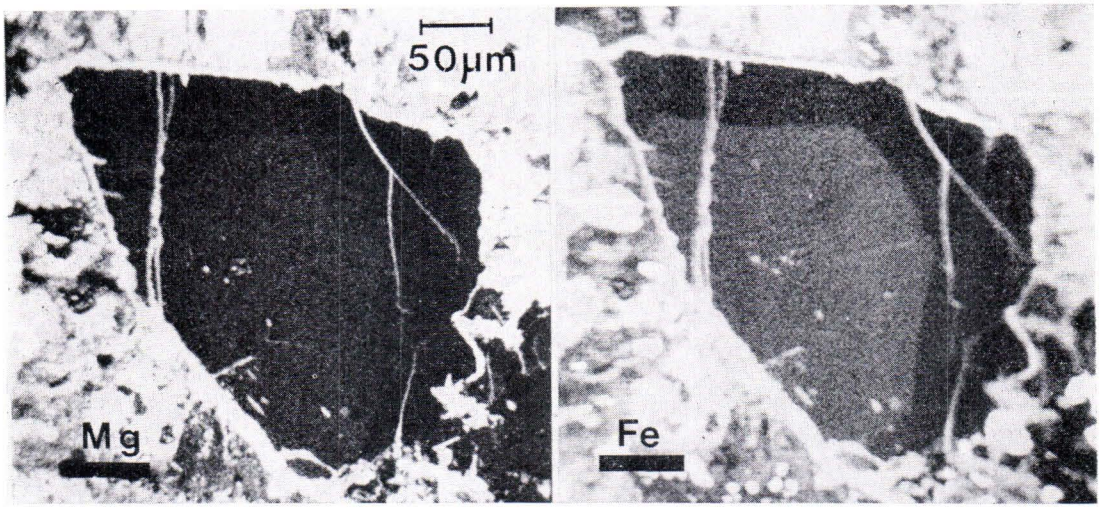

Fig. 38. Distribution of Fe and Mg in andalusite (sample 194 III, garnet-cordierite gneiss). Note the discontinuous zoning.

chlorite, white mica, quartz and a carbonate at the expense of cordierite, garnet and plagioclase. During the same process K-feldspar and biotite were altered into white mica and chlorite. A similar retrograde formation of andalusite + chlorite from cordierite has been described by Lal (1969). In unaltered parts of the rocks studied here the primary sillimanite is still preserved.

In thin section the andalusite is colourless to pinkish and may exhibit zoning with higher birefringence in the core. These cores are higher in Fe and Mg (up to 2.0 weight per cent Fe_2O_3 and 1.6 % MgO) compared to the margins (0.5 % Fe_2O_3, 0.2 % MgO, cf. Table 23). This zoning is discontinuous. The core sometimes shows idiomorphic contours (Fig. 38), but more frequently it is interfingering with the margin. According to the Mössbauer spectrum Fe is mostly in the ferric state.

Whereas elevated Fe_2O_3 contents are common in andalusite, no MgO values higher than 0.3 weight per cent have been reported in the literature (cf. Okrusch and Evans 1970, Deer *et al.* 1962). According to Fig. 39, Mg is negatively correlated to the sum of trivalent cations in octahedral positions ($Al^{VI} + Fe^{3+}$). Since the number of Si atoms remains constant, the charge balance can only be achieved by a concomitant substitution of OH^- for O^{2-} when Mg is introduced for Al. Such coupled substitutions have been postulated by Beran and Zeemann (1969) on the basis of infrared pleochroism.

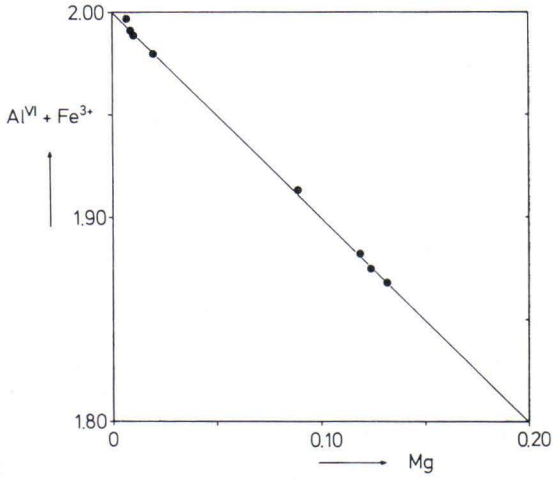

Fig. 39. Correlation between ($Al^{VI} + Fe^{3+}$) and Mg (per 6 cations, see Table 23) in andalusites.

Kyanite

Kyanite has only been encountered as a retrograde product in garnet–cordierite gneisses of the northeastern marginal zone in textural relationship and assemblage similar to those of andalusite as described above. It even may occur together with andalusite.

ORIGIN OF THE SOURCE ROCKS

The chemical composition of magmatogenic rocks may reflect the chemical and mineralogical composition of the hypothetical source materials from which the magmas originated, and the conditions of their formation, if the later metamorphism was essentially isochemical. Arguments supporting this assumption have been given above. The magmatogenic processes and the compositions of the magmas produced can be interpreted by means of experimental data obtained in model systems. For the origin of the basaltic rocks the peridotite system (e.g. Mysen and Boettcher 1975) and for the andesitic and rhyolitic rocks both the peridotite and basalt systems (Mysen and Boettcher 1975, Allen *et al.* 1975) have to be applied. From a comparison of the rock compositions actually present to those of liquids produced in the experiments, the depth of magma generation may be derived. This information serves for a characterization of the paleotectonic setting. The chemical composition of sedimentary source rocks, on the other hand, may shed some light on the processes of weathering, transport and deposition during the Prekarelian.

West Inari schist zone

The *ultramafic rocks* were, judging from the REE patterns, picrites rather than komatiites. Such melts can be produced from mantle garnet peridotites at pressures higher than about 30 kbars (O'Hara 1963, Green and Ringwood 1967). The emplacement of the ultramafic bodies into the rock series of the West Inari schist zone may well have occurred in the solid state during orogenesis. In this case the ultramafic rocks may be unrelated to the basaltic rocks formed in an earlier period.

The source rocks of the *amphibolites* were quartz tholeiites. Such magmas can form by partial melting of peridotite under anhydrous conditions or by fractional crystallization of olivine tholeiites at pressures lower than 5 kbars (Green and Ringwood 1967, Ringwood 1975).

Alternatively they can also result from partial melting of peridotite under hydrous conditions at pressures of 10—20 kbars ($X_{H_2O} \sim 0.4$) and temperatures of 1 100—1 150°C (Mysen and Boettcher 1975). The melts are rather calcic but could easily achieve the composition of the basalts considered here by a minor fractionation of clinopyroxene which can coexist with such melts under these conditions (Allen *et al.* 1975).

The REE distribution patterns of the tholeiitic rocks, with Eu anomalies absent, do not favour an origin by dry partial melting of peridotite or differentiation under pressures lower than 5 kbars, where plagioclase is an important residual or differentiated phase.

The origin of the heterogenous group of the *hornblende gneisses* cannot be described by a simple model, mainly because their major element composition does not change regularly and thus trends resulting from partial melting or fractionation are not evident. However, their source rock is related to that of the amphibolites. Amphibolites and hornblende gneisses are

tholeiitic in terms of the Alk-F-M diagram and have REE distribution patterns and contents of other trace elements similar to tholeiites, except for Ni, Cr and V which are strongly depleted. This indicates that phases with high distribution coefficients for these ferromagnesian elements (i.e. clinopyroxene, spinel and amphibole) coexisted with the melts. Garnet can be excluded because of the flat REE distribution patterns.

Melts corresponding in composition to that of the hornblende gneisses may also be produced by hydrous partial melting of peridotite, but at lower temperatures (950—1 150°C) and higher X_{H_2O} (0.6) than required for the formation of quartz tholeiites (Mysen and Boettcher 1975). The observed compositional variation of the rocks can be achieved by the fractionation of variable amounts of clinopyroxene, amphibole and spinel which have a broad stability field under these PT-conditions in the hydrous quartz tholeiite system (Allen *et al.* 1975).

The origin of the *quartz–feldspar gneisses* is discussed together with the compositionally similar calc-alkaline garnet gneisses of the granulite complex. Both are characterized by a strong depletion of the HREE compared with LREE, suggesting a similar origin.

The metagreywackes (*amphibolites and hornblende gneisses*) are, although discriminating as sediments, chemically similar to the meta-tholeiites and meta-andesites. They have lost alkalies and alumina, and the Ni/MgO and Cr/MgO correlations typical of the magmatogenic rocks vanished. The contents of the other trace elements and the REE distribution patterns were not altered significantly. The changes in chemical composition can be explained best by a partial loss of feldspar component and a rather erratic concentration or depletion of accessory minerals (spinel, pyrrhotite) during the sedimentary process. Abnormally high Zr or Ce contents in a few samples might be due to sedimentary enrichment of zircon or monazite. Because the typical REE distribution patterns of crustal rocks develop rapidly in the sedimentary process, the sediments must have contained a large proportion of unaltered magmatic material.

Granulite complex

The origin of the quartz–tholeiitic source rocks of the *basic hypersthene gneisses* can be described by the same processes already discussed in context with the amphibolites of the West Inari schist zone. In contrast to those source rocks, however, the tholeiitic liquids of the granulite complex must have undergone extensive olivine and clinopyroxene fractionation, as evident from the low Ni and Cr contents as well as the high-alumina-character of the rocks. The fractionation of olivine and clinopyroxene accounts for the enrichment of the REE, and the fractionation of clinopyroxene for the relative enrichment of LREE compared with HREE. Rb, Sr and Ba were also enriched during this process.

The *intermediate hypersthene gneisses and garnet biotite gneisses* display the typical pattern of a calc-alkaline rock series in the Harker diagram of Fig. 7 and the Alk–F–M diagram of Fig. 4. The rocks are chemically closely related to each other as shown by the Ni/MgO, Cr/MgO, Rb/K_2O and Ba/K_2O correlations (Figs. 5, 6). The rocks have the typical trace element abundances of Andean-type calc-alkaline volcanic rocks (Dostal *et al.* 1977, Hörmann and Pichler 1980). It is, therefore, suggested that the source rocks actually were andesites and dacites of a volcanic orogenic sequence. Their REE abundances are characterized by fractionated patterns with LREE enriched compared to HREE (Hörmann and Schock 1980) and Eu anomalies absent or positive. These patterns indicate a derivation of these melts from basalts rather than from dacitic crustal rocks by anatexis which are characterized by Eu anomalies absent or negative.

Experimental evidence suggests that andesitic magmas of the tholeiite series are formed by hydrous partial melting of mantle peridotite (e.g. Mysen and Boettcher 1975). These melts are characterized by high SiO_2 contents, tholeiitic trends in the Alk–F–M diagram, high Ni, Cr, V abundances, and low K, Rb, Ba contents. On the other hand, hydrous anatexis of basaltic matter produces liquids which match closely the major element composition of rocks of the calc-alkaline andesite—dacite series (Holloway and Burnham 1972, Allen *et al.* 1975, Stern and Wyllie 1978).

Melts originating in the hydrous basalt system are andesitic to dacitic and coexist with amphibole and clinopyroxene in a broad stability field. This holds true for the temperature range 850—1 000°C both in the low pressure regime of 4—10 kbars/$X_{H_2O} = 0.6$ (Holloway and Burnham 1972) as well as for an intermediate pressure range of 10—20 kbars/$X_{H_2O} = 1$ (Allen *et al.* 1975). These melts form mainly by the partial breakdown of amphibole to yield clinopyroxene + liquid. At low degrees of partial melting dacitic melts originate which become progressively andesitic with higher degrees of partial melting. The calc-alkaline trend results because the FeO/MgO ratio of the residual amphibole and clinopyroxene is close to 1.

The major element composition of liquids originating by melting of basalts in the low and intermediate pressure regimes corresponds closely to that of the andesitic and dacitic gneisses of the granulite complex. The trace element contents of the anatectic melts will be controlled by the degree of partial melting and the crystal-liquid distribution coefficients of the elements. The trace element abundances in the melts will increase with increasing degree of partial melting for those trace elements with distribution coefficients above 1 for amphibole and clinopyroxene (e.g. Ni, Cr; Wedepohl 1975), but decrease for elements with distribution coefficients below 1 (e.g. Ce, Yb, Rb, Ba; Gill 1978). If garnet would have coexisted with the anatectic melts, a strong depletion of Yb compared to Ce in the melts would be expected because the distribution coefficient D_{Yb}^{Gt} is markedly above 1 (Gill 1978) but D_{Ce}^{Gt} is much lower (Wedepohl 1975). The trends in the trace element concentrations in the andesitic to dacitic rocks (Table 12) conform with an anatectic origin of these rocks in the presence of amphibole and clinopyroxene. The low Ce_N/Yb_N ratios (Hörmann and Schock 1980) exclude the presence of garnet as a liquidus phase during anatexis and consequently restrict the conditions of melt formation to pressures lower than 20 kbars (Allen 1975).

Both the major element and trace element contents of the hypersthene gneisses and garnet–biotite gneisses point, therefore, to an origin by hydrous partial melting of basaltic matter at pressures lower than 20 kbars.

The rhyodacitic and rhyolitic *garnet gneisses* are a chemically heterogeneous group. The origin of the magmas is not explicable by a simple partial melting model.

Rhyodacitic and rhyolitic melts may originate by hydrous partial melting of tholeiitic and andesitic compositions at pressures higher than 20 kbars (Allen 1975, Stern and Wyllie 1978) and temperatures between 800 and 1 200°C. These melts coexist with garnet besides clinopyroxene and kyanite, and a strong enrichment of the LREE compared to the HREE may be expected.

The major element composition of the rocks corresponds fairly well to melts produced from andesitic matter (Stern and Wyllie 1978). Only this process can account for the high potassium contents (Table 9, Fig. 7). In terms of trace element composition, however, two subgroups may be distinguished. One, comprising the rhyodacitic garnet gneisses, with very steep REE distribution patterns, with HREE even depleted below the concentrations in chondrites, and another subgroup (rhyolitic garnet gneisses) with fractionated but very flat REE distributions (Hörmann and Schock 1980). The former subgroup reflects the participation of garnet in

the anatectic process and conforms with the model discussed. The origin of the other subgroup remains obscure.

The metasedimentary rock group, i.e. the garnet–cordierite gneisses as well as part of the garnet–biotite- and hypersthene gneisses originated from the magmatic rocks by a weathering process removing part of the sodium and calcium of clastic plagioclase and thus leading to a decrease in CaO and Na_2O contents, increase in the K_2O/Na_2O ratio, with Al_2O_3 contents little affected. However, the REE distribution patterns are still those inherited from the magmatic parent rocks, indicating immature sediments.

METAMORPHIC CONDITIONS

From the regional development of mineral assemblages as derived in the foregoing sections three zones of different type of metamorphism are distinguished. They correspond to the main geotectonic units (cf. Figs. 8 and 9):

1) amphibolite facies in the part of the West Inari schist zone studied,

2) granulite facies within the granulite complex,

3) amphibolite facies in the granite gneiss complex.

These three metamorphic zones are not separated from each other by abrupt changes in mineral assemblage and composition but show gradational transitions within the marginal zones of the granulite complex.

Mineral assemblages, textural criteria and radiometric dates (Meriläinen 1976) demonstrate that the entire Precambrian crystalline rock series has been subjected to high-grade polyphase metamorphism during the Karelian orogeny: an early high-grade stage of crystallization M1 proceeding simultaneously with the overthrusting of the granulite complex onto the rock series of the West Inari schist zone (Meriläinen 1976) and a later, also high-grade stage of postkinematic metamorphism M2. During this later event the entire rock series recrystallized and, in the central and northeastern part of the granulite complex, an intense anatexis took place. From the petrography alone it cannot be decided whether the two stages of crystallization represent clearly separated metamorphic events or just are parts of a single metamorphic cycle. On the basis of radiometric dates Meriläinen (1976) suggested a time span of 250 Ma for the high-grade metamorphism of the entire granulite complex, starting at an age of 2 150 Ma for M1 and lasting to an age of 1 900 Ma for M2. Because M2 was of high grade, too, it can be expected that the coexisting minerals reequilibrated during this stage. A later low-grade diaphthoritic retrogression affected only narrow zones.

Whereas the PT- conditions during M1 can only be indirectly deduced from the synkinematically grown mineral assemblages, which still are preserved in the West Inari schist zone and in the southwestern part of the granulite complex, there is ample evidence for the conditions prevailing during M2 from the reequilibrated mineral assemblages and the composition of the coexisting minerals. The minor paragenetic changes when passing from M1 to M2 suggest rather similar conditions of metamorphism for both events. A quantitative reconstruction of the physicochemical conditions of metamorphism can only be achieved by an analysis of the composition of coexisting phases and by application of the pertinent equilibria. The following discussion will, therefore, be restricted to the M2 event.

Attainment of equilibrium

Attainment of equilibrium during M2 is demonstrated by the following criteria (cf. Seifert 1978):

1) The parageneses in the rocks are defined by mineral phases in mutual grain contact. This is also true for the rather rare occurrence of reaction textures (e.g. coronas).

2) Zoning in the minerals is absent or weak, even in refractory phases such as garnet and, if present, may be attributed to retrograde effects.

3) The distribution coefficients between minerals defining a paragenesis show little variation, even over the major rock units, and smooth trends (Fig. 45).

4) If any crossing tie-lines show up in the ACF or AFM projections, these can be explained by additional components in the minerals (AFM projection; Ti in biotite, Ca in garnet), fractionation of Mg and Fe^{2+} taken as one component in the ACF projection, and varying activity of water.

Metamorphic conditions in the West Inari schist zone and the southwestern marginal zone

The rather simple mineralogy of the rocks of the West Inari schist zone offers only limited information on the precise physicochemical conditions of metamorphism during M2. From the occurrence of water-filled fluid inclusions in the rocks of this zone (Klatt, pers. comm. 1978) and from the petrographic observations reported in the section on petrography it is concluded that P_{H_2O} was close to P_{total}.

The widespread occurrence of migmatites indicates that the granitic minimum has been surpassed during metamorphism (Tuttle and Bowen 1958), i.e. temperatures were above some 650°C at 5 kbars water pressure. High temperatures are also evident from the total absence of any prograde muscovite. However, the equilibrium curve for the reaction at the second sillimanite isograd

muscovite + quartz $\leftrightarrows$ K-feldspar + sillimanite + vapor

as determined by Chatterjee and Johannes (1974) cannot be applied because the pair K-feldspar + sillimanite is missing even in the gneisses.

The corundum-, sapphirine- and kornerupine-bearing amphibolites described by Haapala *et al.* (1971) from Paaraskalla south of Lisma indicate high pressures and temperatures as well: The experimental data on the stability of sapphirine and kornerupine determined by Seifert (1974, 1975) would suggest minimum pressures of 4.5 kbars and minimum temperatures of 740°C (Fig. 40). However, these data are not strictly applicable since they were determined in the pure system $MgO-Al_2O_3-SiO_2-H_2O$. Additional components such as B_2O_3 in kornerupine and FeO in sapphirine and kornerupine might shift the equilibria, probably towards lower pressures and temperatures.

No aluminium silicates have been encountered in the rocks of the profile studied within the West Inari schist zone, due to restrictions in bulk composition. However, Eskola (1952) reports kyanite–staurolite schists and Meriläinen (pers. comm. 1979) hornblende–staurolite–garnet gneiss from Korvatunturi which lies in an equivalent tectonic position. The occurrence of staurolite + quartz in these rocks suggests temperatures somewhat lower than those of the rocks dealt with here.

Metatroctolites of the southwestern marginal zone of the granulite complex close to Mukkapalo exhibit corona structures (Fig. 20) which can be explained by the reaction

olivine + anorthite $\leftrightarrows$ clinopyroxene + orthopyroxene + spinel.

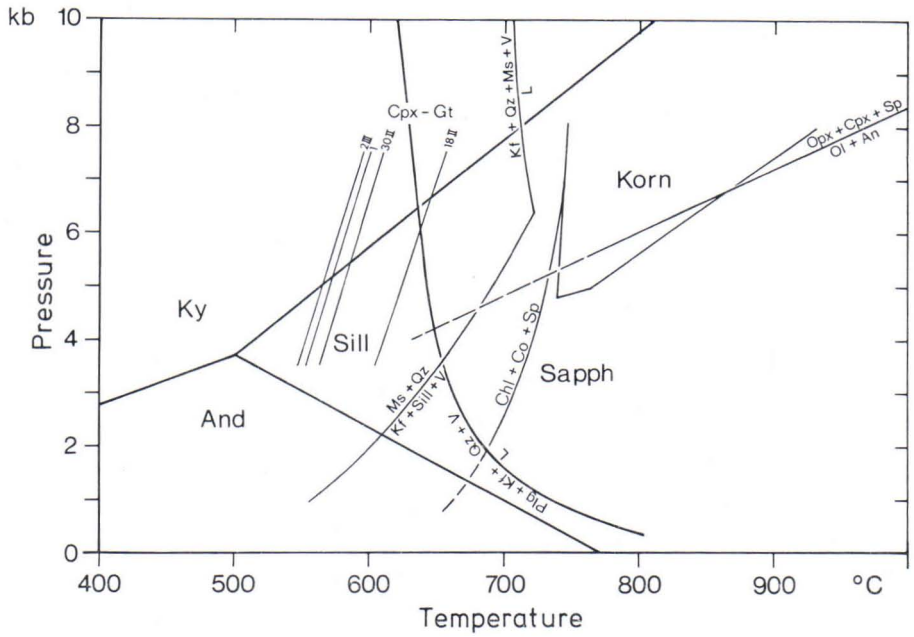

Fig. 40. Stabilities of minerals and assemblages (at $P_{H_2O} = P_{total}$) relevant to the metamorphic conditions attained during M2 in the West Inari schist zone. Stability of aluminum silicates taken from Holdaway (1971), muscovite + quartz from Chatterjee and Johannes (1974), K-feldspar + quartz + muscovite + vapour from Storre and Karotke (1972), sapphirine from Seifert (1974), kornerupine from Seifert (1975), olivine + anorthite from Green and Ringwood (1972), granite minimum melting curve from Tuttle and Bowen (1958), PT-curves obtained from the distribution of Fe and Mg between coexisting garnet and clinopyroxene from Råheim and Green (1974).

This equilibrium has been used to separate low-pressure granulites from intermediate-pressure granulites by Green and Ringwood (1967). However, its location in PTX space is uncertain as discussed by Gardner and Robins (1974). According to these authors the equilibrium curves determined for this reaction by Green and Ringwood (1972) and Ito and Kennedy (1971) are best suited for an application to natural rocks. Using this curve (Fig. 40) the corona texture would originate by lowering of temperature in the vicinity of 700°C at 5 kbars.

The mineral pair garnet—clinopyroxene which shows widespread occurrence in the amphibolites can be used for geothermometry: According to Råheim and Green (1974) the Mg–Fe distribution between these minerals is mainly dependent on temperature and, to a lesser extent, on pressure. The distribution coefficients reported in Table 24 indicate temperatures around 570°C

Table 24

FeO/MgO ratios of coexisting garnet and clinopyroxene, Fe-Mg distribution coefficient and temperature derived from the model given by Råheim & Green (1974), assuming a pressure of 5 kbars.

	West Inari Zone				SW Marginal Zone				GC	NEMZ
	1 LI	2 III	18 II	30 II	47 III	66 II	66 III	67 II	198 I	458 II
$(FeO/MgO)^{Gar}$	5.330	5.579	2.665	4 329	3.990	3.642	3.622	9.184	7.325	4.823
$(FeO/MgO)^{Cpx}$	0.585	0.593	0.374	0.507	0.632	0.760	0.635	1.464	1.144	0.902
$\ln K_D$	2.209	2.242	1.964	2.145	1.843	1.568	1.741	1.836	1.856	1.677
T °C (5 kb)	570	564	618	582	644	709	667	646	641	682

at 5 kbars in the West Inari schist zone proper and 660°C at 5 kbars in the southwestern marginal zone (Figs. 40 and 43). These figures are obviously lower than those derived from the data discussed above. Ca contents of the garnet might account for the low values*.

* After this paper was finished Ellis and Green (1979) published their study on the effect of Ca on the above equilibrium. Applying their equation to our data temperatures of 750 ± 30°C are obtained for both West Inari schist zone and the southwestern marginal zone.

The distribution of Na over the coexisting microcline and plagioclase can be evaluated in terms of temperature and pressure by the models given by Stormer (1975) and Powell and Powell (1977). The temperatures thus derived (at an assumed pressure of 5 kbars) are presented in Table 21 and Fig. 41. They are in the range 400 to 500°C and obviously represent late stage reequilibration temperatures or late stage removal of albite component from the alkali feldspar. Low temperature processes are also documented by the maximum Al–Si order attained in K-feldspar (cf. p. 60—64).

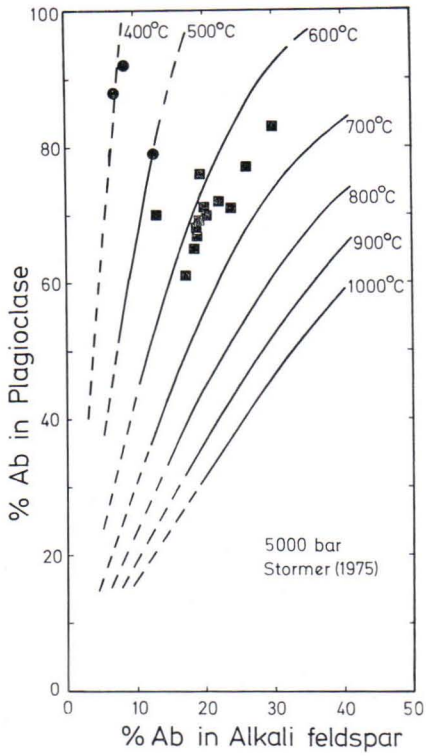

Fig. 41. Mole per cent Ab in plagioclase versus mole per cent Ab in coexisting microcline from quartz-feldspar-gneisses of the West Inari schist zone (dots) and orthoclase from garnet gneisses of the granulite complex (squares). Curves are drawn according to Stormer (1975).

Metamorphic conditions in the granulite complex

Evidence from parageneses:

For estimates of pressure and temperature univariant solid-solid equilibria would be suited best, because these are not affected by fugacities of volatile species. In particular, metamorphism in the granulite complex took place at water pressures less than total pressures, and dehydration equilibria could only be applied if water fugacities were known. From the solid-solid reactions only the stability boundaries of the aluminium silicates are applicable to a major part of the profile studied (Richardson *et al.* 1969, Holdaway 1971). The presence of sillimanite in most garnet gneisses of the granulite complex delimits only a wide field of PT-conditions. Maximum pressures in the range from 6 to 10 kbars can be inferred if temperatures are set to 600—800°C which can be expected for a granulite facies terrain. Due to the uncertainties in the location of the andalusite/sillimanite equilibrium no lower pressure limit can be given.

The presence of the pair K-feldspar + sillimanite and the absence of the alternate tie-line muscovite + quartz indicates either high temperatures (above 700°C at 5 kbars, Chatterjee and Johannes 1974) or low water fugacities, or both (Fig. 42).

The assemblage cordierite + K-feldspar + garnet + biotite + sillimanite + quartz, which is widespread in the central and northeastern part

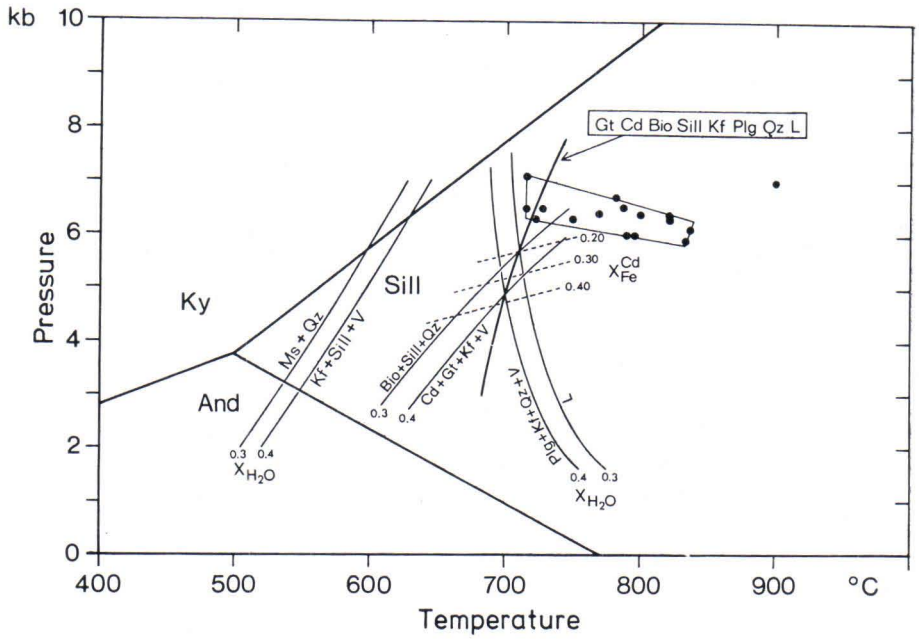

Fig. 42. Stabilities of minerals and assemblages (at $P_{H_2O} < P_{total}$) relevant to the metamorphic conditions attained during M2 in garnet-cordierite gneisses in the central and northeastern parts of the granulite complex. Stability of aluminium silicates taken from Holdaway (1971), muscovite + quartz at varying X_{H_2O} taken from Kerrick (1972), reactions involving the »seven-phase» assemblage garnet + cordierite + biotite + sillimanite + K-feldspar + plagioclase + quartz and a melt taken from Lee and Holdaway (1977). Dots are PT-conditions calculated from the composition of coexisting garnet and cordierite by the model of Thompson (1976 b).

of the granulite complex, corresponds, in terms of the system K_2O-MgO-FeO-Al_2O_3-SiO_2-H_2O and at $P_{H_2O} = P_{total}$, to an univariant equilibrium, expressed by a reaction relationship

biotite + sillimanite + quartz $\leftrightharpoons$ cordierite + garnet + K-feldspar + vapour

and causes the crossing tie-lines in the AFM projections (Fig. 9). An univariant equilibrium, however, contradicts the regional occurrence. A higher variance can be caused by the incorporation of additional components such as Ca into garnet and, in particular, Ti into biotite and Na into K-feldspar. Since H_2O participates in the reaction, a water deficiency (in terms of a closed system) would also make the above assemblage stable over a range of pressures and temperatures. In an open system the silicate assemblage might buffer the composition of the fluid phase (Greenwood 1975) and become stable over a PT range.

A reduced activity of water is evident from the following observations:

1) At $a_{H_2O} = 1$ the equilibrium curve for the above reaction is largely metastable with respect to melts (Lee and Holdaway 1977).

2) The temperatures and pressures calculated on the basis of partitioning equilibria between garnet and cordierite (see below) are, on the average, in the biotite + sillimanite + quartz stability field with respect to the equilibrium curve for $a_{H_2O} = 1$. Neglecting the effects of additional components, the equilibrium can only occur at these lower temperatures if the water activity was low.

3) The composition of the cordierite (X_{Fe} around 0.24, cf. Table 18) in the seven-phase assemblage cordierite + garnet + sillimanite + biotite + K-feldspar + plagioclase + quartz which is widespread in the anatectic gneisses, indicates, according to Lee and Holdaway (1977),

a temperature near 705°C, 5.5 kbars total pressure and an X_{H_2O} of 0.32 (Fig. 42). These figures are obtained from the intersection of the cordierite – garnet – K-feldspar – biotite – sillimanite–quartz equilibrium curve for different X_{H_2O} with those of the minimum melting of granite.

4) Direct evidence for a low activity of water is presented by the fluid inclusions which, in these rocks, largely consist of CO_2 (Klatt, pers.comm. 1978).

5) The $H_2O/(H_2O + CO_2)$ ratios in cordierite indicate X_{H_2O} in the metamorphic gas phase around 0.3.

6) The assemblage graphite + pyrite + pyrrhotite restricts, at 700°C, 5 kbars total pressure, the X_{H_2O} in the gas phase to values below 0.83 (Ohmoto and Kerrick 1977).

Whereas the formation of anatexites was widespread during M2 in the central and northeastern part of the granulite complex, syn- to postkinematic anatexites are subordinate in the southwestern part, although suitable bulk compositions were available and temperatures derived from partitioning data discussed below are similarly high. Therefore, it is concluded that water activities were even lower in this part of the granulite complex.

Evidence from cation distribution and miscibility:

Whereas retrograde reactions producing new tie-lines can be readily recognized from the textural relationships of an assemblage retrograde changes in element distribution between coexisting minerals might not be that evident. Because the cooling rate of the rocks and the kinetics of cation exchange between the individual mineral pairs are essentially unknown, temperatures derived from models using element partitioning data for geothermometry can, at best, represent cut-off temperatures where the equilibria are frozen-in and thus can give only minimum temperatures for M2 (cf. Tracy *et al.* 1976, Seifert 1978). In the following, a number of models for geothermometry and geobarometry based on exchange equilibria and miscibility will be applied to the rocks of the granulite complex.

Mg–Fe distribution between garnet and cordierite: The paragenesis garnet + cordierite + sillimanite + quartz enables the determination of both pressure and temperature from the X_{Fe} of garnet and cordierite. Many contradictory models have been proposed in the literature (e.g. Currie 1971, 1974, Hensen and Green 1971, 1973, Hensen 1977, Thompson 1976 a, b, Wells 1976, Holdaway and Lee 1977). Although Currie's model would yield data which are consistent with the experimental results of Holdaway and Lee (1977) on the »seven-phase» cordierite–garnet assemblage, it has not been employed here because its experimental and thermodynamic bases have been questioned (Holdaway and Lee 1977). The approach of Hensen and Green (1971, 1973) and that of Hutcheon *et al.* (1974) yielded PT-values lying in part outside the sillimanite stability field. For these reasons, the format of calculation given by Thompson (1976) has been preferred. Both garnets and cordierites of the gneisses can be adequately represented by binary (Mg–Fe) solid solutions and the model should therefore be applicable. Reduced water activities do not affect the K_D values and consequently not the temperature readings, but they do affect the composition of the phases and thus the pressure readings (Lee and Holdaway 1977). All these models have, however, recently been questioned by Newton and Wood (1979).

The temperatures obtained range in general between 700 and 825°C and the pressures (uncorrected for $P_{H_2O} < P_{total}$) are generally in a narrow range of 6 to 6.5 kbars (Table 25). These pressures are negatively correlated with temperature, which may be an artifact introduced by the model employed. Considering the low a_{H_2O} (around 0.3, see above) the total pressures have to be lowered by 1 to 2 kbars (Lee and Holdaway 1977).

Additional uncertainties are introduced into the calculations by the minor but systematic zonation of garnet and cordierite. Using the rim

Table 25

X_{Fe} values of cordierite and garnet coexisting with sillimanite and quartz, Fe-Mg distribution coefficient, and PT-conditions calculated according to Thompson (1976 b).

	Cord X_{Fe}	Gar X_{Fe}		Gar-Cord $\ln K_D$		T °C		P kb
		core	rim	Gar_c	Gar_r	Gar_c	Gar_r	
89 I	0.204	0.582	0.594	1.692	1.742	782	755	6.6
89 V	0.226	0.562	0.571	1.494	1.517	861	855	8.1
93 VI	0.259	0.686	0.705	1.832	1.922	722	695	6.3
105 I	0.236	0.633	0.656	1.721	1.820	772	730	6.4
110 III	0.205	0.561	0.557	1.601	1.584	822	820	6.3
119 I	0.240	0.594	0.604	1.532	1.575	838	825	6.1
145 I	0.164	0.557	0.582	1.859	1.960	717	680	7.1
158 I	0.229	0.649		1.836		728		6.5
158 II	0.271	0.657		1.640		795		6.0
158 IV	0.252	0.671	0.686	1.801	1.870	711	710	6.4
160 III	0.236	0.636	0.653	1.733	1.807	737	735	6.5
161 I	0.256	0.670		1.775		750		6.3
161 II	0.261	0.614	0.630	1.505	1.573	834	825	5.9
169 I	0.219	0.538	0.590	1.423	1.636	901	805	7.0
177 I	0.228	0.592	0.621	1.592	1.713	824	775	6.3
194 III	0.271	0.665		1.675		790		6.0
196 III	0.256	0.665	0.729	1.644	2.056	800	655	6.4
424 II	0.290	0.750		2.024		657		6.4

composition of both phases, temperatures generally some 20—40°C lower than those for core compositions are obtained (Table 25). Only strongly retrogressed rocks (with e.g. formation of andalusite) give large differences. As a whole, the formation of the rims must be interpreted as a retrograde reequilibration effect.

Ca distribution between garnet and plagioclase: It has been shown by Ghent (1976, 1977) that the distribution of Ca between garnet and plagioclase in the assemblage with sillimanite and quartz is controlled by the end member reaction

3 anorthite $\leftrightarrows$ 1 grossularite + 2 sillimanite + 1 quartz

and could be used mainly as a geobarometer if the effects of nonideality in the garnet and plagioclase solid solution series were known. With the assumption of ideality, however, approximate values can be obtained. The composition of coexisting garnets and plagioclases has been determined both by microprobe and by physical methods, with identical results. Neglecting a possible andradite component in the garnet solid solution, a distribution coefficient

$$\log K_D = \log \frac{(X_{Ca}^{garnet})^3}{(X_{Ca}^{plagioclase})^3}$$

ranging from —2.7 to —3.4 (average —3.0) has been calculated. According to Ghent's model (1977, Equ. 7.12) this corresponds to a pressure of 5.5 kbars at 720°C (Fig. 43). Mössbauer spectroscopic data demonstrate that the andradite component does not exceed a concentration of 1 mole per cent. Even such small concentrations would lower the pressure derived by some 2 kbars. On the other hand, the activity terms for plagioclase and garnet, which are set unity in the model but probably have higher values, tend to increase the pressure reading (Ghent 1977). Effects of nonideality are evident from the clear correlation of log K_D with An content in the plagioclase (Fig. 44), which reflects the CaO/(CaO + Na_2O) ratio of the rock (Fig. 29). In contrast, log K_D is not markedly correlated to X_{Ca}^{garnet} but depends strongly on the Mg/Fe^{2+} ratio of the garnet. Therefore, the assumption of ideality is also invalid for the garnet and a refined model has to take into account the Margules

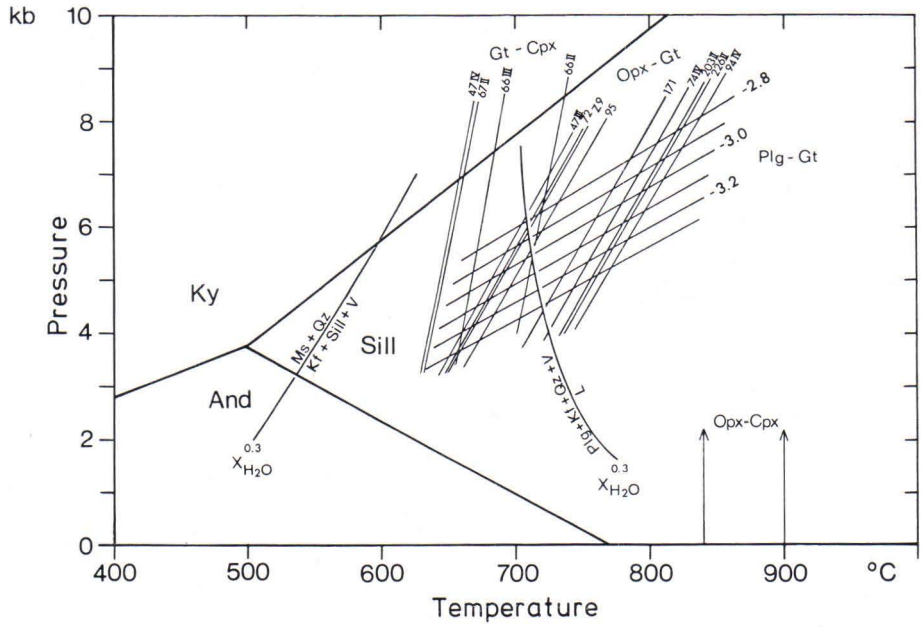

Fig. 43. Stabilities of minerals and assemblages relevant to the metamorphic conditions attained during M2 in the hypersthene-plagioclase rocks and sillimanite-garnet gneisses of the granulite complex. Stability of aluminum silicates taken from Holdaway (1971), muscovite + quartz stability at $X_{H_2O} = 0.3$ taken from Kerrick (1972), minimum melting of granite at $X_{H_2O} = 0.3$ taken from Lee and Holdaway (1977), univariant PT-curves for mineral pairs calculated by the models of Råheim and Green (1974, garnet-clinopyroxene), Wood (1974, garnet-orthopyroxene), Ghent (1976, 1977, plagioclase-garnet, with log K_d values given). For the mineral pair orthopyroxene-clinopyroxene the range of temperatures obtained from the models of Wood and Banno (1973) and Wells (1977) is indicated.

interaction parameters in the garnet solid solution (Schmidt and Wood 1976, Ganguly and Kennedy 1974). Incorporation of these parameters and of the activity terms of the plagioclase solid solution (Orville 1972) leads to a decrease in the scatter of the activity-corrected log K values indicating rather uniform conditions of metamorphism. — It might thus be fortuitous that the incorrected data closely match those derived by the model of Lee and Holdaway (1977).

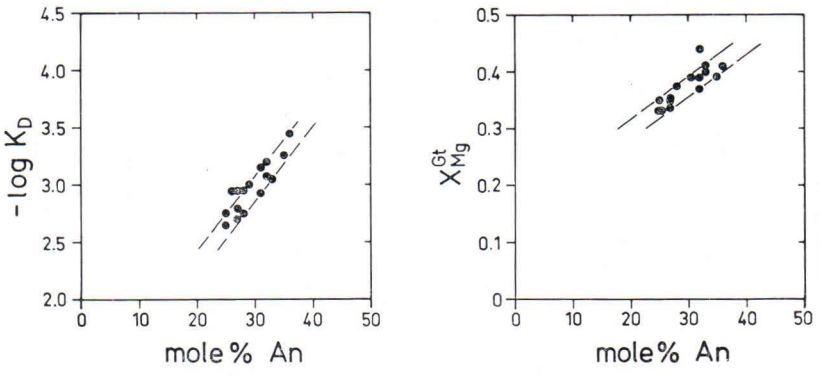

Fig. 44. Relations relevant to the garnet-plagioclase geothermometer and -barometer (Ghent 1976). For discussion see text.

Table 26

Compositional parameters of coexisting garnet and orthopyroxene from the granulite complex and the southwestern marginal zone (samples: Z9, 47III), and temperatures calculated from Equ. 12 of Wood (1974), assuming a pressure of 5 kb.

	Gar X_{Mg}	Gar X_{Ca}	Opx $X_{Fe^{2+}}$	Opx X^{M1}_{Al}	Wood 1974 T °C/5 kb
Z 9	0.27	0.06	0.46	0.064	690
47 III	0.16	0.20	0.51	0.035	682
72 I	0.43	0.07	0.32	0.070	688
74 IV	0.31	0.09	0.37	0.083	748
94 IV	0.30	0.07	0.45	0.093	767
95 I	0.33	0.07	0.44	0.066	700
171 I	0.29	0.06	0.45	0.081	735
203 II	0.33	0.05	0.41	0.097	757
226 II	0.28	0.04	0.44	0.099	760

Al contents in orthopyroxene coexisting with garnet: The Al contents of orthopyroxene in this assemblage are, at moderate pressures, mainly governed by temperature (e.g. Anastasiou and Seifert 1972). The related equilibrium for the pure system $MgO-Al_2O_3-SiO_2$ can be formulated as

enstatite + Mg-Tschermak's component $\leftrightarrows$ pyrope

$Mg_2Si_2O_6$ $MgAlAlSiO_6$ $Mg_3Al_2Si_3O_{12}$

For the complex natural system the dependence of the Al content on the $Fe^{2+}/(Fe^{2+} + Mg)$ ratio and the nonideality in the garnet and orthopyroxene solid solutions has to be taken into account in addition. For the purpose of the present paper equation (12) of Wood (1974) has been used exclusively for a determination of the pressure-temperature relationships. However, since Fe^{3+} contents in orthopyroxene are known, octahedral Al (instead of $Al_{total}/2$) was used in the calculations. It should be pointed out that this equilibrium does not depend on water fugacity because no hydrous phase is involved.

The mineral pair orthopyroxene + garnet occurs only in a few types of basic to intermediate rocks of the granulite complex. Evaluating only those occurrences with unaltered orthopyroxene in grain contact with garnet, the data presented in Table 26 and Fig. 43 are obtained. The samples, which come from the entire granulite complex, define a rather narrow band of pressure — temperature conditions, ranging, at 5 kbars total pressure, from 680 to 770°C, with a mean value of 725°C. Samples with altered orthopyroxene or with orthopyroxene not in grain contact with garnet generally yielded lower temperatures (down to 580°C at 5 kbars).

Composition of garnet in the assemblage with orthopyroxene, plagioclase, and quartz: The Ca content of garnet is not only determined by pressure and temperature in the assemblage with plagioclase, sillimanite and quartz (Ghent 1976) but also in the paragenesis with orthopyroxene, plagioclase and quartz. This potential geobarometer and geothermometer has, so far, not been calibrated (Hensen 1976). The pertinent equilibrium can be formulated as follows:

garnet solid solution + quartz $\leftrightarrows$ anorthite + enstatite

$CaMg_2Al_2Si_3O_{12}$ SiO_2 $CaAl_2Si_2O_8$ $Mg_2Si_2O_6$

The large ΔV of this reaction (+23.4 cm³/mole, corresponding to 14.3 %) already indicates that the equilibrium will be markedly pressure-dependent, higher pressures shifting the reaction to the left. For the complex natural assemblages an equilibrium constant has to be defined:

$$K = \frac{a^{\text{plagioclase}}_{\text{anorthite}} \cdot a^{\text{orthopyroxene}}_{\text{enstatite}}}{a^{\text{garnet}}_{Ca\,Mg_2Al_2Si_3O_{12}}}$$

Without the knowledge of the activities of the individual species in the minerals this term cannot be evaluated at present. However, an empirical distribution coefficient may be derived (cf. Table 27):

$$K_D = \frac{X^{\text{plagioclase}}_{Ca} \cdot (X^{M1}_{Mg} \cdot X^{M2}_{Mg})^{\text{orthopyroxene}}}{X^{\text{garnet}}_{Ca\,Mg_2Al_2Si_3O_{12}}}$$

On the basis of thermochemical data available (Hensen 1977, Ghent 1976, Hensen and Essene 1971) it can be shown that rising temperatures or decreasing pressures will increase the K_D as defined above but the absolute values of K_D and the slope of the lines with constant K_D in a PT diagram cannot be evaluated. Nevertheless, this mainly pressure-dependent equilibrium, in combination with the strongly temperature-dependent Al_2O_3 content in orthopyroxene coexisting with garnet (Wood 1974, see Fig. 43) may, in the future, enable the determination of both pressure and temperature from the assemblage orthopyroxene + garnet + plagioclase + quartz*.

Table 27

Compositional parameters of coexisting plagioclase, orthopyroxene and garnet, and K_D values as defined in the text.

	Plag X_{An}	Opx M1 X_{Mg}	Opx M2 X_{Mg}	Gar $X_{Ca\,Mg_2}$	K_D
Z 9	0.30	0.397	0.454	0.190	0.284
47 III	0.40	0.470	0.444	0.231	0.372
72 I	0.43	0.597	0.679	0.221	0.774
74 IV	0.40	0.537	0.612	0.258	0.509
94 IV	0.40	0.461	0.544	0.200	0.502
95 I	0.40	0.484	0.551	0.202	0.529
171 I	0.37	0.468	0.546	0.166	0.568
203 II	0.38	0.489	0.580	0.139	0.774
226 II	0.34	0.472	0.553	0.127	0.699

The superscripts M1 and M2 refer to the two different octahedral positions in the orthopyroxene structure.

Table 28

Compositional parameters of coexisting clinopyroxene and orthopyroxene, activity terms and K_D values as defined by Wood & Banno (1973). Temperatures derived by the models given by Wood & Banno (1973) and Wells (1977).

	Opx $X_{Fe^{2+}}$	Cpx a_{En}	Opx a_{En}	$\ln K_D$	Temperature °C Wood & Banno	Temperature °C Wells
46 II	0.22	0.53	0.537	2.316	932.6	909.5
47 III	0.52	0.015	0.196	2.570	737.2	747.5
57 I	0.41	0.037	0.301	2.096	838.3	864.9
58 I	0.27	0.100	0.501	1.611	1 003.3	1 032.1
66 II	0.51	0.022	0.211	2.261	773.0	797.1
70 I	0.41	0.047	0.309	1.883	864.6	903.7
70 III	0.38	0.053	0.336	1.847	887.1	924.7
84 I	0.38	0.019	0.342	2.890	764.1	750.5
85 I	0.35	0.036	0.378	2.351	841.5	846.1
100 I	0.25	0.046	0.534	2.452	896.8	871.0
109 I	0.30	0.054	0.435	2.086	908.9	916.2
116 III	0.35	0.047	0.380	2.090	874.3	892.4
168 I	0.38	0.027	0.338	2.527	803.8	805.1
170 II	0.28	0.033	0.376	2.433	900.7	861.4

* After this manuscript was finished Wells (1979) published his evaluation of the above equilibrium. Pressures obtained here with his format of calculation are in the range 7.5 to 5.5 kbars at 750°C.

Fe-Mg distribution between clinopyroxene and orthopyroxene: The Fe-Mg distribution between coexisting pyroxenes is, in the temperature range considered here, almost exclusively a function of temperature (Wood and Banno 1973, Wells 1977). Temperature values derived (Tab. 28) are 859 $\pm$ 72 °C for the Wood and Banno model and 866 $\pm$ 75 °C for the Wells model. It has been shown by other investigators (e.g. Hewins 1975) that temperatures calculated for natural assemblages generally are on the high side (by about 50°C). Another cause for the unreasonably high temperature values might be the high Al and Fe^{3+} contents in the orthopyroxenes.

Fe-Mg distribution between garnet and biotite: For pressure—temperature conditions of metamorphic rocks this equilibrium is largely a function of temperature. Recent models have been proposed by Goldman and Albee (1977), Thompson (1976 a, b), Ferry and Spear (1978). The latter two models are based on empirical Fe–Mg distribution coefficients ($K_D = (Fe/Mg)^{garnet} \cdot (Mg/Fe)^{biotite}$) and thus are particularly sensitive to any nonideality in these phases, whereas the model proposed by Goldman and Albee takes the effects of additional components into account. The temperature dependence of K_D has been calibrated by oxygen isotope temperature measurements (Goldman and Albee 1977) or temperature estimates from the mineral assemblages (Thompson 1976) but has been determined experimentally by Ferry and Spear. High Ti concentrations in biotite may jeopardize the application of these models (Ferry and Spear 1978).

Evaluation of the composition of coexisting garnets and biotites from the different types of garnet gneisses according to these models yielded wide ranges of temperatures (790$\pm$ 100°C, Ferry and Spear model; 730$\pm$70°C, Thompson model; 660$\pm$70°C, Goldman and Albee model). Generally, garnet-biotite pairs from cordierite-bearing gneisses give systematically higher temperatures. The discrepancies between the individual models and the large standard deviation in the temperature readings may be attributed to the inherent simplifying assumptions quoted above or to the fact that biotite is particularly sensitive to reequilibration during cooling (Tracy *et al.* 1976).

Feldspar thermometry: Based on the distribution of albite component between coexisting plagioclase and K-feldspar and its pressure dependence a thermometer has been proposed by Stormer (1975) and later refined by Powell and Powell (1977). Setting total pressure to 5 kbars the temperatures listed in Table 21 are obtained (Fig. 41). In the granulite complex they average to 623$\pm$31°C for the Stormer thermometer and to 595$\pm$29°C for the model of Powell and Powell. They are thus distinct from the much lower values encountered in the West Inari schist zone. In addition, the temperatures derived for the rocks of the granulite complex represent minimum temperatures: Taking into account the antiperthite exsolution of K-feldspar component in the plagioclase which is in the order of 10 volume per cent, nominal temperatures some 40°C higher than the values reported above would result. The temperatures obtained are therefore rather close to those derived for the thermal peak of metamorphism M2 by other thermometers (some 700 to 750°C) and compositional changes of feldspars during cooling obviously only play a minor role in the rocks of the granulite complex. This contrasts to the relationships encountered in the West Inari schist zone where the feldspars indicate temperatures of only some 400°C due to reequilibration during cooling and removal of an albite component from the K-feldspar. The difference in the behaviour of the feldspars during cooling may be attributed to a high activity of water in the West Inari schist zone as opposed to a rather dry environment in the rocks of the granulite complex.

Metamorphic conditions in the granite gneiss complex

The simple and rather uniform mineral assemblages encountered in the rocks of the granite gneiss complex within the profile studied do not allow a precise characterization of the conditions of metamorphism. However, the high-grade amphibolite-facies assemblages and the widespread occurrence of migmatites point to metamorphism under hydrous conditions in the upper temperature part of the amphibolite facies (i.e. temperatures above 650°C at 5 kbars with water pressure close to total pressure). We assume that the physicochemical conditions of the postkinematic M2 event here were similar to those prevailing in the northeastern part of the West Inari schist zone.

Regional variation of pressure — temperature conditions

Whereas so far the three main rock units have been treated as entities with respect to metamorphic grade it is the purpose of this section to investigate gradients of $P-T-X_{fluid}$ conditions within these units as well as to establish the changes of these conditions in the transition zones between the units (i.e. the marginal zones). Such changes already demonstrated in the section on metamorphic zones and episodes are certainly only slight because rather uniform pressure and temperature values have been obtained for the entire profile. Since the various geothermometers and geobarometers discussed above yield only approximate values of pressure and temperature most of them are not suited for detection of minor regional variations of conditions. However, relative changes might be recognized by a number of parameters such as distribution coefficients or mineral chemistry in buffered assemblages.

Fe-Mg distribution among minerals from metabasic rocks: Fig. 45 shows the Fe-Mg distribution between all ferromagnesian minerals except biotite, because the Fe/Mg ratio of the latter is mainly controlled by its Ti content. The band widths of the individual K_D values are generally rather narrow in the West Inari schist zone and the southwestern part of the granulite complex. Whereas the composition of basic rocks in the West Inari schist zone is quite uniform and such a behaviour might be expected, the rocks considered in the granulite complex range chemically from tholeiitic to andesitic. Therefore, it is concluded that the distribution coefficients presented in Fig. 45 are not strongly influenced by bulk rock chemistry but by varying pressure—temperature conditions.

The K_D between garnet and hornblende decreases within the West Inari schist zone and the southwestern marginal zone steadily from 5.8 to 4.0 from the southwest towards the northeast, whereas that between clinopyroxene and hornblende increases from 0.55 to 0.75 in the same direction. These trends can be explained by rising temperatures (cf. Kretz and Jen 1978). The role of changing temperature is emphasized by the decrease in the K_D for garnet–clinopyroxene from 10 to 6 (Råheim and Green, 1974), which would correspond to a ΔT of about 100°C, see Fig. 40.

These trends can be followed into the southwestern part of the granulite complex where the K_D for clinopyroxene–hornblende continues without break. The Fe-Mg distribution between the mineral pairs orthopyroxene–hornblende, orthopyroxene–clinopyroxene and garnet–orthopyroxene defines narrow bands of rather uniform trends in the southwestern part of the granulite complex. Proceeding towards the northeast, the slopes change roughly where cordierite appears in the adjacent gneisses. The bands of all K_D values become ill-defined and poorly documented in the northeastern part of the granulite complex, the northeastern marginal zone and the granite gneiss complex. The spread might be attributed to the higher chemical

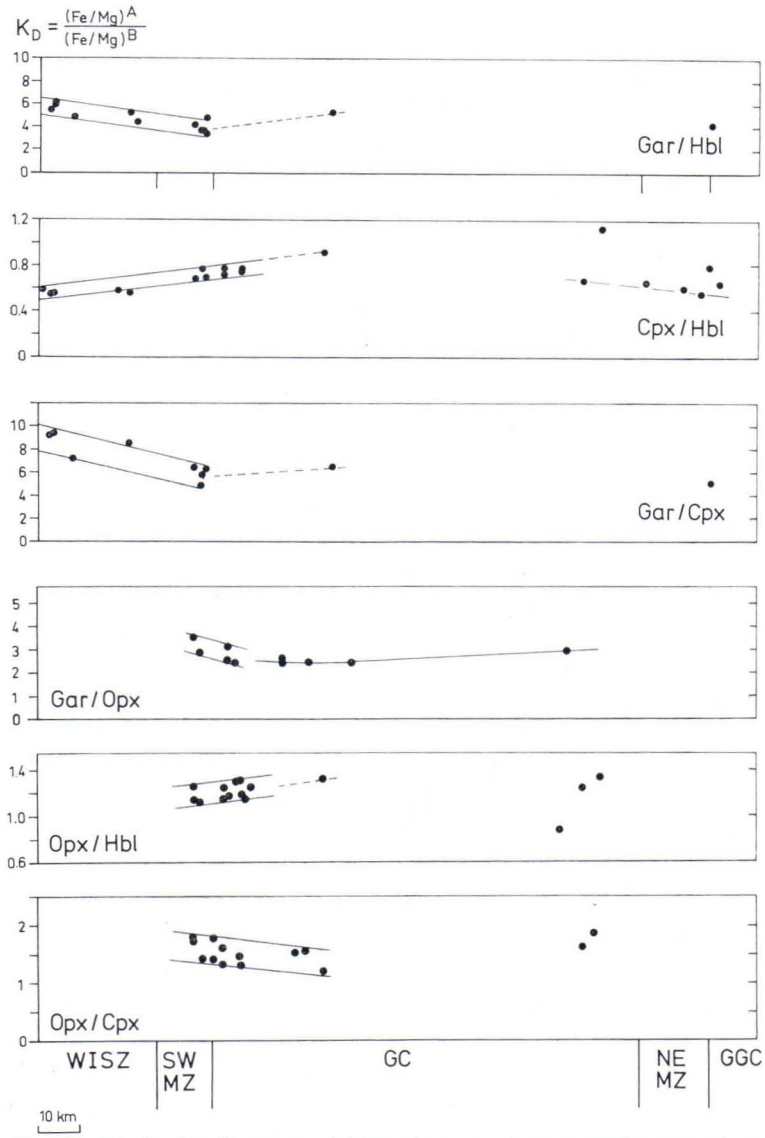

Fig. 45. Mg-Fe distribution coefficients between ferromagnesian minerals in basic to intermediate rocks along the Ivalojoki—Inarijärvi profile.

variability or, more probably, to the stronger retrogression of these rocks.

All these observations would be consistent with the assumption of a temperature maximum within the southwestern part of the granulite complex but other explanations cannot be excluded.

Fe-Mg distribution coefficients between ferromagnesian minerals of the garnet gneisses do not show systematic regional variations. It has been shown above that the Ca distribution coefficient between garnet and plagioclase is affected by the nonideality of the solid solutions involved. It can, therefore, not be used as an indicator of regional trends in metamorphic conditions.

Variation in mineral chemistry: The main features of the regional variation in mineral chemistry

have already been discussed in the section on mineral chemistry and only the relevant conclusions need to be repeated here.

The TiO_2 contents in biotite, hornblende and clinopyroxene coexisting with excess Ti phases (such as sphene, ilmenite, rutile) all show a well-defined regional trend with a systematic increase within the West Inari schist zone (where sphene is the excess Ti phase), and a maximum in the southwestern part of the granulite complex. Further towards the northeast, the hornblende exhibits rather constant TiO_2 values, the TiO_2 in clinopyroxene decreases continously, whereas biotite shows much scatter, probably due to retrogression of the rocks within the northeastern marginal zone (Fig. 28). In the rocks of the granulite complex, the northeastern marginal zone, and the granite gneiss complex ilmenite or rutile form the excess Ti phase. Although the nature of the excess Ti phase will influence the absolute TiO_2 concentrations in the minerals considered, the trends must be interpreted as being due mainly to a temperature maximum in the southwestern part of the granulite complex.

The Al contents of orthopyroxene coexisting with garnet exhibit a strong increase in the southwestern marginal zone and the adjoining southwestern part of the granulite complex and then essentially remain constant (Fig. 22). These Al contents should be positively correlated with temperature, which is, surprisingly, not reflected in the temperatures calculated from the Wood (1974) model.

Similarly, extreme values in a number of other chemical parameters appear in the same position of the profile, with steady and strong changes towards the southwest and less pronounced changes towards the northeast: Among these are the Al content in clinopyroxene (Fig. 22), the Na + K contents and Al^{VI}/Al^{IV} and $(Al^{IV} + Na + K)/Si$ ratios in hornblende (Fig. 19).

Taking all the evidence together, it is concluded that temperatures during M2 varied without major breaks along the profile and attained maximum values in the southwestern part of the granulite complex. The difference between the extreme values in temperature along the profile is estimated to be less than 100°C (650 to 750°C, see above). No data on pressure variation can be given. Higher pressures expected from the geological setting in the parts of the West Inari schist zone overthrusted by the granulite complex during M1 need not necessarily have been present during the post-kinematic M2 event.

Regional variation in fluid phase composition

Fluid inclusion studies (Klatt, pers. comm. 1978) have demonstrated that the trapped fluids in quartz consist of H_2O only in the rocks of the West Inari schist zone whereas in quartz from the granulite complex both CO_2- and H_2O-rich inclusions are present. Exact composition, i.e. H_2O/CO_2 ratios, could not be measured due to the small size of the inclusions. The essentially water-filled inclusions in quartz from rocks of the granulite complex are considered to represent a later (retrogressive) stage of metamorphism. Thus, during M2, the composition of the intergranular fluid phase varied from water-rich in the West Inari schist zone to CO_2-rich in the granulite complex. For the granite gneiss complex a water-rich environment has been inferred. Regional trends within the individual rock units cannot be recognized so far from these studies. They are, however, evident from the $H_2O/(H_2O + CO_2)$ ratios of the fluid enclosed in the channels of the cordierite structure: In the central and northeastern part of the granulite complex this ratio decreases from about 0.77 to 0.65 (disregarding analytical problems) from the northeast to the southwest (Fig. 24). At 600°C, 5 kbars fluid pressure this would correspond to

a change in X_{H_2O} from 0.35 to 0.25 (Johannes and Schreyer 1977). An average X_{H_2O} of 0.32 had also been derived from the »seven-phase» assemblage data of Lee and Holdaway (1977). The trend observed obviously continues into the southwestern part of the granulite complex devoid of cordierite, where an even lower X_{H_2O} is indicated by the absence of significant anatexis during M2. An abrupt change in the fluid phase composition must have occurred within the southwestern marginal zone.

SUMMARY AND CONCLUSIONS

From the chemical data of the metabasic rocks of the West Inari schist zone and their petrological interpretation it is concluded that quartz–tholeiitic magmas which were generated by hydrous partial melting of peridotite in depths of 30—70 km (10—20 kbars) extruded into an oceanic environment or into an area with thin continental crust. The basaltic rocks do not display the typical trace element abundances and REE distribution patterns of oceanic tholeiites but of those intermediate between continental basalts on the one side and basalts and andesites of the island arcs on the other side. These rocks are tholeiitic in terms of the Alk–F–M diagram. Associated dacitic and plagidacitic rocks belong to the series. Such tholeiitic dacites are also encountered in the outer tholeiitic arcs of the modern island arc systems. The ultramafic rocks of the sequence are either komatiites or picrites.

Because the rock compositions are identical to those encountered in the Tertiary island arc system in front of the North Andes (Basic Igneous Complex) a similar geotectonic setting is assumed for the generation of magmas in the West Inari schist zone, i.e. the existence of a Prekarelian island arc.

The rocks of sedimentary origin within the West Inari schist zone which are chemically closely related to the tholeiitic basalts and andesites were mainly greywackes.

In the southwestern marginal zone of the granulite complex the rock compositions become calc-alkaline and are thus more similar to the source-rocks of the granulite complex than to those of the West Inari schist zone.

The rocks of magmatic origin of the granulite complex are members of a series which is calc-alkaline in terms of the Alk–F–M diagram. Basaltic compositions are less abundant and of the high-alumina type. Andesitic and dacitic compositions predominate by far. The calc-alkaline trend, the trace element abundances and the REE distribution patterns relate these rocks closely to the volcanic rocks of the Andean type, i.e. an inner arc on a continental basement.

From a comparison with experimental data it is concluded that the andesitic and dacitic source rocks of the granulite complex originated by hydrous partial melting of basalt, possibly of the composition of the tholeiites of the West Inari schist zone, at depths of 30—70 km (10—20 kbars). The rhyodacitic source rocks may have formed at depths of 70—100 km (20—30 kbars) by hydrous partial melting of andesite.

Rocks of sedimentary origin are more abundant in the granulite complex than in the West Inari schist zone. They are greywackes, subgreywackes, arkoses and quartzites, but pelitic rocks are rare. The primitive character of most sediments is emphasized by similarities to the magmatic parent rocks with respect to the REE distribution patterns and the major element chemistry.

Only limited chemical information is available at present on the rocks of the granite gneiss complex. With respect to the major elements the acid gneisses are closely related to the plagidacitic-rhyolitic rocks of the granulite complex, and possibly of similar origin.

The model proposed for the generation of magmas now forming the magmatogenic rocks of the granulite complex requires a subduction of basalts and andesites chemically similar to the source rocks of the West Inari schist zone. Since the age relations in the West Inari schist zone are only incompletely known, it cannot be decided whether this subducted arc system belonged to the West Inari schist zone itself or represented an even older (>2 800 Ma) island arc.

According to the radiometric age data (Meriläinen 1976) at least two main metamorphic cycles (at 2 500 Ma and in the time span 2 150—1 900 Ma) affected the rocks after emplacement. For the latter Karelian metamorphism the petrologic data indicate two distinct episodes. In particular, in the granulite complex an older (M1) synkinematic granulite facies event at 2 150 Ma could be distinguished from a younger (M2) mainly postkinematic high-grade metamorphic stage at 1 900 Ma. This last metamorphic event which affected the entire Precambrian terrain of northern Lapland during the Karelian Orogeny took place under rather uniform conditions of pressure and temperature without major breaks between the individual rock units. Temperatures ranged from about 650 to 750°C. From the southwest towards the northeast an increase of temperature of metamorphism is observed within the West Inari schist zone. The temperature attained a maximum value in the southwestern part of the granulite complex and then decreased again at a very slow rate towards the northeast. Total pressure ranged from 5 to 6 kbars within the granulite complex but might have been higher in the West Inari schist zone. Opposed to these slight regional changes in the parameters temperature and total pressure there is a marked variation in the composition of the intergranular fluid phase during M2, with X_{H_2O} close to 1 in the West Inari schist zone and the granite gneiss complex but X_{H_2O} close to 0.3 and X_{CO_2} close to 0.7 within the granulite complex. This difference in fluid phase composition lead to the formation of water-saturated amphibolite facies assemblages and widespread anatexis in the West Inari schist zone and the granite gneiss complex, but to rather dry granulite facies assemblages within the granulite complex. Within the latter rock unit, the lowest values of X_{H_2O} are encountered in the southwestern part thus preventing thorough recrystallization and anatexis and still preserving the textures and assemblages of the older M1 event. On the other hand, further in the northeast, X_{H_2O} was higher during M2 and led to a rather complete overprint of M1 by anatexis, metamorphic reactions and recrystallization.

Although the regional chemical variation in the gneisses is only slight, these differences cause the formation of rather distinct mineral assemblages. Within the granulite complex cordierite-garnet-bearing anatexites of the northeastern part are significantly lower in Ca/(Ca + Mg + Fe) and higher in sulfur than the cordierite-free gneisses of the southwestern part. Thus, the appearance of cordierite does not mark an isograd in the field. Similarly, the occurrence of sillimanite in the granulite complex and the lack of aluminium silicates in the quartz–feldspar gneisses of the West Inari schist zone and the granite gneiss complex is controlled by bulk rock chemistry.

Although the basic and intermediate rocks also exhibit systematic chemical differences between the individual units, the paragenetic changes can be modelled by balanced chemical reactions. The appearance of orthopyroxene in the southwestern marginal zone and its disappearance in the northeastern marginal zone define isograds.

After the climax of the M2 event decreasing pressures and temperatures led locally to retrogression. These effects are particularly pronounced in the northeastern part of the granulite complex and the northeastern marginal zone probably because there X_{H_2O} was rather high. The decreased temperatures and possibly also decreased pressures are reflected by the appearance of andalusite in the central and north-

eastern parts of the granulite complex and of kyanite and andalusite in the northeastern marginal zone. In the northeastern marginal zone even lower temperatures are recorded by the appearance of chlorite, epidote, and prehnite. This strong retrogression might be related to late tectonic movements between the granulite complex and the granite gneiss complex (cf. Meriläinen 1976).

Summarizing the evidence from the age data (Meriläinen 1976), the geochemistry of the source rocks and the evolution of the metamorphic rocks in space and time the following development of the Precambrian crystalline rocks of northern Lapland can be deduced from the studies in the Ivalojoki—Inarijärvi profile:

1) The formation of the source rocks for all three major rock units considered took place at an age before at least 2 500—2 800 Ma. The depth of formation for the magmatic liquids of the West Inari schist zone was about 30—70 km, whereas magmatic liquids in the granulite complex originated from depths of about 70—100 km. If genetic relations exist between the magmatic rocks of the West Inari schist zone and the granulite complex, then the overall picture corresponds to the architecture of a modern continental margin system, e.g. the North Andes, with the West Inari schist zone as an outer tholeiitic arc, the granulite complex and the granite gneiss complex as calc-alkaline inner arc systems, and a stable continental block farther in the northeast. The present-day geological setting of the rock units might still reflect this old geotectonic structure. — The sedimentary environment at that time is characterized by clastic sedimentation and incomplete removal of feldspar leading to greywackes, arkoses, and only subordinate quartzites and pelites.

2) The next well-documented event is a high-grade metamorphism still preserved in the southwestern part of the granulite complex (M1) at about 2 150 Ma. The time span between source rock formation and this Karelian event is hidden by the veil of geological history, and only isotope data hint to an amphibolite facies event at 2 500 Ma (Meriläinen 1976) in the granulite complex and the granite gneiss complex. During M1 the granulite complex was metamorphosed under granulite facies conditions and suffered intense shearing. The granite gneiss complex and the granulite complex were probably welded during this period into a single unit and overthrusted onto the West Inari schist zone along a plane subparallel to the hypothetical subduction zone postulated for the generation of magmas. During the overthrusting of the hot granulite complex onto the West Inari schist zone no appreciable amount of water have been released because otherwise the dry granulite facies assemblages and the platy quartz textures would not have been preserved. Consequently it must be postulated that the central and northeastern parts of the West Inari schist zone were already in amphibolite facies during M1. The large scale metamorphic zoning within the West Inari schist zone ranging from greenschist facies in the Peltotunturi zone to amphibolite facies in its northeastern parts is thus not or not only due to heat transfer from the overthrusted granulite complex. However, the small-scale variation encountered in the southwestern marginal zone and the lack of any break in pressure and temperature conditions at the border between the West Inari schist zone and the granulite complex might be related to heat transfer.

3) The Karelian metamorphic evolution ended with a mostly postkinematic event at about 1 900 Ma (M2) which affected the West Inari schist zone, the granulite complex, as well as the granite gneiss complex. It is assumed that in the time span between M1 and M2 the metamorphic grade did not change significantly, i.e. M1 and M2 only represent two paroxysms of a rather extensive metamorphic cycle. At least in the granulite complex the pressure—temperature conditions during M2 were similar to those during M1 and in the West Inari schist zone the

preexisting metamorphic gradient was preserved or even reinforced. At the border between the West Inari schist zone and the granulite complex (i.e. the southwestern marginal zone) no significant exchange of gas phases took place. However, transfer of H_2O generated by amphibolite facies metamorphism and anatexis in the granite gneiss complex into the granulite complex might be responsible for the widespread anatexis and more hydrous assemblages in the northeastern parts of the granulite complex.

4) Late tectonic movements along fault zones led to partial retrogression under conditions of low-grade amphibolite or even greenschist facies. The intrusion of discordant postorogenic granites (Nattanen-type, 1 730 Ma) terminates the Karelian orogenetic cycle.

ACKNOWLEDGMENTS

Support and cooperation by the Geological Survey of Finland, in particular Drs. K. Meriläinen and I. Haapala, is gratefully acknowledged. The research program was made possible through grants from Deutsche Forschungsgemeinschaft, Bonn-Bad Godesberg. S. Bilâl, A.v. Doetinchem, H. Lechner and F. Wiens contributed to the project through their diploma theses. E.Klatt kindly made available unpublished results of fluid inclusion studies. The microprobe used was procured by Volkswagen Foundation. Assistance by the technical staff of Mineralogisches Institut, Universität Kiel, is gratefully acknowledged. The manuscript has kindly been reviewed by Dr. K. Meriläinen (Espoo), Profs. G. Müller (Clausthal), W. Schreyer (Bochum) and K. H. Wedepohl (Göttingen).

REFERENCES

Alexander, P. O. & Gibson, L. L., 1977. Rare earth abundances in Deccan trap basalts. Lithos 10, 143—147.

Allen, J. C., Boettcher, A. L. & Marland, G., 1975. Amphiboles in andesite and basalt: I. Stability as a function of P-T-f_{O_2}. Am. Mineral. 60, 1 069—1 085.

Anastasiou, P. & Seifert, F., 1972. Solid solubility of Al_2O_3 in enstatite at high temperatures and 1—5 kb water pressure. Contrib. Mineral. Petrol. 34, 272—287.

Bambauer, H. U., Corlett, M., Eberhard, E. & Viswanathan, K., 1967. Diagrams for the determination of plagioclases using X-ray powder methods. Schweiz. Mineral. Petrogr. Mitt. 47, 333—350.

Baragar, W. R. A., 1966. Geochemistry of Yellowknife volcanic rocks. Can. J. Earth Sci. 3, 9—30.

Baragar, W. R. A. & Goodwin, A. M., 1969. Andesites and Archean volcanism of the Canadian shield. Proc. Andesite Conf., Oregon State Dept. Min. Ind. Bull. 65, 121—142.

Bayley, R. W., Proctor, P. O. & Condie, K. C., 1973. Geology of the South Pass area, Wyoming. U.S. Geol. Surv. Prof. Pap. 793. 39 p.

Beran, A. & Zemann, J., 1969. Messung des Ultrarot-Pleochroismus von Mineralen. VII. Der Pleochroismus der OH-Streckfrequenz in Andalusit. Tschermaks Mineral. Petrogr. Mitt. 13, 285—292.

Bilâl, S., 1978. Metavulkanite und Metasedimente in der Granulitserie von Finnisch-Lappland. Diploma Thesis, Univ. Kiel. 82 p.

Blais, S., Auvray, B., Capdevilla, R., Jahn, B. M., Bertrand, J. M. & Hameurt, J., 1978. The Archean greenstone belts of Karelia (eastern Finland) and their komatiitic and tholeiitic series. *In:* Windley, B.F. and Naqvi, M. (eds.), Archean geochemistry. Elsevier, Amsterdam 1978, 87—107.

Burri, C., Parker, R. L. & Wenk, E., 1967. Die optische Orientierung der Plagioklase. Birkhäuser Verlag, Basel. 334 p.

Carswell, D. A. & Dawson, J. B., 1970. Garnet peridotite xenoliths in South African kimberlite pipes and their petrogenesis. Contrib. Mineral. Petrol. 25, 163—184.

Chatterjee, N. D. & Johannes, W., 1974. Thermal stability and standard thermodynamic properties of synthetic $2M_1$ muscovite, $KAl_2\ AlSi_3O_{10}(OH)_2$. Contrib. Mineral. Petrol. 48, 89—114.

Clark, S. P., Schairer, J. F. & deNeufville, J., 1962. Phase relations in the system $CaMgSi_2O_6$-$CaAl_2SiO_6$-SiO_2 at low and high pressure. Carnegie Inst. Wash. Year Book 61, 59—68.

Condie, K. C., 1972. A plate tectonics evolutionary model of the South Pass Archean greenstone belt, southwestern Wyoming. 24th Int. Geol. Congr. Montreal, Sect. 1, 104—112.

Condie, K. C. & Baragar, W. R. A., 1974. Rare earth element distributions in volcanic rocks from Archean greenstone belts. Contrib. Mineral. Petrol. 45, 237—246.

Currie, K. L., 1971. The reaction 3 cordierite = 2 garnet + 4 sillimanite + 5 quartz as a geological thermometer in the Opinion Lake region, Ontario. Contrib. Mineral. Petrol. 33, 215—226.

— **, 1974.** A note on the calibration of the garnet-cordierite geothermometer and geobarometer. Contrib. Mineral. Petrol. 44, 35—44.

Deer, W. A., Howie, R. A. & Zussman, J., 1971. Rock-forming minerals. Longmans, London.

v. Doetinchem, A., 1977. Die Paragenese Granat-Cordierit-Sillimanit-Biotit in den Granuliten Lapplands, Nordfinnland. Diploma Thesis, Kiel Univ. 108 p.

Dostal, J., Zentilli, M., Caelles, J. C. & Clark, A. H., 1977. Geochemistry and origin of volcanic rocks of the Andes (26°-28° S). Contrib. Mineral. Petrol. 63, 113—128.

Ellis, D. E., 1978. Stability and phase equilibria of chloride and carbonate bearing scapolites at 750°C and 4 000 bar. Geochim. Cosmochim. Acta 42, 1 271—1 281.

Ellis, D. E. & Green, D. H., 1979. An experimental study of the effect of Ca upon garnet-clinopyroxene Fe—Mg exchange equilibria. Contrib. Mineral. Petrol. 71, 13—22.

Engel, A. E. J. & Engel, C., 1960. Progressive metamorphism and granitization of the major paragneiss, northwest Adirondack Mountains, New York. Part 2, Mineralogy. Geol. Soc. Am. Bull. 71, 1—58.

Eskola, P., 1939. Die metamorphen Gesteine. *In:* Barth, T. F. W., Correns, C. W. & Eskola, P., Die Entstehung der Gesteine. Springer Verlag Berlin, 263—407.

—, **1952.** On the granulites of Lapland. Am. J. Sci., Bowen Volume, Pt. 1, 133—171.

Ewart, A., Bryan, W. B. & Gill, J., 1973. Mineralogy and geochemistry of the younger volcanic islands of Tonga, S. W. Pacific. J. Petrol. 14, 429—465.

Ferry, J. M. & Spear, F. S., 1978. Experimental calibration of the partitioning of Fe and Mg between biotite and garnet. Contrib. Mineral. Petrol. 66, 113—117.

Frey, F. A., 1969. Rare earth abundances in a high-temperature peridotite intrusion. Geochim. Cosmochim. Acta 33, 1 429—1 447.

Ganguly, J. & Kennedy, G. C., 1974. The energetics of natural garnet solid solution. I. Mixing of the aluminosilicate end-members. Contrib. Mineral. Petrol. 48, 137—148.

Gardner, P. M. & Robins, B., 1974. The olivine–plagioclase reaction: geological evidence from the Seiland petrographic province, Northern Norway. Contrib. Mineral. Petrol. 44, 149—156.

Gélinas, L., Lajoie, J. & Brooks, C., 1977. The origin and significance of Archean ultramafic volcanoclastics from Spinifex Ridge, Lamotte Township, Quebec. Geol. Assoc. Canada Spec. Paper 16, IV, Archean greenstone belts, 297—309.

Ghent, E. D., 1976. Plagioclase–garnet–Al_2SiO_5–quartz: a potential geobarometer–geothermometer. Am. Mineral. 61, 710—714.

—, **1977.** Applications of activity - composition relations to displacement of a solid - solid equilibrium grossular = anorthite + kyanite + quartz. *In:* Greenwood, H. J. (ed.), Short Course in applications of thermodynamics to petrology and ore deposits. Mineral. Ass. Canada, 99—108.

Gill, J. B., 1978. Role of trace element partition coefficients in models of andesite genesis. Geochim. Cosmochim. Acta, 42, 709—724.

Goldman, D. S. & Albee, A. L., 1977. Correlation of Mg/Fe partitioning between garnet and biotite with $^{18}O/^{16}O$ partitioning between quartz and magnetite. Am. J. Sci. 277, 750—767.

Goldsmith, J. R. & Laves, F., 1954. Potassium feldspars structurally intermediate between microcline and sanidine. Geochim. Cosmochim. Acta 6, 100—118.

Goldsmith, J. R. & Newton, R. G., 1977. Scapolite-plagioclase relations at high pressures and temperatures in the system $NaAlSi_3O_8$ - $CaAl_2Si_2O_8$ - $CaCO_3$ - $CaSO_4$. Am. Mineral. 62, 1 063—1 081.

Goodwin, A. M., 1977. Archean volcanism in Superior Province, Canadian shield. Geol. Assoc. Canada Spec. Paper 16, IV, Archean greenstone belts, 205—241.

Goossens, P. J., Rose, W. I. & Flores, D., 1977. Geochemistry of tholeiites of the Basic Igneous Complex of northwestern South America. Geol. Soc. Am. Bull. 88, 1 711—1 720.

Green, D. H. & Ringwood, A. E., 1967. The genesis of basaltic magmas. Contrib. Mineral. Petrol. 15, 103—190.

Green, D. H. & Ringwood, A. E., 1972. A comparison of recent experimental data on the gabbro–garnet granulite–eclogite transition. J. Geol. 80, 277—288.

Greenwood, H. J., 1975. Buffering of pore fluids by metamorphic reactions. Am. J. Sci. 275, 573—593.

Guidotti, C. V., Cheney, J. T. & Guggenheim, S., 1977. Distribution of titanium between coexisting muscovite and biotite in pelitic schists from northwestern Maine. Am. Mineral. 62, 438—448.

Gunn, B. M., 1976. A comparision of modern and Archean oceanic crust and island arc petrochemistry. *In:* Windley, B. F. (ed.), The early history of the Earth. Wiley, London, 389—403.

Haapala, I., Siivola, J., Ojanperä, P. & Yletyinen, V., 1971. Red corundum, sapphirine and kornerupine from Kittilä, Finnish Lapland. Bull. Geol. Soc. Finland 43, 221—231.

Hamm, H.-M. & Vieten, K., 1971. Zur Berechnung der kristallchemischen Formel und des Fe^{3+}-Gehaltes von Klinopyroxenen aus Elektronenstrahl-Mikroanalysen. N. Jb. Mineral. Mh., 1971, 310—314.

Heier, K. S., 1960. Petrology and geochemistry of high-grade metamorphic and igneous rocks on Langøy, Northern Norway. Norges. Geol. Unders. 207, 1—246.

—, **1962.** Spectrometric uranium and thorium determinations on some high-grade metamorphic rocks on Langøy, Northern Norway. Norsk Geol. Tidsskr. 42, 143—155.

Heier, K. S. & Adams, J. A. S., 1965. Concentration of radioactive elements in deep crustal material. Geochim. Cosmochim. Acta 29, 53—61.

Henry, J., 1974. Garnet–cordierite gneisses near the Egersund-Ogna anorthositic intrusion, southwestern Norway. Lithos 7, 207—216.

Hensen, B. J., 1976. The stability of pyrope–grossular garnet with excess silica. Contrib. Mineral. Petrol. 55, 279—292.

—, **1977.** Cordierite–garnet-bearing assemblages as geothermometers and barometers in granulite facies terranes. Tectonophysics 43, 73—88.

Hensen, B. J. & Essene, E. J., 1971. Stability of pyrope-quartz in the system $MgO–Al_2O_3–SiO_2$. Contrib. Mineral. Petrol. 30, 72—83.

Hensen, B. J. & Green, D. H., 1971. Experimental study of the stability of cordierite and garnet in pelitic compositions at high pressure and temperature. I. Compositions with excess alumino-silicate. Contrib. Mineral. Petrol. 33, 309—330.

Hensen, B. J. & Green, D. H., 1973. Experimental study of the stability of cordierite and garnet in pelitic compositions at high pressure and temperature. III. Synthesis of experimental data and geological implication. Contrib. Mineral. Petrol. 38, 151—166.

Herrmann, A. G., Blanchard, D. P., Haskin, L. A., Jakobs, J. W., Knake, D., Korotev, R. L. & Brannon, J. C., 1976. Major, minor and trace element compositions of peridotitic and basaltic komatiites from the Precambrian crust of Southern Africa. Contrib. Mineral. Petrol. 59, 1—12.

Hewins, R. H., 1975. Pyroxene geothermometry of some granulite facies rocks. Contrib. Mineral. Petrol. 50, 205—209.

Hörmann, P. K. & Pichler, H., 1980. Geochemistry and petrology of Cenozoic volcanic rocks from the Andes of Ecuador. In preparation.

Hörmann, P. K. & Schock, H. H., 1980. Rare earth element distributions in gneisses of the West Inari schist zone and the granulite complex of northern Finland. In preparation.

Holdaway, M. J., 1971. Stability of andalusite and the aluminium silicate phase diagram. Am. J. Sci. 271, 97—131.

Holdaway, M. J. & Lee, S. M., 1977. Fe-Mg cordierite stability in high-grade pelitic rocks based on experimental, theoretical and natural observations. Contrib. Mineral. Petrol 63, 175—198.

Holloway, J. R. & Burnham, C. W., 1972. Melting relations of basalt with equilibrium water pressure less than total pressure. J. Petrol. 13, 1—29.

Hutcheon, I., Froese, E. & Gordon, T. M., 1974. The assemblage quartz–sillimanite–garnet–cordierite as an indicator of metamorphic conditions in the Daly Bay Complex, N. W. T. Contrib. Mineral. Petrol. 44, 29—34.

Ito, K. & Kennedy, G. C., 1971. An experimental study of the basalt–garnet granulite–eclogite transition. *In:* J. G. Heacock (ed.), The structure and physical properties of the earth's crust. Am. Geophys. Union Geophys. Mon. 14, 303—314.

Jahn, B. M.,1977. Trace element geochemistry of Archean volcanic rocks and its implication for the chemical evolution of the upper mantle. Bull. Soc. Geol. France (7), XIX, 1 259—1 269.

Jakeš, P. & White, A. J. R., 1972. Major and trace element abundances in volcanic rocks of orogenic areas. Geol. Soc. Am. Bull. 83, 29—40.

Johannes, W. & Schreyer, W., 1977. Verteilung von H_2O und CO_2 zwischen Mg-Cordierit und fluider Phase. Fortschr. Mineral. 55, Beih. 1, 64—65.

Johannes, W. & Schreyer, W., 1979. Experimental introduction of CO_2 and H_2O into Mg-cordierite. Am. J. Sci. In the press.

Kerrick, D. M., 1972. Experimental determination of muscovite + quartz stability with $P_{H_2O} < P_{total}$. Am. J. Sci. 272, 946—958.

Köhler, A. & Raaz, F., 1951. Über eine neue Berechnung und graphische Darstellung von Gesteinsanalysen. N. Jb. Mineral. Mh. 247—264.

Kretz, R. & Jen, L. S., 1978. Effect of temperature on the distribution of Mg and Fe^{2+} between calcic pyroxene and hornblende. Canad. Mineral. 16, 533—537.

Krishnamurthy, P. & Cox, K. G., 1977. Picrite basalts and related lavas from Deccan of western India. Contrib. Mineral. Petrol. 65, 53—75.

Kussmaul, S., Hörmann, P. K., Ploskonka, E. & Subieta, T., 1977. Volcanism and structure of southwestern Bolivia. J. Volcanol. Geotherm. Res. 2, 73—111.

Kwak, T. A. P., 1968. Ti in biotite and muscovite as an indication of metamorphic grade in almandine amphibolite facies rocks from Sudbury, Ontario. Geochim. Cosmochim. Acta 32, 1 222—1 229.

Lal, R. K., 1969. Retrogression of cordierite to kyanite and andalusite at Fishtail Lake, Ontario, Canada. Mineral. Mag. 37, 466—471.

Lambert, I. B. & Heier, K. S., 1968. Geochemical investigations of deep-seated rocks in the Australian shield. Lithos 1, 30—53.

Langer, K. & Schreyer, W., 1969. Infrared and powder X-ray diffraction studies on the polymorphism of cordierite, $Mg_2(Al_4Si_5O_{18})$. Am. Mineral. 54, 1 442—1 459.

Langer, K. & Schreyer, W., 1976. Apparent effects of molecular water on the lattice geometry of cordierite: a discussion. Am. Mineral. 61, 1 036—1 040.

Lasnier, B., 1977. Persistance d'une série granulitique au coeur du Massif Central Français, Haut Allier. Les termes basiques, ultrabasiques et carbonatés. Thèse, Nantes. 351 p.

Leake, B. E., 1965. The relationship between tetrahedral aluminium and the maximum possible octahedral aluminium in natural calciferous and subcalciferous amphiboles. Am. Mineral. 50, 843—851.

Lechner, H., 1978. Seriengliederung, Tektonik und Metamorphose der Gesteinsserien in der SW-Randzone des Granulit-Komplexes östlich Repojoki (Finnisch-Lappland). Diploma Thesis, Univ. Kiel.

Lee, S. M. & Holdaway, M. J., 1977. Significance of Fe-Mg cordierite stability relations on temperature, pressure, and water pressure in cordierite granulites. The Earth's crust. AGU, Washington. Geophys. Monogr. Series Vol. 20, 79—94.

Lewis, J. D. & Spooner, C. M., 1973. K/Rb ratios in Precambrian granulite terranes. Geochim. Cosmochim. Acta 31, 1 111—1 118.

Martin, R. F., 1969. The hydrothermal synthesis of low albite. Contrib. Mineral. Petrol. 23, 323—339.

Meriläinen, K., 1965. Pre-Quaternary rocks, Sheet C8-9, Inari Utsjoki. General Geological Map of Finland, 1 : 400 000.

—, **1976.** The granulite complex and adjacent rocks in Lapland, northern Finland. Geol. Surv. Finland, Bull. 281. 129 p.

Mikkola, E., 1941. Kivilajikartan selitys. Lehdet-Sheets B7-C7-D7, Muonio-Sodankylä-Tuntsajoki. English summary. General Geological Map of Finland, 1 : 400 000. 286 p. (Maps published 1936, 1937, 1936).

Mikkola, E. & Sahama, Th. G., 1936. The region to the South-West of the »Granulite Series» in Lapland and its ultrabasics. C. R. Soc. Géol. Finlande 9, 357—371; *also:* Bull. Comm. Géol. Finlande 115.

Miyashiro, A., 1957. Cordierite–indialite relations. Am. J. Sci. 255, 43—62.

—, **1974.** Volcanic series in island arcs and active continental margins. Am. J. Sci. 274, 321—355.

Morse, S. A., 1968. Revised dispersion method for low plagioclase. Am. Mineral. 53, 105—115.

Mysen, B. O. & Boettcher, A. L., 1975. Melting of a hydrous mantle: I. Phase relations of natural peridotite at high pressures and high temperatures with controlled activities of water, carbon dioxide and hydrogen. J. Petrol. 16, 520—548. II. Geochemistry of crystals and liquids formed by anatexis on mantle peridotite at high pressures and high temperatures as a function of controlled activities of water, hydrogen and carbon dioxide. J. Petrol. 16, 549—593.

Nesbitt, R. W., 1972. Skeletal crystal forms in the ultramafic rocks of the Yilgarn block, western Australia; evidence for an Archean ultramafic liquid. Geol. Soc. Australia Spec. Pub. 3, 331—350.

Newton, R. C. & Wood, B. J., 1979. Thermodynamics of water in cordierite and some petrologic consequences of cordierite as a hydrous phase. Contrib. Mineral. Petrol. 68, 391—405.

Nisbet, E. G., Bickler, M. J. & Martin, A., 1977. The mafic and ultramafic lavas of the Belingue greenstone belt, Rhodesia. J. Petrol. 18, 521—566.

Nissen, H. U., 1974. Exsolution phenomena in bytownite plagioclase. *In:* W. S. Mackenzie and J. Zussman (Eds.), The Feldspars. Manchester University Press, Manchester, 491—521.

O'Hara, M. J., 1963. Melting of garnet peridotite and eclogite at 30 kilobars. Carnegie Inst. Washington Yearbook 62, 71—77.

Ohmoto, H. & Kerrick, D., 1977. Devolatilization equilibria in graphitic systems. Am. J. Sci. 277, 1 013—1 044.

Okrusch, M. & Evans, B. W., 1970. Minor element relationship in coexisting andalusite and sillimanite. Lithos 3, 261—268.

Orville, Ph. M., 1972. Plagioclase cation exchange equilibria with aqueous chloride solution: Results at 700°C and 2 000 bars in the presence of quartz. Am. J. Sci. 272, 234—272.

—, **1975.** Stability of scapolite in the system Ab-An-NaCl-$CaCO_3$ at 4 kb and 750°C. Geochim. Cosmochim. Acta 39, 1 091—1 105.

Pichler, H. & Zeil, W., 1972. The Cenozoic rhyolite-andesite association of the Chilean Andes. Bull. Volcanol. 35, 424—452.

Powell, M. & Powell, R., 1977. Plagioclase - alkali-feldspar geothermometry revisited. Mineral. Mag. 41, 253—256.

Raase, P., 1974. Al and Ti contents of hornblende, indicators of pressure and temperature of regional metamorphism. Contrib. Mineral. Petrol. 45, 231—236.

Råheim, A. & Green, D. H., 1974. Experimental determination of the temperature and pressure dependence of the Fe-Mg partition coefficient for coexisting garnet and clinopyroxene. Contrib. Mineral. Petrol. 48, 179—203.

Rankama, K. 1948. New evidence of the origin of pre-Cambrian carbon. Geol. Soc. Am. Bull. 59, 389—416.

Richardson, S. W., Gilbert, M. C. & Bell, P. M., 1969. Experimental determination of kyanite–andalusite and andalusite–sillimanite equilibria; the aluminum silicate triple point. Am. J. Sci. 267, 259—272.

Riley, J. S., 1958. The rapid analysis of silicate rocks and minerals. Anal. Chim. Acta 19, 413—428.

Ringwood, A. E., 1975. Composition and petrology of the Earth's mantle. Mc Graw-Hill, New York. 618 p.

Rittmann, A., 1929. Die Zonenmethode. Schweiz. Min. Petr. Mitt. 9, 1—46.

Rivalenti, G., 1976. Geochemistry of metavolcanic amphibolites from south-west Greenland. *In:* Windley, B. F. (ed.) The early history of the Earth. Wiley, London, 213—223.

Rye, D. M. & Roy, R. F., 1978. The distribution of thorium, uranium, and potassium in Archean granites from northeastern Minnesota. Am. J. Sci. 278, 354—378.

Sahama, Th. G., 1933. Struktur und Bewegungen in der Granulitformation des finnischen Lapplands. C. R. Soc. Géol. Finlande 6, 82—90; *also:* Bull. Comm. Géol. Finlande 101.

— , **1936.** Die Regelung von Quarz und Glimmer in den Gesteinen der finnisch-lappländischen Granulitformation. Bull. Comm. Géol. Finlande 113. 110 p.

— , **1945.** Spurenelemente der Gesteine im südlichen Finnisch-Lappland. Bull. Comm. Géol. Finlande 135. 86 p.

Schau, M., 1977. «Komatiites» and quartzites in the Archean Prince Albert Group. Geol. Assoc. Canada, Spec. Paper 16, IV, Archean greenstone belts, 341—354.

Schmid, R. & Wood, B. J., 1976. Phase relationships in granulitic metapelites from the Ivrea-Verbano Zone (Northern Italy). Contrib. Mineral. Petrol. 54, 255—279.

Seifert, F., 1974. Stability of sapphirine: A study of the aluminous part of the system $MgO-Al_2O_3-SiO_2-H_2O$. J. Geol. 82, 173—204.

— , **1975.** Boron-free kornerupine: A high-pressure phase. Am. J. Sci. 275, 57—87.

— , **1978.** Bedeutung und Nachweis von thermodynamischem Gleichgewicht und die Interpretation von Ungleichgewichten. Fortschr. Mineral. 55, 111—134.

Seifert, F. & Schreyer, W., 1970. Lower temperature stability limit of Mg-cordierite in the range 1-7 kb water pressure: A redetermination. Contrib. Mineral. Petrol. 27, 225—238.

Seifert, F. & Virgo, D., 1975. Kinetics of the Fe^{2+}-Mg, order-disorder reaction in anthophyllites: Quantitative cooling rates. Science 188, 1 107—1 109.

Shaw, D. M., 1960. The geochemistry of scapolite, part I and II. J. Petrol. 1, 218—285.

— , **1972.** The origin of the Aspley gneiss, Ontario. Canad. J. Earth Sci. 9, 18—35.

Shaw, D. M., Dostal, J. & Keays, R. R., 1976. Additional estimates of continental surface Precambrian shield composition in Canada. Geochim. Cosmochim. Acta 40, 73—86.

Simonen, A., 1953. Stratigraphy and sedimentation of the Svecofennidic, early Archean supracrustal rocks in southwestern Finland. Bull. Comm. Géol. Finlande 160, 7—64.

Smith, J. V., 1974. The feldspar minerals. Vols. 1 and 2. Springer-Verlag, Heidelberg, 627 and 690 p.

Sobolev, V. S. (ed.), 1972. The facies of metamorphism. Part 1 (translated by D. A. Brown). Australian National University Press, Canberra, A. C. T. 417 p.

Stern, Ch. R. & Wyllie, P. J., 1978. Phase compositions through crystallization intervals in basalt–andesite–H_2O at 30 kbar with implications for subduction zone magmas. Am Mineral. 63, 641—663.

Stewart, D. B. & Ribbe, P. H., 1969. Structural explanation for variations in cell parameters of alkali feldspars with Al/Si ordering. Am. J. Sci. 267-A, 444—462.

Stewart, D. B. & Wright, T. L., 1974. Al/Si order and symmetry of natural alkali feldspars, and the relationship of strained cell parameters to bulk composition. Bull. Soc. Fr. Mineral. Cristallogr. 97, 356—377.

Stormer, J. C. Jr., 1975. A practical two feldspar geothermometer. Am. Mineral. 60, 667—674.

Storre, B. & Karotke, E., 1972. Experimental data on melting reactions of muscovite + quartz in the system $K_2O-Al_2O_3-SiO_2-H_2O$ to 20 kb water pressure. Contrib. Mineral. Petrol. 36, 343—345.

Stout, J. H., 1975. Apparent effects of molecular water on the lattice geometry of cordierite. Am. Mineral. 60, 229—234.

Sun, S. S. & Nesbitt, R. W., 1978. Petrogenesis of Archean ultrabasic and basic volcanics: Evidence from rare earth elements. Contrib. Mineral. Petrol. 65, 301—325.

Taylor, S. R., 1969. Trace element chemistry of andesites and associated calc-alkaline rocks. Proc. Andesite Conf., Oregon State Dept. Min. Ind. Bull. 65, 43—63.

Thompson, A. B., 1976a. Mineral reactions in pelitic rocks: I. Prediction of P–T–X (Fe–Mg) phase relations. Am. J. Sci. 276, 401—424.

— , **1976b.** Mineral reactions in pelitic rocks: II. Calculation of some P–T–X (Fe–Mg) phase relations. Am. J. Sci. 276, 425—454.

Tracy, R. J., Robinson, P. & Thompson, A. B., 1976. Garnet composition and zoning in the determination of temperature and pressure of metamorphism, central Massachusetts. Am. Mineral. 61, 762—775.

Tröger, W. E., 1971. Optische Bestimmung der gesteinsbildenden Minerale. Teil 1 Bestimmungstabellen. 4. Aufl., Schweizerbart'sche Verlagsbuchhandlung, Stuttgart.

Tsuboi, S., 1934. A straight-line diagram for determining plagioclases by the dispersion method. Japan Geol. Geogr. 11, 325—326.

Tuttle, O. F. & Bowen, N. L., 1958. Origin of granite in the light of experimental studies in the system $NaAlSi_3O_8-KAlSi_3O_8-SiO_2-H_2O$. Geol. Soc. Am. Mem. 74. 153 p.

Viljoen, M. J. & Viljoen, R. P., 1969. The geology and geochemistry of the lower ultramafic unit of the Onverwacht Group and a proposed new class of igneous rocks. Geol. Soc. South Africa, Spec. Publ. no. 2, 55—85.

Wedepohl, K. H., 1969—1978. Handbook of Geochemistry, I, II 1—5, Springer, Berlin.

— , **1975.** The contribution of chemical data to assumptions about the origin of magmas from the mantle. Fortschr. Mineral. 52, 141—172.

Wells, P. R. A., 1976. Late Archean metamorphism in the Buksefjorden region, southwest Greenland. Contrib. Mineral. Petrol. 56, 229—242.

— , **1977.** Pyroxene thermometry in simple and comlex systems. Contrib. Mineral. Petrol. 62, 129—139.

— , **1979.** Chemical and thermal evolution of Archaean sialic crust, southern Greenland. J. Petrol. 20, 187—226.

Wiens, F., 1978. Seriengliederung, Tektonik und Metamorphose der Gesteinsserien der SW-Randzone des Granulitkomplexes östlich Repojoki (Finnisch-Lappland). Diploma Thesis, Univ. Kiel.

Winchell, H., 1958. The composition and physical properties of garnets. Am. Mineral. 43, 595—600.

Windley, B. F. (ed.), 1976. The early history of the Earth. Wiley, London. 619 p.

Wones, D. R. & Eugster, H. P., 1965. Stability of biotite: experiment, theory and application. Am. Mineral. 50, 1 228—1 272.

Wood, B. J., 1974. Solubility of alumina in orthopyroxene coexisting with garnet. Contrib. Mineral. Petrol. 46, 1—15.

Wood, B. J. & Banno, S., 1973. Garnet–orthopyroxene and orthopyroxene–clinopyroxene relationships in simple and complex systems. Contrib. Mineral. Petrol. 42, 109—124.

Wright, T. L. & Stewart, D. B., 1968. X-ray and optical study of alkali feldspar I. Determination of composition and structural state from refined unit-cell parameters and 2 V. Am. Mineral. 53, 38—87.

Wynne-Edwards, H. R. & Hay, P. W., 1963. Coexisting cordierite and garnet in regionally metamorphosed rocks from the Westport area, Ontario. Can. Mineral. 7, 453—478.

Appendix

Sample number, rock type, rock complex, and mineral content

WISZ = West Inari schist zone, SWMZ = southwestern marginal zone of the granulite complex, GC = granulite complex, NEMZ = northeastern marginal zone of the granulite complex, GGC = granite gneiss complex.

act = actinolite
amph = amphibole
and = andalusite
anth = anthophyllite
ap = apatite
bio = biotite
chalc = chalcopyrite
carb = carbonate
chl = chlorite
cord = cordierite
cpx = clinopyroxene
ep = epidote
gar = garnet
graph = graphite
hem = hematite
hbl = hornblende
ilm = ilmenite
kf = alkalifeldspar
ky = kyanite
mt = magnetite
mus = muscovite
ol = olivine
opx = orthopyroxene
ore = opaques
pic = picotite
plag = plagioclase
pre = prehnite
pyr = pyrite
pyrr = pyrrhotite
qtz = quartz
rut = rutile
scap = scapolite
ser = sericite
serp = serpentine
sill = sillimanite
sph = sphene
spi = spinel
staur = staurolite
tc = talc
zois = zoisite

No.	rock type	rock complex	mineral content main and minor minerals	accessories	secondary minerals
1LI	garnet amphibolite	WISZ	hbl, plag, gar, qtz, cpx	sph, zirc	
2I	amphibolite		hbl, plag, qtz, cpx	sph, zirc	act, ep, ore
2III	garnet-clinopyroxene amphibolite; foliated		hbl, plag, cpx, gar	sph, pyr	carb, ep
4I	amphibolite, banded		hbl, plag, cpx, qtz	sph, pyr	act
5I	ultramafic rocks		hbl, ol, spi, chl	pic	serp, carb
6I	quartz-feldspar gneiss; grey		qtz, plag, kf, bio, gar	ap, zirc	chl, mus, ore
8I	garnet amphibolite; banded		hbl, plag, gar, qtz	sph, zirc, ore	
8II	quartz-feldspar gneiss; grey, schlieric		qtz, plag, kf, bio, gar	zirc	chl, mus
8IV	amphibolite		hbl, plag, qtz, bio	sph, ap	scap, ep
9I	amphibolite		hbl, plag, cpx, qtz		scap, ep, sph
14I	corundum amphibolite		hbl, corundum		chl, zois
16I	granite gneiss; grey (Hetta-type)		qtz, plag, kf, bio		chl, mus, ep
17I	amphibolite		hbl, plag, qtz	sph, ore	carb
18I	garnet amphibolite		hbl, gar, qtz, plag, cpx	sph	ep, ore
18II	garnet amphibolite		hbl, gar, plag, cpx, qtz	sph, ap, pyr	ep
19I	amphibolite		hbl, plag, cpx, gar		scap, ep, sph
19II	quartz-feldspar gneiss; reddish		qtz, plag, kf, bio		chl, mus, ep, ore
20I	amphibolite		hbl, plag, qtz, gar	sph, ap	ep
21I	amphibolite		hbl, plag, qtz	ore, sph, ap	chl, ep
22I	ultramafic rock		opx, ol		serp, carb, tc, chl, amph
23IV	amphibolite		hbl, plag, bio, staur	ore	
24I	amphibolite		hbl, plag, qtz	sph	ep, ore
24II	quartz-feldspar gneiss; reddish grey		kf, qtz, plag, bio	sph, ore	ep, mus
25I	hornblende gneiss; lineated		qtz, kf, plag, hbl, gar	sph, ore	
26I	quartz-feldspar gneiss; reddish	↓	kf, qtz, plag, hbl, bio	ore, sph	carb

Appendix, contd

No.	rock type	rock complex	mineral content main and minor minerals	accessories	secondary minerals
27I	amphibolite	WISZ	hbl, plag, qtz, cpx	sph	
29I	amphibolite		hbl, plag, qtz	sph	
30LI	meta-dolerite		plag, cpx, bio	ore, ap	hbl, gar
30II	garnet amphibolite		hbl, plag, gar, qtz, cpx	ilm, pyr, sph, ap	ep
31I	biotite gneiss; grey		qtz, plag, bio, gar, hbl		ep
34I	quartz-diorite		plag, hbl, qtz, bio		ep, chl, sph
36I	garnet amphibolite; banded		hbl, plag, gar, qtz, cpx	sph	carb
38I	ultramafic rock		ol, opx, carb	ore	chl, serp, amph, tc
38II	ultramafic rock; sheared		amph, ol, carb, chl, opx		serp
39I	ultramafic rock; sheared		amph, chl		tc, ore
40I	quartz-feldspar gneiss; reddish		kf, qtz, plag, hbl, bio	ore, sph	
41I	quartz-feldspar gneiss; reddish grey		kf, qtz, hbl, plag, bio	mt, sph	
42I	quartz-feldspar gneiss; reddish	SWMZ	kf, qtz, plag, hbl, bio	ore, zirc, sph	
42II	quartz-feldspar gneiss; schlieric reddish		qtz, plag, kf, hbl, bio	ore, zirc, sph, ap	
43I	quartz-feldspar gneiss; grey		qtz, plag, cpx, gar	sph	ore
43IV	amphibolite; banded		hbl, plag, qtz, opx, bio	ap, ilm	
44I	amphibolite		hbl, plag, cpx, qtz	sph	
46I	garnet-quartz-feldspar gneiss; reddish		qtz, kf, plag, gar	ilm, mt	
46II	meta-troctolite		plag, ol		opx, cpx, spi, amph
46III	pyroxene gneiss; grey, banded		plag, qtz, cpx, hbl, opx, bio	sph, ore	
47I	garnet-quartz-feldspar gneiss; light, sheared		qtz, kf, plag, gar, bio	ore, zirc	ser, ep, chl
47III	garnet-pyroxene-amphibole rock, migmatized		plag, hbl, cpx, opx, gar, qtz, bio, kf	pyr	
48I	clinopyroxene-quartz-feldspar gneiss; greyish		plag, qtz, cpx, hbl	ilm, sph	carb
51I	hornblende-plagioclase gneiss; meta-quartzdiorite		plag, qtz, hbl, bio	ilm, mt, ap	mus, chl
52I	quartz-feldspar gneiss; light, sheared		qtz, plag, kf, bio	zirc	chl, sph
53I	garnet-biotite-hornblende gneiss; foliated		plag, qtz, gar, bio, hbl, kf	ore, ap, zirc	chl
54I	hornblende-plagioclase gneiss; meta-quartzdiorite		plag, hbl, qtz	ore, ap	ep, ser, chl, pre
55I	garnet-hornblende gneiss; foliated		plag, qtz, hbl, gar	ore, ap, zirc	
57I	hypersthene-plagioclase gneiss; brown	GC	plag, opx, bio, qtz	ilm, mt, pyrr	
58I	hypersthene-plagioclase rock; brown	GC	opx, plag, bio, cpx, hbl	ore, ap	
58III	quartz-feldspar augengneiss		qtz, plag, bio, kf	ore, rut, zirc, ap	mus, ep, chl, scap
59I	sillimanite-garnet gneiss; foliated		qtz, kf, gar, plag, bio, sill	ore, rut	
59II	hypersthene-plagioclase rock; dark brown		plag, bio, opx, qtz	ilm, pyr, pyrr, ap	
62I	sillimanite-garnet gneiss	SWMZ	qtz, kf, gar, plag, bio, sill	ore, zirc, rut	
63I	quartz-feldspar gneiss; greyish, retrogressed		qtz, plag, cpx, hbl	zirc	scap, ep, carb, chl, ser
65I	sillimanite-garnet gneiss; banded		qtz, kf, gar, bio, plag, sill	rut, ilm, pyr	
65III	garnet-quartz-feldspar gneiss; banded, light		qtz, kf, plag, gar, bio	rut, sill	ep, mus, carb
66I	pyroxene-plagioclase gneiss; banded		qtz, plag, hbl, cpx, opx, bio	ilm, ap, sph	scap, carb
66II	pyroxene gneiss; dark		opx, cpx, plag, hbl, gar	ilm, pyrr, ap	chl, carb
66III	garnet-clinopyroxene amphibolite, dark		cpx, plag, hbl, gar	ilm, pyrr, ap	act
67I	garnet-plagioclase amphibolite; foliated		plag, hbl, qtz, gar, bio	pyr, ap, zirc	ep, chl
67II	garnet-hornblende gneiss; grey		plag, qtz, hbl, gar, cpx	ilm, mt, ap, zirc	
69II	garnet-quartz-feldspar gneiss; light	GC	qtz, plag, gar, bio	ore, rut, zirc	ep
69III	sillimanite-garnet gneiss; greyish		qtz, plag, kf, gar, bio, sill	rut, graph, zirc	

Appendix, contd

No.	rock type	rock complex	mineral content main and minor minerals	accessories	secondary minerals
70I	hypersthene-plagioclase rock; dark	GC	plag, opx, hbl, cpx	ilm, mt, pyr, ap	
70II	garnet-quartz-feldspar gneiss; banded		qtz, plag, kf, gar, bio	ilm, mt, pyr, zirc	
70III	hypersthene-plagioclase rock; dark		plag, opx, hbl, cpx, bio	ore, ap	
71I	garnet-quartz-feldspar gneiss; light		qtz, kf, gar, plag, bio	ore, rut	
72I	garnet-hypersthene-plagioclase gneiss		plag, gar, opx, bio, qtz	ilm, mt, pyr, pyrr, ap	
74I	hypersthene-plagioclase gneiss		plag, opx, bio, qtz	ilm/hem, mt, pyr, scap, ap	
74IV	garnet-hypersthene-plagioclase gneiss		plag, bio, gar, hyp, qtz, kf	ilm, mt, pyr, zirc, ap	
76I	garnet-quartz-feldspar gneiss; light		kf, qtz, plag, gar, bio, sill	zirc	
76II	sillimanite-garnet gneiss; banded		qtz, plag, kf, gar, bio, sill	rut, zirc	
80I	hypersthene-plagioclase rock		plag, qtz, opx, kf, bio, amph	ilm/hem, mt, pyr, ap, zirc	ep, chl
83I	hypersthene-plagioclase gneiss		plag, opx, qtz, bio	ilm/hem, mt, pyr, ap	
84I	hornblende-pyroxene-plagioclase rock		plag, opx, amph, cpx, bio, qtz	ilm/hem, mt, pyr, ap	ep, ser
85I	hypersthene-plagioclase gneiss		plag, opx, qtz, amph, bio, cpx, kf	ilm/hem, mt, pyr, ap	ep, ser
88I	hypersthene-plagioclase rock		plag, opx, bio, amph, cpx, qtz, scap	ilm/hem, mt, pyr, ap	
89I	garnet-cordierite gneiss; schlieric		kf, qtz, cord, plag, gar, bio, sill	ilm, pyr, pyrr	
89V	garnet-cordierite anatexite		qtz, kf, plag, gar, cord, bio, sill	ilm, mt, pyr, pyrr, zirc, spi	
91I	hypersthene-plagioclase rock		plag, opx, bio, qtz, kf	ilm, mt, pyr, ap	
93I	garnet-quartz-feldspar gneiss		qtz, kf, plag, gar, bio	ore, ap	ser, chl, ep
93II	hypersthene-plagioclase gneiss		plag, opx, bio, qtz	ilm, pyr, ap	
93IV	garnet-quartz-feldspar gneiss; light		qtz, plag, gar, kf, bio		chl, ser, carb, ore
93VI	garnet-cordierite anatexite; pegmatoid		qtz, plag, cord, bio, gar, sill	pyr, zirc	
94IV	hypersthene-plagioclase gneiss		plag, kf, opx, qtz, bio, gar	ilm, mt, pyr, ap, zirc	
95I	garnet-hypersthene-plagioclase gneiss; banded		plag, qtz, opx, bio, gar, kf	ilm, mt, pyr, ap, zirc	
96I	garnet-quartz-feldspar gneiss; light		qtz, kf, plag, gar, sill, bio	ilm, pyr, rut, zirc	
97I	hypersthene-plagioclase rock		plag, opx, bio	ilm, mt, pyr, ap	
97II	hypersthene-plagioclase rock		plag, opx, bio	ilm/hem, mt, pyr, ap	
100I	biotite-bronzite rock (ultramafic)		opx, bio, plag, cpx, amph	ap	
105I	sillimanite-garnet-cordierite gneiss; banded		kf, qtz, cord, gar, sill, bio, plag	ore, rut, zirc	
109I	biotite-bronzite rock (ultramafic)		opx, plag, bio, cpx, qtz	pyrr	
110III	sillimanite-garnet-cordierite gneiss; banded		kf, qtz, gar, cord, sill, bio, plag	rut, zirc	
111I	garnet-biotite-plagioclase gneiss		plag, qtz, gar, bio	ilm, pyrr, ap, zirc	ser, chl, ep
116I	garnet-quartz-feldspar gneiss; banded		qtz, kf, gar, plag, bio, sill	ilm/hem, pyr, pyrr	
116III	hypersthene-plagioclase rock		plag, opx, amph, cpx, bio	ilm/hem, mt, pyr, pyrr, ap	
119I	sillimanite-garnet-cordierite gneiss; schlieric		qtz, kf, gar, cord, sill, bio, plag	ore, rut, zirc	
125I	hypersthene-plagioclase gneiss		plag, opx, bio, qtz	ilm, pyr, ap	
128I	garnet-biotite-plagioclase gneiss		plag, qtz, gar, bio, kf	ore, rut, zirc	ser
130I	quartz-feldspar gneiss; light		kf, qtz, plag	ore, zirc	
140III	garnet-hypersthene-plagioclase gneiss		plag, opx, bio, gar, qtz	pyr, pyrr	
141I	hypersthene-plagioclase rock		plag, opx, bio, qtz	ilm, pyr, pyrr, ap	
143I	garnet-quartz-feldspar gneiss; light	↓	kf, qtz, plag, gar	ore, rut	ser

Appendix, contd

No.	rock type	rock complex	mineral content main and minor minerals	accessories	secondary minerals
145I	garnet gneiss; foliated	GC	qtz, gar, plag, bio, cord, and	ore	chl, ser
148I	garnet-biotite gneiss; banded		qtz, kf, plag, gar, bio, sill	ore, zirc, rut	ser, chl
150I	garnet-quartz-feldspar gneiss; schlieric		qtz, plag, kf, gar, bio, sill	ilm, rut, zirc	
154I	garnet-quartz-feldspar gneiss; light		kf, qtz, plag, sill, gar		
156I	garnet-quartz-feldspar gneiss; schlieric		kf, qtz, gar, plag, sill, bio	ore, rut	
158I	garnet-cordierite anatexite		kf, qtz, cord, gar, sill, bio, plag	ilm, rut, pyr, pyrr, zirc	
158II	garnet-cordierite anatexite		qtz, cord, kf, gar, sill, bio	ilm, rut, pyr, pyrr, zirc	chl
158IV	garnet-cordierite anatexite		qtz, cord, kf, gar, sill, bio, plag	ilm, rut, pyr, pyrr, zirc	
160III	garnet-cordierite anatexite		kf, qtz, cord, gar, bio, plag, sill	ilm, rut, pyrr, zirc	
161I	garnet-cordierite anatexite		qtz, kf, cord, plag, gar, bio, sill	ilm, pyr, pyrr, zirc	
161II	garnet-cordierite anatexite		kf, qtz, plag, cord, gar, bio, sill	ore, zirc	
164I	garnet-cordierite anatexite		kf, cord, gar, qtz, plag, sill, bio, and	ore, zirc	chl, ser, carb
168I	hypersthene-plagioclase rock		plag, opx, hbl, cpx, bio, qtz	ilm/hem, mt, pyr, ap	
169I	garnet-cordierite anatexite; schlieric		qtz, kf, plag, gar, cord, bio, sill	ilm, pyr, pyrr, rut, zirc	
170II	hypersthene-plagioclase rock		opx, plag, bio, cpx, hbl	ilm, rut, pyrr, ap	
171I	garnet-hypersthene-plagioclase gneiss		plag, qtz, bio, gar, opx	ore, ap, zirc	ser
174II	amphibolite		plag, hbl, cpx, qtz	ilm, mt, ap	ser
177/I	garnet-cordierite anatexite		plag, bio, gar, qtz, cord, sill	ilm, pyr, pyrr, zirc, spi	
J1I	hypersthene-plagioclase gneiss		plag, qtz, opx, bio, kf	ilm, mt, pyr, pyrr, ap	
J3I	garnet-quartz-feldspar gneiss		plag, qtz, gar, bio	ilm, rut, zirc, ap	
J5II	garnet-quartz-feldspar gneiss; banded		qtz, plag, kf, gar, bio, sill	ore, rut, ap	chl, ser
J7I	garnet-biotite-plagioclase gneiss		plag, qtz, gar, bio	pyr, chalc, zirc	ser, chl
J12I	hypersthene-plagioclase gneiss		plag, opx, hbl, bio, qtz, kf	ilm/hem, mt, ap	
190I	garnet-cordierite gneiss		kf, qtz, cord, gar, plag, bio, sill	ore, rut, zirc	
194II	garnet-cordierite anatexite		qtz, kf, cord, gar, plag, bio, sill	ore, rut, zirc	
194III	garnet-cordierite anatexite		qtz, cord, plag, gar, bio, sill, and	ore, rut, zirc, ap	ser, chl
195I	garnet-cordierite anatexite		qtz, kf, cord, gar, plag, bio, sill, and	ore, zirc, spi	
196III	garnet-cordierite anatexite; very coarse-grained		kf, cord, qtz, gar, and		chl, ser
198I	garnet-pyroxene-plagioclase rock; fine-grained		qtz, plag, cpx, gar, opx?, hbl	ore	ep, carb
198III	garnet-cordierite anatexite; schlieric		kf, qtz, cord, gar, plag, bio, sill	ore, rut, zirc	
203II	garnet-hypersthene gneiss; light		kf, qtz, plag, gar, opx, bio	ilm, mt, zirc	
204I	garnet-cordierite gneiss; schlieric		kf, qtz, gar, cord, plag, bio, sill	ore, zirc, sph	
205I	garnet-cordierite gneiss; banded		kf, qtz, cord, gar, plag, bio, sill	ore, zirc	
206I	clinopyroxene-plagioclase rock		plag, qtz, cpx, scap	ore, ap	sph, ser
211II	sillimanite-garnet gneiss		qtz, kf, gar, bio, plag, sill	ore, rut, zirc	
215I	garnet-cordierite anatexite		plag, qtz, gar, cord, bio, sill, and	ore, zirc	ser, carb
217I	garnet-cordierite gneiss; banded	NEMZ	kf, bio, gar, cord, qtz, plag, sill	ore, zirc	
219I	amphibolite		plag, hbl, cpx	ilm, ap, zirc	
220II	garnet-cummingtonite-plagioclase rock		plag, cumm, gar, bio, qtz	ilm, pyrr, ap	amph

Appendix, contd

No.	rock type	rock complex	mineral content main and minor minerals	accessories	secondary minerals
222III	anthophyllite-plagioclase rock	GC	plag, anth, bio, qtz	ilm, pyrr, ap, zirc	
223I	sillimanite-garnet gneiss; banded		kf, qtz, bio, gar, plag, sill	rut, zirc	
226II	garnet-hypersthene-plagioclase rock		plag, qtz, opx, bio, gar, kf	ore	ser, chl, ep
228I	biotite-plagioclase gneiss		plag, qtz, bio, kf	ore, zirc	ser, carb
232I	garnet-cordierite anatexite; schlieric	↓	kf, plag, qtz, gar, bio, cord, sill	ore, zirc, spi	
424II	biotite-garnet gneiss	NEMZ	plag, qtz, bio, gar, cord, sill, ky	pyr, mt, zirc	chl, ser
426II	biotite-garnet gneiss		plag, qtz, bio, cord, gar, sill, and, ky	ore, zirc	ser, chl
458II	garnet amphibolite; banded	↓	plag, hbl, gar, qtz, cpx, bio, cumm	ilm, pyrr, sph, ap	ep, carb, chl
460II	amphibolite	GGC	hbl, plag, cpx, qtz	pyr	ep
464II	amphibolite	NEMZ	hbl, plag, qtz, cpx, bio	ilm, pyr, ap, sph, zirc	
465II	amphibolite	GGC	hbl, plag, qtz, bio	ilm, ap, sph, zirc	ser, ep, chl, prehn
470II	amphibolite	↓	hbl, plag, cpx, kf, qtz	ap	carb, ep
Z9	garnet-hypersthene rock	SWMZ	gar, opx, qtz, plag, bio	ore	cumm/anth

ISBN 951-690-122-0
ISSN 0367-522X